UCLA Samueli
School of Engineering

Summer Undergraduate Research Program at the Engineering Student Resource Center
Office of Academic and Student Affairs
UCLA Samueli School of Engineering
420 Westwood Plaza, 6288 Boelter Hall, Los Angeles, CA, 90095-1600
310.825.9478 | www.samueli.ucla.edu

UCLA Samueli
School of Engineering

SUMMER
UNDERGRADUATE
RESEARCH PROGRAM

2019

RESEARCH JOURNAL

Table of Contents

Student Research Abstracts & Posters

Poster Symposium and Awards Ceremony | August 16, 2019

First Floor Engineering VI: Mong Auditorium, Lobby and Patio

11:00 AM - 11:05 AM Announcement (William Herrera)

11:05 AM - 12:30 PM Poster Galley Walk

11:45 AM - 12:30 PM Hors d'oeuvres service begins

12:30 PM - 2:00 PM Awards Ceremony

DEAN'S MESSAGE

The Summer Undergraduate Research Program (SURP) provides participants with an intensive 8-week summer research experience in a wide range of engineering fields. Undergraduate students participate in research with UCLA Samueli School of Engineering faculty and research teams to gain real-world lab experience. As part of this program, SURP students:

- Meet and network with peers who have similar goals and interests
- Learn to communicate research outcomes by participating in weekly Technical Presentation Labs
- Create a professional scientific poster of their research
- Write and publish a research abstract
- Present a detailed Summary of Project
- Become more competitive when applying to engineering graduate schools

This year, 39 undergraduate students were selected to join the 2019 SURP cohort. I would like to congratulate this SURP class on completion of their amazing research projects. Creating new knowledge is a very important, and a very difficult, task. These high-performing students have done an outstanding job working through the rigors and challenges of full time research. They should be very proud of the abstracts and posters they have published today. I encourage you to meet the students, ask questions about their projects, and learn about the cutting-edge knowledge that is being created here at the UCLA Samueli School of Engineering.

Sincerely,

Jayathi Murthy
Ronald and Valerie Sugar Dean

LAB NAME
Signal Processing and Circuit Engineering Laboratory

FACULTY ADVISOR
Professor Sudhakar Pamarti

GRADUATE STUDENT DAILY LAB SUPERVISOR
Shi Bu

DEPARTMENT
Electrical and Computer Engineering

Neha Adhlakha

Electrical Engineering

Second Year

UCLA

Filter Behavior Characterization and Verification Utilizing Analog to Digital Converter and Digital Signal Processing

High-performance integrated electrical filters are desired in almost every aspect and found in almost all electronic devices. In realizing very sharp and linear analog filters with enhanced wave filtering applications, our lab began utilizing an intentional use of time varying circuits. However, for such filters to be truly useful, it needs precise characterization with fast, and preferably automated processes. Developing this automation involved signal generators and an analog-to-digital converter to create a quick and precise characterization of the behavior of various filters which would otherwise be done manually which is time consuming and inefficient. The ADC board combined with two synchronized signal generators allows the signal to be sent to a MATLAB algorithm and hence obtain the desired magnitude and phase responses of the filter. The signal generation and process is more complex than sweeping the input frequency because the automation produces many challenges including equipment noise. My research aims to overcome these obstacles with digital signal processing. Our process of characterizing the parameters of a filter quickly and precisely will contribute to our labs development of a frequency-channelized ADC that will use tens of such filters to separate the spectrum into multiple pieces.

UCLA | Samueli School of Engineering | Summer Undergraduate Research Program

Fast Track to SUCCESS summer scholars program

Filter Behavior Characterization and Verification Utilizing Analog to Digital Converter and Digital Signal Processing

UCLA Department of Electrical and Computer Engineering

N. Adhlakha, A. Bakhshandeh, S. Bu, S. Pamarti

Introduction

High-performance integrated electrical filters are desired in almost every aspect and found in almost all electronic devices. In realizing very sharp and linear analog filters with enhanced wave filtering applications, our lab began utilizing an intentional use of time varying circuits. However, for such filters to be truly useful, it needs precise characterization with fast, and preferably automated processes. This automation created a quick and precise characterization of the behavior of various filters which would otherwise be done manually which is time consuming and inefficient. The techniques developed in this research used off-the-shelf filters for proof of concept and will be used to measure the fabricated LPTV-circuit-based chips so that we will build the frequency-channelized ADC.

Measurement Principles and Setup

The setup below is used with two synchronized Signal Generators in phase which sends two signals, one at a high frequency, and one at a low frequency through a power combiner. Then the two-tone signal is passed through the low pass filter and into the ADC for data collecting and sent through a MATLAB algorithm.

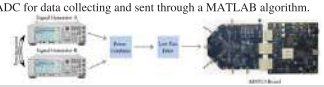

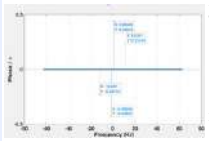

Phase

The use of a power combiner in the setup above allowed the relative phases between an input signal 12 MHz) and a synchronized (1 MHz) signal to be represented on the graph to the left. The calculated phase of a signal in itself is irrelevant; its relative phase to an accompanying synchronized signal is used due to the fact that the at low frequencies, the filter adds negligible delay.

Amplitude

The amplitude of the signal was extracted with the use of the FFT function as well as taking the FFT processing gain into consideration. Spectrum leakage has also been taken into account. The resulting amplitude magnitude is compared to data sheets to verify the filter.

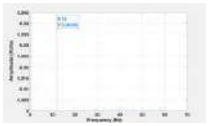

Acknowledgements

I would like to acknowledge the 2019 Summer Undergraduate Scholars Program for this amazing research opportunity, Professor Pamarti for giving us this project to contribute to his influential research, and Shi Bu our daily lab supervisor for guiding us through this project and answering all of our questions to make sure this is a huge learning experience for us.

Automation

GPIB

In order to manually automate the synchronized E4422b signal generators, we connected them with GPIB and a NI GPIB board which connects through usb to a computer. Then the signal generators are controlled by MATLAB code which sweeps the frequency of both generators by 1MHz until the algorithm is stopped.

Visual Analog

The signal data is processed through Visual Analog software, which we use for sampling and automation to extract the magnitude and phase. The data is sent through the input formatter, data router, and pattern saver which saves the data in a new txt file in a folder every 1000 ms. This allows the data to be sent through an automation algorithm to characterize the filter at each frequency.

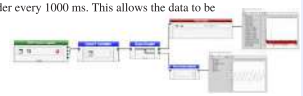

Characterization Aspects

Challenges

- The two-tone set up is necessary because the absolute phase of one sinusoidal signal depends on when the sampling starts and is therefore useless. So, the relative phase is obtained by comparing it with a reference low-frequency signal, for which the filter has negligible delay.

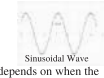

- The phase of the two signal generators might be out of lock after changing the frequency which may need to be solved by using a dummy ADC setup that capturers the signal prior to it passing through the filter and then compare the relative phase.

Filter Verification

To verify that the low pass filter being used worked correctly, the magnitude response was measured with a signal passing through the filter and sent through the spectrum analyzer. The results were graphed (top) and compared to the online specification (bottom), the visual drop in loss at 12 MHz verifies our filter.

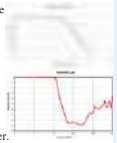

Future Work and Conclusion

In conclusion, digital signal processing is a complicated task which requires many verifications of processes and obstacles to overcome with equipment use. However, the automation of characterizing filters involves synchronized Signal Generators, ADC Boards, Visual Analog Software, and a MATLAB algorithm. In the end we are able to fully characterize a filters magnitude and phase and graph the results in order to understand their precise response.

Our process of characterizing the parameters of a filter quickly and precisely will contribute to our labs development of a frequency-channelized ADC that will use tens of integrated LPTV-circuit-based filters to separate the spectrum into multiple pieces. The filters are one of the sharpest integrated filters to date and the ability to use multiple filters and characterize them precisely and accurately will allow development for advanced technology.

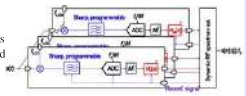

LAB NAME

Terahertz Devices and Intersubband Nanostructures Group Laboratory

FACULTY ADVISOR

Professor Ben Williams

GRADUATE STUDENT DAILY LAB SUPERVISOR

Parastou Mortazavian

DEPARTMENT

Electrical and Computer Engineering

Nathan Atkinson

Computer Engineering

Third Year

UCLA

Diamond as an output coupler for chip-scale terahertz external cavity quantum cascade lasers

External cavity quantum cascade lasers are an integral source of terahertz radiation. However, heat removal from the devices is critical in order to achieve continuous wave operation. We introduce a chip-scale output coupler for a quantum cascade vertical external-cavity surface emitting laser (QC-VECSEL) through a 500 um thick synthetic polycrystalline diamond plate. This design brings two primary benefits: a method of dissipating heat from the laser's bias region and a mechanically stable output coupler with no need for alignment. The diamond is mounted directly on top of the metasurface, replacing an existing design involving an externally mounted quartz output coupler. Initial electromagnetic simulations indicate acceptably high reflectance at a resonant lasing frequency of 3.4 THz and a bandwidth of about 140 GHz. Thermal simulations will be conducted to predict the expected improvements to operating temperature and heat dissipation for the VECSEL's metasurface. Possible areas of concern include high threshold current and increased thermal losses due to an adjusted ridge geometry that features a high fill factor.

Diamond as a chip-scale output coupler for terahertz quantum cascade lasers

Nathan Atkinson, Parastou Mortazavian, Christopher Curwen, and Benjamin Williams

Department of Electrical and Computer Engineering, University of California, Los Angeles

Abstract

External cavity quantum cascade lasers are an integral source of terahertz radiation. However, heat removal from the devices is critical in order to achieve continuous wave operation. We introduce a chip-scale output coupler for a quantum cascade vertical external-cavity surface emitting laser (QC-VECSEL) through a 500 um thick synthetic polycrystalline diamond plate. This design brings two primary benefits: a method of dissipating heat from the laser's bias region and a mechanically stable output coupler with no need for alignment. The diamond is mounted directly on top of the metasurface, replacing an existing design involving an externally mounted quartz output coupler. Initial electromagnetic simulations indicate acceptably high reflectance at a resonant lasing frequency of 3.4 THz and a bandwidth of about 140 GHz. Thermal simulations will be conducted to predict the expected improvements to operating temperature and heat dissipation for the VECSEL's metasurface. Possible areas of concern include high threshold current and increased thermal losses due to an adjusted ridge geometry that features a high fill factor.

VECSEL Coupled with Diamond

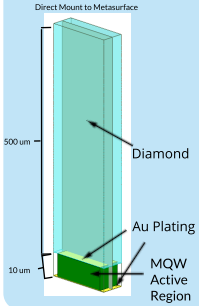

Diamond is a superb thermal conductor and a strong electrical insulator. Consequently, it serves as a viable output coupler and heat spreader for the metasurface. Placing diamond on top of the metasurface serves to remove the external cavity and create a pseudo-monolithic system which may offer improved mechanical stability in applied settings. The diamond introduces a lossy medium through which the laser beam must travel. Carbon vapor deposition (CVD) diamond has been observed to have an optical refractive index of about 2.378.[2] This changes the beam's resonant frequency; the ridge geometry must be adjusted to realign the resonance with the target 3.4 THz. As such, this design features a much shorter ridge gap than previous VECSELs.

Candidate Active Region

The VECSEL will be fabricated on an existing wafer design (VB0988) which has a maximum current density of about 1000 A/cm^2. Given a fill factor of 84.5%, the nominal bias region diameter was chosen to be 1 mm. This implies a peak current of 6.6 A.

Possible areas of concern moving forward primarily involve thermal performance. 500 um thick diamond may not adequately dissipate heat from the bias region.

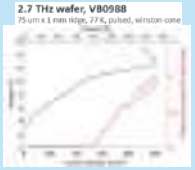

VECSEL Design

VECSEL Ridge Active Region Geometry

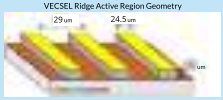

- Designed metasurface is a periodic array of coupled metal-metal ridges
- Chip-scale ridges consist of a layered multiple quantum well (MQW) semiconductor structure
- Laser cavity comprised of metasurface and a partially reflective output coupler
- Width and distance between ridges on the metasurface determine the resonant frequency, as does the distance of the output coupler from the metasurface

Output Coupler with Metasurface

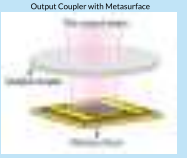

- Previous output coupler made of quartz
- Vacuum cavity separates metasurface and output coupler
- 3.4 THz is a standard frequency for which the VECSELs are designed[1]

Response at Resonant Frequency

Reflectance for VECSEL with Quartz Window

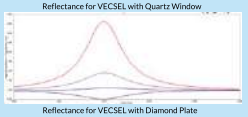

Reflectance for VECSEL with Diamond Plate

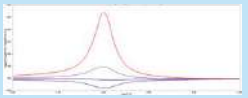

- Simulated reflectance maintains similar values from previous design
- Expected peak reflectance at resonant frequency (3.4 THz)
- Full-width half max bandwidth is 140 GHz at 40 cm^{-1} gain
- Free spectral range (FSR) is 126 GHz; single mode lasing expected

Electric Field Magnitude Profile

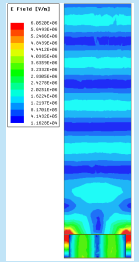

In electromagnetic simulations, the electric field profile appears uniform with no indication of diffraction. The high intensity patterns located periodically between ridges suggests that the device will behave similarly to a distributed feedback laser (DFB). A radiative pattern indicative of wave propagation in the normal direction is observed.

Acknowledgments

We would like to thank the National Science Foundation and the UCLA HSSEAS Summer Undergraduate Research Program for providing funding for and the opportunity to publish our research, as well as the UCLA Electrical Engineering Fast Track to Success Program for its continued support of undergraduate research and studies.

References

1. Xu, L., et al. "Metasurface external cavity laser." Applied Physics Letters, **107**, (2015).
2. Kubarev, V., et al. "Optical properties of CVD-diamond in terahertz and infrared ranges". Nuclear Instruments and Methods in Physics Research A, **603**, (2009).

LAB NAME

Signal Processing and Circuit Engineering Laboratory

FACULTY ADVISOR

Professor Sudhakar Pamarti

GRADUATE STUDENT DAILY LAB SUPERVISOR

Shi Bu

DEPARTMENT

Electrical and Computer Engineering

Abbas Bakhshandeh

Electrical Engineering

Second Year

UCLA

Filter Behavior Verification and Characterization Utilizing Analog to Digital Converter and Digital Signal Processing

Electronic filters are utilized almost everywhere. However, while integrated filters are demanded in modern high-complexity systems, for them to be truly useful, we need to fully characterize them with great precision. While such characterization and testing may appear to be straightforward, many difficulties arise in practice. For example, such characterization needs to be fast and accurate, with multiple aspects being measured simultaneously. Measurement equipment non-idealities, such as noise and non-linearity, had to have been addressed with careful consideration. Our utilization of an Analog to Digital Converter (ADC) enabled an automated process with high precision, as the ADC's output could be processed digitally for better handling of various error sources. Our use of an ADC in addition to signal generators and MATLAB algorithms allowed us to automate the process of verifying the veracity of a filter's intended behavior; this process allowed us to extract properties such as magnitude and phase, some of the most important parameters to our interest. These now characterized filters can be utilized in more complex integrated systems for various communication applications. For example, the aid from the automated, precise characterization of filters will allow the building of a hybrid filter bank - which would consist of tens of filters - to achieve signal reconstruction with much less difficulty, which is key to realizing a wideband frequency-channelized ADC for high-dynamic-range and low-power applications.

Filter Behavior Verification and Characterization Utilizing Analog to Digital Converter and Digital Signal Processing

Abbas Bakhshandeh, Neha Adhalaka, Shi Bu, Sudhakar Pamarti

Department of Electrical and Computer Engineering, University of California - Los Angeles

Introduction

High-performance integrated electronic filters are desired in almost every aspect and found in almost all electronic devices. It is desirable to know their responses, and in some applications, it is preferable that precise measurements of the filter's frequency responses be measured. Without this step, there will be performance degradation. The utilization of the ADC enabled an automated process with high precision, as the ADC's output could be processed digitally for better handling of various error sources. Our use of an Analog to Digital Converter (ADC) in addition to signal generators and Matlab algorithms allowed us to automate the process of verifying the veracity of a filter's intended behavior; this process allowed us to extract properties such as magnitude and phase, some of the most important parameters to our interest. In our specific case, we intend to use such measurements to create a hybrid filter bank that utilizes alias cancellation. This filter bank will allow for high-dynamic range and low-power applications.

Filter Verification Setup and Process

A

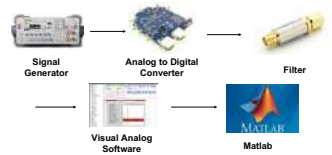

(**A**) The signal generator – or multiple signal generators in sync with one another to produce multiple signals - constructs a signal which is sent to the analog digital converter, which in turn passes through the filter on its way to the Visual Analog Software. The data set produced through this software is extracted, and then sent to Matlab for analyzation. Within Matlab, Fast Fourier Transforms in addition to various other functions are utilized to extract the amplitude and relative phase of the signal, from which the filter's properties can be characterized and confirmed.

Utilization of Matlab Algorithms and Power Combiner to Extract Amplitude and Relative Phase

A

(**A**) The amplitude of the signal was extracted with the use of the fft function as well as taking the FFT processing gain into consideration. Spectral leakage has also been taken into account. The resulting amplitude magnitude is compared to data sheets to verify the filter's frequency response.

(**B**) The Power Combiner uses two input ports to combine two input signals into a single output signal. This is necessary in the case of analyzing the phase of a signal, as the relative phase of one signal to another is what is really desired. The power combiner allows both signals to be graphed and analyzed within one set of data.

B

C

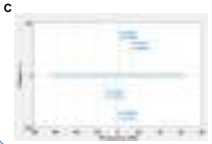

(**C**) The use of a power combiner allowed the relative phases between an input signal (12 MHz in this case) and a synchronized (1 MHz) signal to be represented within one graph. The calculated phase of a signal in itself is irrelevant; its relative phase to an accompanying synchronized signal reveals its true behavior and allowed the filter to be fully characterized. This is based on the notion that at low frequencies, the filter adds negligible delay.

Spectral Leakage

A

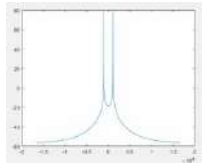

(**A**) Whenever the period of time being analyzed does not contain an integer number of periods, spectral leakage occurs. While performing a Fast Fourier Transform, this leakage causes sharp junctions, which in turn increase the perceived frequency content of the signal. This must be accounted for in order to extract the correct relative phase value of the signal, and hence to characterize the filter effectively. This is possible to do since we know the signal frequency, which we chose as the input.

B

(**B**) To solve the issue of spectrum leakage, we are truncating the sequence such that it has an integer number of periods. This will make the sample being analyzed an better representation of the original signal. This is necessary because the FFT function assumes the data being analyzed can be reconstructed exactly as the input signal. The process of windowing, which includes the use of weighting functions, can solve this issue.

Lock-In Amplifier

A

$$U_{\text{out}}(t) = \frac{1}{T}\int_{t-T}^{t} \sin[2\pi f_{\text{ref}} \cdot s + \varphi] U_{\text{in}}(s)\, ds$$

(**A**) The methods associated with a lock in amplifier must be utilized in order to decrease the noise surrounding the signal. This is important because at frequencies where the filter greatly attenuates the signal, the input to the ADC will be too small, which will cause it to be overwhelmed by noise. Therefore, we need a lock-in amplifier to de-noise it to get the signal. The properties of a lock in amplifier were simulated in Matlab by multiplying and then integrating the data set by a reference signal of the same frequency to eliminate the effects of all frequencies not of importance.

Conclusions and Future Work

A

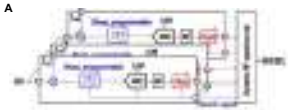

(**A**) Looking forward, the algorithms developed will allow for the accurate verification and characterization of the self made filters in the lab. These verified filters can be utilized in more complex integrated systems for various communication applications. A filter bank can now be constructed which will facilitate more efficient signal reconstruction; this in turn will be useful in realizing high-dynamic range and low-power applications. Additionally, our process of characterizing the parameters of a filter quickly and precisely will contribute to our labs development of a frequency-channelized ADC that will use tens of integrated LPTV-circuit-based filters to separate the spectrum into multiple pieces.

Acknowledgments

This work was supported by the Fast Track to Success Summer Scholars Program. It has also been supported and much gratitude is given to Professor Pamarti as well as Shi Bu, our daily lab supervisor, for their input on the project. Abbas Bakhshandeh is participating in the Summer Undergraduate Scholars Program at the Henry Samueli School of Engineering at UCLA.

LAB NAME

Algorithmic Research in Network Infromation Flow Laboratory

FACULTY ADVISOR

Professor Christina Fragouli

GRADUATE STUDENT DAILY LAB SUPERVISOR

Yahya Ezzeldin

DEPARTMENT

Electrical and Computer Engineering

Pranav Balgi

Computer Engineering

Third Year

UCLA

Rodent Path Reconstruction using Hippocampal Rate Coding

The goal of this project is to use neural spike readings from a rat to determine its position in an enclosure. The spike readings are taken from several neurons in the hippocampus, a part of the brain that is associated with spatial memory. The spike readings are condensed into spike rates for each neuron, which are believed to hold information about the stimulus (the rat's position). The spike rate of each neuron is modeled as a Poisson process with an unknown parameter that is a function of the stimulus. A neural network is used to determine the parameter for every neuron at every position in the enclosure. Different sets of features from the stimulus can be used as the input to the neural network. The parameters and spike rate data are then fed into a decoder to reconstruct the original path. There are many different feature extractions, neural network architectures, and decoding schemes that can be used in this framework. The goal is to select the features, design the neural network, and build the decoder that will minimize error in the reconstructed path. Some of the decoding algorithms that have been explored in this project include one-shot decoding, greedy decoding, Viterbi decoding, and adaptive decoding. A high-performance decoder could possibly be adapted to improve brain-machine interfaces.

Rodent Path Reconstruction using Hippocampal Rate Coding

Pranav Balgi, Yahya Ezzeldin, Christina Fragouli

Algorithmic Research on Networked Information Flow (ARNI)

Department of Electrical and Computer Engineering, University of California, Los Angeles

Introduction

Goal: use neural spike readings* from a rat to determine its position in an enclosure

- spike readings are taken from multiple neurons in the rat's hippocampus
- hippocampus is a part of the brain that is associated with spatial memory
- spike readings are condensed into spike rates for each neuron,
- spike rates are believed to hold information about the stimulus (the rat's position)
- a high-performance decoder could possibly be adapted to improve decoding of neural responses which is a key interest for brain-machine interfaces

*data was provided by the W. M. Keck Center for Neurophysics at UCLA

Neural Encoding

- spike rate of each neuron (N=73) is modeled as a Poisson process
- Poisson parameters are functions of the stimulus
- different sets of features from the stimulus can be used as the input to the model
- model is trained to determine the parameter for every neuron at every position in the enclosure
- a neural network can be used for feature extraction

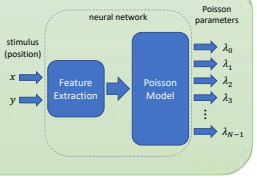

Path Decoding

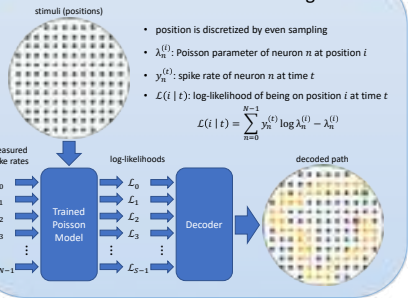

- position is discretized by even sampling
- $\lambda_n^{(i)}$: Poisson parameter of neuron n at position i
- $y_n^{(t)}$: spike rate of neuron n at time t
- $\mathcal{L}(i \mid t)$: log-likelihood of being on position i at time t

$$\mathcal{L}(i \mid t) = \sum_{n=0}^{N-1} y_n^{(t)} \log \lambda_n^{(i)} - \lambda_n^{(i)}$$

Decoding Methods

One-Shot Decoder

- selects position with maximum likelihood at each time
- $s(t)$: decoded position at time t

$$s(t) = \underset{i}{\operatorname{argmax}}\, \mathcal{L}(i \mid t)$$

Greedy Decoder

- selects position that is within a fixed distance r of the previous position

$$s(t) = \underset{i}{\operatorname{argmax}}\, \mathcal{L}(i \mid t) \;\; s.t. \;\; \|\boldsymbol{p}(i) - \boldsymbol{p}(s(t-1))\| \leq r$$

Viterbi Decoder

- selects path with maximum likelihood out of all possible paths
- $s(i,t)$: maximum likelihood previous position from position i at time t
- $m(i,t)$: path metric on position i at time t

$$s(i,t) = \underset{j}{\operatorname{argmax}}\, m(j, t-1) + \mathcal{L}(i \mid t) \;\; s.t. \;\; \|\boldsymbol{p}(i) - \boldsymbol{p}(j)\| \leq r$$
$$m(i,t) = \mathcal{L}(s(i,t) \mid t-1) + \mathcal{L}(i \mid t)$$

Adaptive Decoding

- selects position that is within a variable distance r of the previous position
- r is proportional to current speed

$$s(t) = \underset{i}{\operatorname{argmax}}\, \mathcal{L}(i \mid t)$$
$$s.t. \;\; \|\boldsymbol{p}(i) - \boldsymbol{p}(s(t-1))\| \leq \alpha \|\boldsymbol{p}(s(t-1)) - \boldsymbol{p}(s(t-2))\|$$

Results

- Viterbi decoding performs the best, but at the cost of running time
- adaptive decoding slightly improves the greedy decoder, but not the Viterbi decoder
- performance decreases as the testing interval moves away from the training interval
- decoders perform better when trained on future intervals rather than past intervals
- all of these decoders can run in real time, with the Viterbi decoders requiring a delay
- one-shot decoding performs the worst, showing that more sophisticated decoding algorithms can improve performance

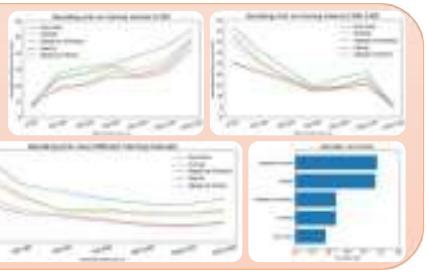

Future Work

- explore more decoding algorithms
- try out different neural network architectures for encoding
- try out new feature extractions for encoding
- select different combinations of neurons to use

LAB NAME
Terahertz Electronics Laboratory

FACULTY ADVISOR
Professor Mona Jarrahi

GRADUATE STUDENT DAILY LAB SUPERVISOR
Dr. Nezih Yardimci and Dean Turan

DEPARTMENT
Electrical and Computer Engineering

Arhison Bharathan

Electrical Engineering

Second Year

UCLA

A High-Speed, Low-Cost, and Compact Optical Delay Stage for Terahertz Time-Domain Spectroscopy Systems

Terahertz Time-Domain Spectroscopy (THz-TDS) is an application of the terahertz band of the electromagnetic spectrum with advanced capabilities in chemical identification, material characterization, and nondestructive material analysis. Recent developments in THz emitter and detector technology have established improved signal-to-noise ratios within these systems, increasing the viability of THz-TDS in commercial applications. However, the weight and speed of these systems are also limited by a component known as the delay stage, a mechanical device used to vary laser optical path length. The focus of our research has been to create a miniaturized, high-speed delay stage to address this need.

While laboratory delay stages offer sub-micron accuracies, these systems are often large and expensive due to the extra functionality they provide. We have opted to explore alternative mechanisms to achieve compact and cost-effective designs that suit our application. Utilizing 3D printing and machining, we have created prototype stages using crank and crank-inspired mechanisms that achieve reciprocation frequencies of 10.4 Hz (as compared to 1.2 Hz by a laboratory stage). Through comparisons of THz-TDS results between a laboratory stage and our stages in the clarity and accuracy of absorbed THz waves measured through air, we have also been able to classify the efficacy of each iteration of our device. Looking at areas other than performance, our stages are lighter (211 g to 17 kg) and cheaper (about $200 to $10k) as well.

A High-Speed, Low-Cost, and Compact Optical Delay Stage for Terahertz Time-Domain Spectroscopy Systems

Arhison Bharathan, Madeline Taylor, Nezih Yardimci, Deniz Turan, Mona Jarrahi

Department of Electrical and Computer Engineering, University of California – Los Angeles

Background – What is THz-TDS?

Terahertz Time-Domain Spectroscopy (THz-TDS) is a well-established technology within the field of terahertz (THz) research. Created in the early 90's, this technology exploits the electromagnetic absorption properties of matter in the THz waveband for purposes of chemical identification, material characterization, and nondestructive material analysis.

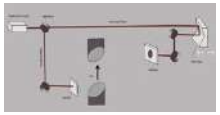

THz-TDS System Operation:

- THz emitter - receives a femtosecond IR pulse and emits THz radiation towards sample
- THz detector - upon receiving a femtosecond IR pulse and THz pulse, acts as a switch to allow current pass when struck simultaneously
- Delay Stage – moves two mirrors at 90° on a carriage to vary the optical path length of the IR pulse to the detector. This allows for time-domain reconstruction of the pulse (see Figure 1). A Fourier transform of this reconstruction yields the frequency-domain characteristics of the pulse (see Figure 2).

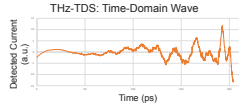

Figure 1 – Reconstructed THz wave through air using a laboratory delay stage

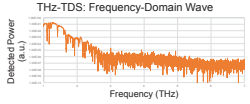

Figure 2 – Fourier transform of Figure 1 from which absorbed THz frequencies can be determined

Objective

Recent technological advancements in THz-TDS systems—due to the creation of more powerful sources and more sensitive emitters which offer better signal-to-noise ratios—have made the use of this technology practical at a commercial scale. To optimize the size and speed of such systems, another necessity is to create a compact, high-speed delay stage to increase system portability and usability.

Our research objective is to develop this miniaturized delay stage. By leveraging speed, cost, and size, we aim to create a delay stage at a size suitable for commercial use. To gauge the progress of our designs, we compare the THz wave detection results from our stage and a laboratory delay stage, looking the clarity and accuracy of absorbed frequencies. Other statistics like travel, weight, and size are also considered.

Crank Mechanism - Proof of Concept

We have chosen to use a crank mechanism to drive our stage since it trivially achieves smooth, consistent, reciprocating linear motion. Unlike a laboratory stage, the path a crank mechanism follows is invariable so a trivial h-bridge motor controller suffices to actuate the mechanism. A lab scale prototype of this mechanism allows us to compare THz measurements between a laboratory stage and crank actuated stage to determine the viability of this mechanism for this THz-TDS.

Laboratory Stage – Newport Motorized Linear Stage IMS300LM-S
Produces accurate and precise motion at the expense of size, cost, and, speed. This stage is only practical in a laboratory setting.

Frequency	1.2 Hz
Total Travel	30 cm
Weight	17 kg
Size	55.6 cm x 18 cm x 8.9 cm
Price	about $10,000

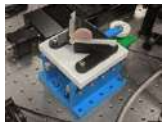

Laboratory Scale Crank Stage
This is a prototype to find out whether a crank mechanism can provide any THz-TDS measurements at all. This stage is 3D printed and uses linear slides and a stepper motor to drive the carriage.

Frequency	2.2 Hz
Total Travel	2 cm
Weight	861 g
Size	18 cm x 12.2 cm x 8.9 cm
Price	about $150

THz Wave Absorption Through Air (Frequency-Domain) Results

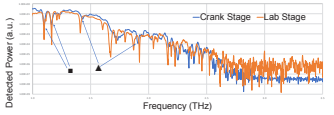

Crank Stage exhibits:

- Shallow absorption lines (■)
- Shifted absorption lines (▲)

We believe these errors are systematic nature. Since we can account for such errors through post-processing, we conclude that a crank mechanism shows promise in a THz-TDS system.

Current Work – Mechanism Miniaturization

We use an iterative design approach to create smaller, high-speed versions of the crank mechanism we previously tested. To improve precision we employ stereolithography printing and CNC routing to create the stage and actuate the carriage on linear bearings on shafts.

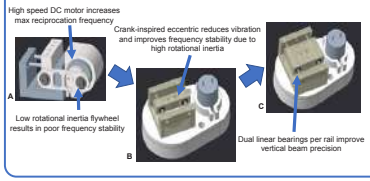

Stage	A	B	C
Frequency (Hz)	N/A[1]	10.4	N/A[2]
Total Travel (cm)	1.2	0.7	1.1
Weight (g)	101	211	N/A[2]
Size (cm^3)	7.4 x 6.6 x 4.6	9.4 x 6.2 x 5.4	
Price	$220	$260	$300

1. Frequency instability makes this value nonessential
2. N/A statistics have not been measured due to work in progress

Conclusion and Future Work

A crank mechanism presents promising results for use in the actuation of a THz-TDS delay stage. Once our stage is mechanically complete, we plan to develop a motor control scheme utilizing position feedback to further improve frequency stability. Utilizing superior manufacturing techniques (e.g. CNC machining) will also contribute to stage precision and speed.

Acknowledgments:

- UCLA Summer Undergraduate Research Program (SURP)
- Terahertz Laser Lab
- Mona Jarrahi, Nezih Yardimci, Deniz Turan
- UCLA Rieber Makerspace

LAB NAME

Actuated Sensing & Coordinated Embedded Networked Technologies Laboratory

FACULTY ADVISOR

Professor William Kaiser

GRADUATE STUDENT DAILY LAB SUPERVISOR

Susie Tan

DEPARTMENT

Electrical and Computer Engineering

Jason Bustani

Computer Science

Third Year

UC Berkeley

Approaching Human Motion Through A Tri-Axial Accelerometer Mapping of Geometric Shapes

Accurately detecting human motion via electronic signals is a feat that has yet to be mastered. It remains to be one of the most difficult and complex motions to be detected by an accelerometer, and its mastery could lead to many new technologies in the medical and sports field. Digital signals are by their nature probabilistic and stochastic, and mapping simple to complex shapes merely on a 2-dimensional plane is challenging. The initial hypothesis was to collect data using a 10 x 10 cm square and writing the outputs in a notebook and calculate the errors to find a consistent pattern. A consequent hypothesis was to play with the filters to attune the signal for a desired result. By changing the resonance frequency for the High-Pass Filter, a chaotic signal came within a decent amount of precision for mapping rectilinear and curved figures that come close to human motions projected onto a 2-dimensional plane. The errors were dependent completely on the filter and on the setup of the device. Proper sensor placement to avoid the effect of gravity and finding the right constant for the filter lead to successful results.

Approaching Human Motion Through A Tri-Axial Accelerometer Mapping Of Geometric Shapes

Jason Bustani, Susie Tan[1], William Kaiser[1]

1. Department of Electrical and Computer Engineering

Motivation

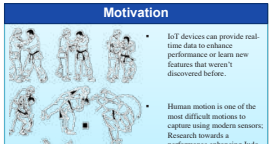

- IoT devices can provide real-time data to enhance performance or learn new features that weren't discovered before.
- Human motion is one of the most difficult motions to capture using modern sensors; Research towards a performance enhancing Judo IoT device can further the field of capturing and analyzing human motion digitally.
- Beginning with 2-Dimensional projection of the footwork is a great steppingstone towards more complex 3-Dimensional Motions.

Introduction

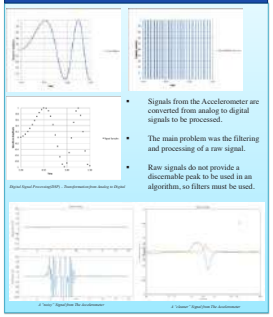

- Signals from the Accelerometer are converted from analog to digital signals to be processed.
- The main problem was the filtering and processing of a raw signal.
- Raw signals do not provide a discernable peak to be used in an algorithm, so filters must be used.

Materials and Methods

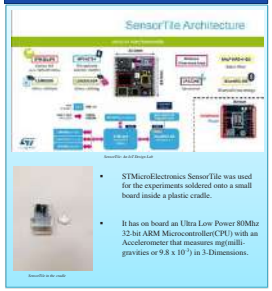

- STMicroElectronics SensorTile was used for the experiments soldered onto a small board inside a plastic cradle.
- It has on board an Ultra Low Power 80Mhz 32-bit ARM Microcontroller(CPU) with an Accelerometer that measures mg(milli-gravities or 9.8 x 10^{-3}) in 3-Dimensions.

- A 10 x 10 cm square was drawn on a piece of paper with the SensorTile following the path.
- The State-Machine method was used when designing the algorithm with 4 states total.

  1) SensorTile moving up (positive Y).

  2) SensorTile moving left (negative X).

  3) SensorTile moving down (negative Y).

  4) SensorTile moving right (positive X).

- The Values of The Peaks Were Recorded Using Output From the SensorTile Into A Matplotlib Python Script Before the Resonance Frequency For High Pass Filter Is Adjusted.
- Data of the measurements from the accelerometer in displacement(millimeters) were recorded and then compared to the actual measurement to check for the percent error, where:

  (Actual – Measured) / Actual X 100 = Percent Error

Path	Trial 1	Trial 2	Trial 3
Up	75%	90%	60%
Left	40%	25%	60%
Down	10%	10%	5%
Right	50%	30%	50%

Path	Trial 1	Trial 2	Trial 3
Up	77%	67%	70%
Left	86%	92%	91%
Down	89%	94%	86%
Right	63%	60%	60%

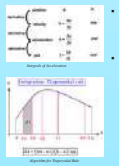

- Trapezoidal integration is implemented into the algorithm to find displacement, which was the measurement used for the experiments.
- Low pass filter (anti-aliasing) filter is initial applied to the raw acceleration signal, then a high pass filter is applied to each successive integration.

- The resonance frequency for the High-Pass filter is changed from 0.3 to 0.8 to fine tune the signal for more desirable results. The higher frequencies are attenuated for lower ones creating more consistent, but large, errors that are more manageable and predictable.

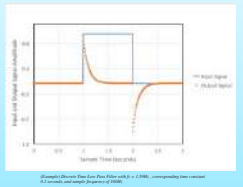

Results

- The proper motion of a square was recognized, when the resonance frequency of the High-Pass Filter was adjusted to give more consistent but smaller values from the accelerometer.
- The LED on-board of the SensorTile was used to indicate the successful recognition of each state.

Conclusion

- The development of the square motion state-machine demonstrates that proper signal processing is required to yield desired results. The complexity of the algorithm and innovative solutions reach a limit, when confronted with the reality of unfettered signals. Therefore, a well-designed approach to processing the signals could lead to optimal results. These conclusions apply only to 2-dimensional motion. 3-dimensional motion will most likely lead to more complexities, including the mapping of motions that are inclusive to Judo.

Future Works

- A new technology coming out of Dr. Kaiser's lab is embedded machine learning. Embedded machine learning is compact and can fit inside IoT device's firmware to allow more flexibility.
- Embedded ML would make this project easier, and would allow new technologies such as Machine Learning built into security cameras to detect potential threats.

Acknowledgments

- (NSF) National Science Foundation
- UCLA Samueli School of Engineering and Applied Sciences
- (SURP) Summer Undergraduate Research Program
- (WHI) Wireless Health Institute
- (MESA) El Camino College Mathematics, Engineering, and Science Achievement
- (TSSRP) Transfer Student Summer Research Program

LAB NAME

Terahertz Devices and Intersubband Nanostructures Laboratory

FACULTY ADVISOR

Professor Benjamin Williams

GRADUATE STUDENT DAILY LAB SUPERVISOR

Anthony Kim

DEPARTMENT

Electrical and Computer Engineering

Cindy Chang

Electrical Engineering

Second Year

UCLA

Analyzing and Quantifying Laser Beam Quality Using the Knife Edge Technique to Calculate the M^2 Factor

A laser's beam quality is a critical parameter in the performance of the laser in the laboratory or for industrial use. Describing the beam quality entails measuring the beam's spot size, a fundamental problem in laser diagnostics as laser beams are often irregular in shape. This is due to the various modes in a laser beam. The ideal Gaussian beam consists of the fundamental lowest-order TEM00 mode and has an irradiance beam profile described by a Gaussian function. We demonstrate a beam quality factor measurement of a terahertz quantum-cascade vertical external cavity surface-emitting laser (QC-VECSEL). The external cavity ideally allows for lasing at the fundamental Gaussian mode. Using a knife-edge measurement scheme, the M^2 factor can be extracted, which describes the extent to which the beam is diffraction limited.

The knife edge technique uses a converging lens to focus on the beam and makes a series of stepped measurements with a knife-edge in two different transverse directions at and around the lens's focus where the beam radius is minimized. This allows the calculation of the beam's spot size, the radius of the beam containing the majority of the power, by measuring the transmitted power with the shift of the knife in the transverse directions. By analyzing the behavior of the beam radius across the optic axis, the divergence of the beam is characterized.

Analyzing and Quantifying Laser Beam Quality Using the Knife Edge Technique to Calculate the M^2 Factor

Cindy Chang, Anthony Kim, and Professor Benjamin Williams

Introduction

A laser beam is created by photons bouncing between two mirrors. The longitudinal mode determines the frequency, wavelength, and thus color of the beam. The transverse modes are described by the distribution of the irradiance along the radial direction. An ideal laser beam only consists of the fundamental lowest-order TEM_{00} mode and has an irradiance beam profile described by a Gaussian function; however, real lasers are not ideal and typically oscillate in the lowest and possibly higher-order modes. To quantify the beam quality of a laser, the knife edge technique takes the waist measurements from stepping a knife incrementally through a beam. The MATLAB curve fitting calculates the M^2 factor in the transverse directions.

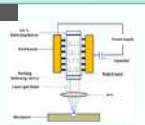

Figure 1. Diagram of the various main parts used in laser beam machining

Figure 2. Various TEM modes described by irradiance profile

Apparatus

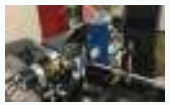

Figure 3. Experimental laser setup consisting of the laser, mirrors, lenses, motor, and the detector

Figure 4. The knife edge used to take stepped measurements

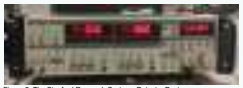

Figure 5. The Stanford Research Systems Detector Device

Terahertz Laser

Terahertz laser or far-infrared laser is a laser with an output wavelength in the far infrared, terahertz frequency band of the electromagnetic spectrum between 30-1000 μm. The laser used in this experiment is the quantum-cascade (QC) vertical-external-cavity surface-emitting-laser (VECSEL). The metasurface acts as an amplifying mirror in the external cavity allowing for an increased beam quality. The experiment's specific laser operates with 1.7 mW average power, pulsed mode, 10% duty cycle at 3.44 THz, 77K operating temperature.

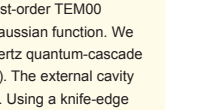

Figure 6. Irradiance profile of terahertz laser

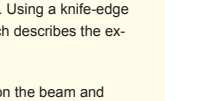

Figure 7. Diagram of terahertz laser

Future Work

The small M^2 values were most likely due to diffraction effects from the experimental set up and the knife edge effects. Several mirrors were used to reflect the beam before detecting the irradiance. Altering the experimental set up to limit these diffraction effects in future work will make the experiment and results more accurate.

The experimental setup also had to take into account that while the x and y movements were motorized, the z steps had to be done manually, significantly slowing down the data acquisition process. Using a motor to turn the z position would aid in future M^2 calculations.

Additionally, making the labview programmatically calibrate the start and final z positions will make the experiment notably more efficient.

Figure 8. An Irradiance vs Distance graph obtained during data acquisition

$$w_x^2(z) = w_{0x}^2\left[1+\left(\frac{z-z_{0x}}{z_{Rx}}\right)^2\right]$$

$$z_{0x} = z\,offset$$

$$z_{Rx} = \frac{\pi w_{0x}^2}{\lambda}$$

$$w_x^2(z) = w_{0x}^2 + M_x^4\left(\frac{\lambda}{\pi w_{0x}}\right)(z-z_{0x})^2$$

Figure 9. The equations used to curve fit the x waist measurements. The same were used for the y measurements.

Methods

With the labview program, the knife edge makes stepped movements in the transverse directions, taking and storing the detector's irradiance measurements in a textfile along with the x, y, and z positions of the knife. The apparatus holding the knife is then moved to a different location along the z axis. The program pauses until the user indicates that the knife is in position for another set of measurements and the program loops again for the transverse directions in the new z position.

To ensure the program made at least five measurements within one Rayleigh length and at least five outside, the z measurements spanned several millimeters with the step size determined from the Rayleigh length.

The error function was fitted to wash out drastic effects of diffraction. The 10-90% criteria for the beam waist was then used to determine waist measurements. This 10-90% criteria was chosen because of the clip levels rationalized using variances in the transverse directions[3]. It defined the waist size as the width where 10-90% of the total irradiance was measured. Curve fitting was then used to find the equation of the hyperbola that most accurately described our experimental data. This provided the value of beam waist constant, w_0, which was then used in our M^2 calculations for the transverse directions.

Results

Figure 10. Waist Size vs Z Position for X

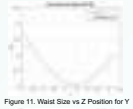

Figure 11. Waist Size vs Z Position for Y

Figure 12. Irradiance vs X position at the 5mm z position

The beam waist for the x and y directions were 0.17 mm and 0.20 mm respectively, as shown by Figures 10 and 11. The M_x^2 and M_y^2 values were calculated as 1.12 and .8612 respectively. The obtained value being under unity implies that there were errors in the measurement. This discrepancy was most likely due to diffraction effects during the knife-edge measurements.

Optical responses involved in the diffraction at metal edges are dependent on the laser's polarization[4]. This laser used was horizontally linearly polarized, resulting in different diffraction behaviors between the two transverse directions. Orienting the knife at a 45 degree angle to the polarization may have suppressed these differences.

Figure 12 shows these effects in the integrated intensity data before the fitting. The small peaks in the plot indicate disturbances in the optical alignment due to the knife-edge diffraction. This will ultimately influence our final results.

References

[1] Siegman, A. E. "Defining, measuring, and optimizing laser beam quality." Proc. SPIE 1868, *Laser Resonators and Coherent Optics: Modeling, Technology, and Applications*, 13 August 1993.

[2] Siegman, A. E. "How to (Maybe) Measure Laser Beam Quality." *DPSS (Diode Pumped Solid State) Lasers: Applications and Issues*, 1998.

[3] Siegman, A.E., et al. "Choice of Clip Levels for Beam Width Measurements Using Knife-Edge Techniques." *IEEE Journal of Quantum Electronics*, vol. 27, no. 4, 1991, pp. 1098–1104.

[4] Suzuki, Kenta, et al. "Spatio-Temporal Imaging of Terahertz Electric-Field Vectors: Observation of Polarization-Dependent Knife-Edge Diffraction." *Applied Physics Express*, vol. 12, no. 5, 2019, p. 052015., doi:10.7567/1882-0786/ab12fc.

We would like to thank the National Science Foundation for providing funding for our undergraduate research. We would also like to extend our thanks to the UCLA Electrical Engineering Fast Track to Success Program and UCLA Samueli Engineering SURP for its continued and valued support in research and academic studies.

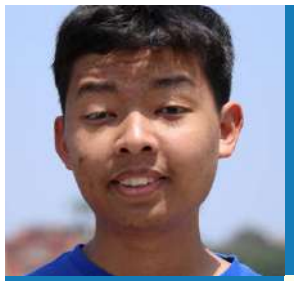

LAB NAME
UCLA Visual Machines Group Laboratory

FACULTY ADVISOR
Professor Achuta Kadambi

GRADUATE STUDENT DAILY LAB SUPERVISOR
Guangyuan Zhao

DEPARTMENT
Electrical and Computer Engineering

Brian Chap

Electrical Engineering

First Year

UCLA

Implementing Kinematic Prediction via Physics-Guided Neural Networks

Physics-guided neural networks (PGNNs) are crucial for modeling resistive behaviors in real- life scenarios ranging from vehicle tracking to aerial trajectories. In prior papers, bounding box construction for videos would entail construction for every individual frame, hindering progress in terms of speed-up without significant computational power. This paper aims to bridge the divide between inage and video object detection, utilizing kinematic priors to predict the motion of subjects via the incorporation of affine transformations and per- spective consideration (horizon, side-to-side, overhead, etc.). Approaches based on optical flow algorithms and tubelet architectures are considered, and blended with physical mod- ules to harness spatiotemporal coherence among individual frames. PyTorch 1.0 acts as the framework for code development, and all code is expected to be open-source for future development.

Implementing Kinematic Prediction via Physics-Guided Neural Networks

Brian Chap, Lucas He, Irfan Syed
Guangyuan Zhao, Achuta Kadambi
Department of Electrical and Computer Engineering, UCLA

Using Physics-Based Machine Learning to Track Objects

Physics-guided neural networks (PGNNs) are crucial for modeling resistive behaviors in real life scenarios ranging from vehicle tracking to aerial trajectories. In prior papers, bounding box construction for videos would entail construction for every individual frame, hindering progress in terms of speed without significant computational power. This paper aims to bridge the divide between image and video object detection, utilizing kinematic priors to predict the motion of subjects via the incorporation of affine transformations and perspective consideration (horizon, side-to-side, overhead, etc.). Approaches based on optical flow algorithms and tubelet architectures are considered and blended with physical modules to harness spatiotemporal coherence among individual frames. PyTorch 1.0 acts as the framework for code development and all code is expected to be open-source for future development.

Regional Convolutional Neural Networks

Figure 1 : Improvements such as clearer annotations and bounding box representations were made on a Faster R-CNN framework with 20 different classifications of objects. The physics model resulted from this framework of Faster R-CNN.

Dataset

Applications of physics-based calculations on the Faster R-CNN framework were tested on a self-made dataset of videos that captured optimal scenarios, including drops, tosses, and object sliding on surfaces to model the effects of gravity, resistance, and object motion. The added complexity of object occlusion was captured for the purpose of modeling realistic difficulties in object detection and motion prediction.

Physics-Based Model

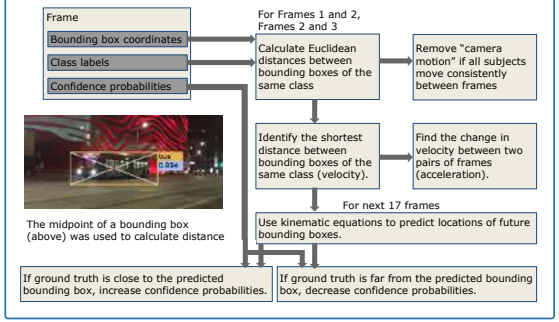

The midpoint of a bounding box (above) was used to calculate distance

Future Plans

The proposed physics model performs with high confidence values in the ideal scenarios created within the dataset. Expectations for future improvements include higher efficiency rates, faster processing rates, greater accuracy between multiple objects, and more accurate predictions for accounted complexities such as occlusions, lighting, and camera motion.

Limitations of current model:

Inability to account for changing acceleration
Inability to predict object motion with occlusions
Prediction model accounts for only 2D object transformations.
Unidentified objects lack physics-based machine learning

Applications:

Self-Driving	Defense Industry
Autonomous Drones	Movement Prediction

Preliminary Results


Figure 4: Bottle detection without physics-based learning (left) and with physics-based learning (right)


Figure 5: Multiple object detection without physics-based learning (left) and with physics-based learning (right)

The physics-based model results indicate significant increases in the accuracy of the model when compared with simply the Faster R-CNN framework. Faster R-CNN with physics-based machine learning increases the confidence of object detection and removes classification errors for objects.

References

Saha, Sumit. A Comprehensive Guide to Convolutional Neural Networks — the ELI5 Way. *Towards Data Science*, (2018).

Lei, F.-F. et al. Detection and Segmentation. *Stanford University*, (2017).

Girshick, R. Fast R-CNN. CoRR 1504.08083 (2015).

Girshick, R., et al. Rich feature hierarchies for accurate object detection and semantic segmentation. CoRR 1311.2524 (2013).

Ren, S., et al. Faster R-CNN: Towards Real-Time Object Detection with Region Proposal Networks. CoRR 1506.01497 (2015).

Redmon, J., et al. You Only Look Once: Unified, Real-Time Object Detection. CoRR 1506.02640 (2015).

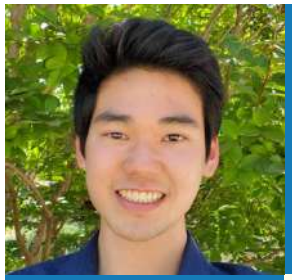

LAB NAME
Networked and Embedded Systems Laboratory

FACULTY ADVISOR
Professor Mani Srivastava

GRADUATE STUDENT DAILY LAB SUPERVISOR
Dr. Luis Garcia

DEPARTMENT
Electrical and Computer Engineering

Sean Dao

Computer Science

Third Year

El Camino College

Environmental Detection Using Mobile Sensors

Machine learning has made significant strides in enhancing human situational awareness with respect to recollection. In order to improve this cognitive ability, it is necessary to have a baseline understanding of the environment, which can also provide context to particular applications. Although localization of a human combined with background knowledge of an area (e.g., having a map of a place) can provide some intrinsic understanding of an environment, there are limitations for both components. Typically, localization in outdoor settings relies on GPS, while indoor localization is dependent on existing infrastructure. In addition, it is neither scalable nor generalizable to rely on background information of an area for exploring new environments. In this work, we aim to provide a semantic understanding of human movement through different spaces using a mobile phone attached to the subject. In particular, we simplify the problem by detecting room-to-room movement instead of fine-grained localization. We further show that detecting room-to-room movement can be implemented using ubiquitous phone sensors that provide a less invasive means of interaction compared to that of a camera. Knowing when a user traverses from one room to another can provide a significant amount of information to make inferences about a specific location. These inferences can then be applied to a variety of applications, such as correlating environment with episodic brain activity.

Environmental Detection Using Mobile Sensors

Tyler Kaplan, Sean Dao, Mani Srivastava, Luis Garcia, Joseph Noor

UCLA Wireless Health Institute

Networked and Embedded Systems Laboratory (NESL)

Motivation

- IoT and Ubiquitous computing has led to the advancement of medical technology and innovation
- Detecting room to room movement can correlate environment to brain activity and recollection
- Can be implemented on nearly any phone and is much more private than a camera

Background

- Localization has been done in outside environments through the use of GPS signals
- Indoor positioning systems rely on pedometers, speedometers, and predetermined maps
- Using sound and its properties may be the key to pinpointing someone's position regardless of location

Methods

- Recorded 800, three-second audio clips at 4 different locations
- Sample Set A – 400 samples with a High-Frequency Tone (HFT) of 22 kHZ played from an external source
- Sample Set B – 400 samples without HFT
- Extracted audio features from the data to train supervised machine learning classification model based on a Random Forest algorithm

Phone Lanyard

Fig 1) mobile device attached to plastic lanyard for capturing data

Results

Bruin Walk

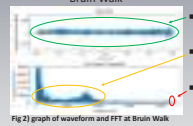

Fig 2) graph of waveform and FFT at Bruin Walk

- the overall loudness is greater in this outside area
- there is also a plethora of frequencies and noises occurring
- 22 kHZ can barely be heard, hardly any reverberations

Library

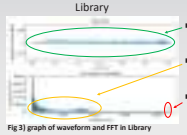

Fig 3) graph of waveform and FFT in Library

- the overall loudness is much quieter compared to outside
- however, there is still numerous sounds occurring
- 22 kHZ is louder; the area is quite large, but there is still some reverberations

Hallway

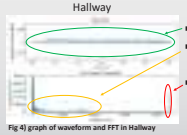

Fig 4) graph of waveform and FFT in Hallway

- the hallway is very quite
- there isn't that much ambient noise either
- however, the 22 kHZ is the loudest here; the most reverberations of any location

Without HFT Model – Results

	Bruin Walk	Student Store	Hallway	Library	NESL
Precision	100	90	100	96	100
Recall	100	100	90	96	100
Overall Accuracy			97 %		

Fig 5) specific results of Random Forest classifier model based on data without HFT

Conclusion and Future Works

- Utilize a variety of mobile sensors with time synchronization to dramatically increase accuracy of room detection
- Implement a neural network to learn distinguishing factors as much more data is collected
- Train better models based on better locations, more samples, and more representative audio features

References

- Lu, Hong, et al. "SoundSense: scalable sound sensing for people-centric applications on mobile phones." Proceedings of the 7th international conference on Mobile systems, applications, and services. ACM, 2009.
- Mao, Wenguang, Mei Wang, and Lili Qiu. "Mobile Imaging Using Acoustic Signals." GetMobile: Mobile Computing and Communications 22.4 (2019): 35-38.
- Shih, Oliver, and Anthony Rowe. "Can a phone hear the shape of a room?." Proceedings of the 18th International Conference on Information Processing in Sensor Networks. ACM, 2019.

LAB NAME

Interconnected & Integrated Bioelectronics Laboratory

FACULTY ADVISOR

Professor Sam Emaminejad

GRADUATE STUDENT DAILY LAB SUPERVISOR

Chris Yeung

DEPARTMENT

Electrical and Computer Engineering

Gustavo Diaz

Computer Science and Engineering

Fourth Year

UCLA

Programable Transdermal Drug Delivery with a Iontophoretically Enhanced Microneedle System

Transdermal drug delivery (TDD) has sparked great interest within the medical field due to its painlessness, ease of use, and reduced risk of infection in comparison to conventional methods such as hypodermic needle injection. Additionally, the growth of the wearable health monitoring device market has spurred the demand for programmable closed-loop personal health systems that can deliver drug treatments in response to physiological changes. To further develop TDD and programmable delivery, investigation of new techniques are required. To this end, we combined hollow microneedle-arrays (MNA) and iontophoresis (ITP) in an effort towards achieving programmable delivery. The MNA serves the purpose of creating tiny pores in the stratum corneum that act as drug delivery channels. In conjunction, ITP utilizes a small electric field in order to drive ionized drug molecules into the skin using electrostatic forces. Additionally, ITP allows for fine control over the delivery rate by adjusting the current strength. We tested the ITP-enhanced MNA by delivering fluorescent-dyed insulin into porcine skin samples at various time intervals and currents. The skin was then analysed using confocal laser scanning microscopy (CLSM) to determine the penetration depth of the insulin. CLSM imaging and fluorescent intensity analysis revealed that the ITP-enhanced MNA have a significantly greater penetration depth than individually applying either one. The ITP-enhanced MNA system proved to be an effective delivery strategy for larger molecule drugs in a small form factor and with easily-programmable control. Further testing of ITP-enhanced MNA with larger molecules could expand the range of suitable drugs for TDD applications.

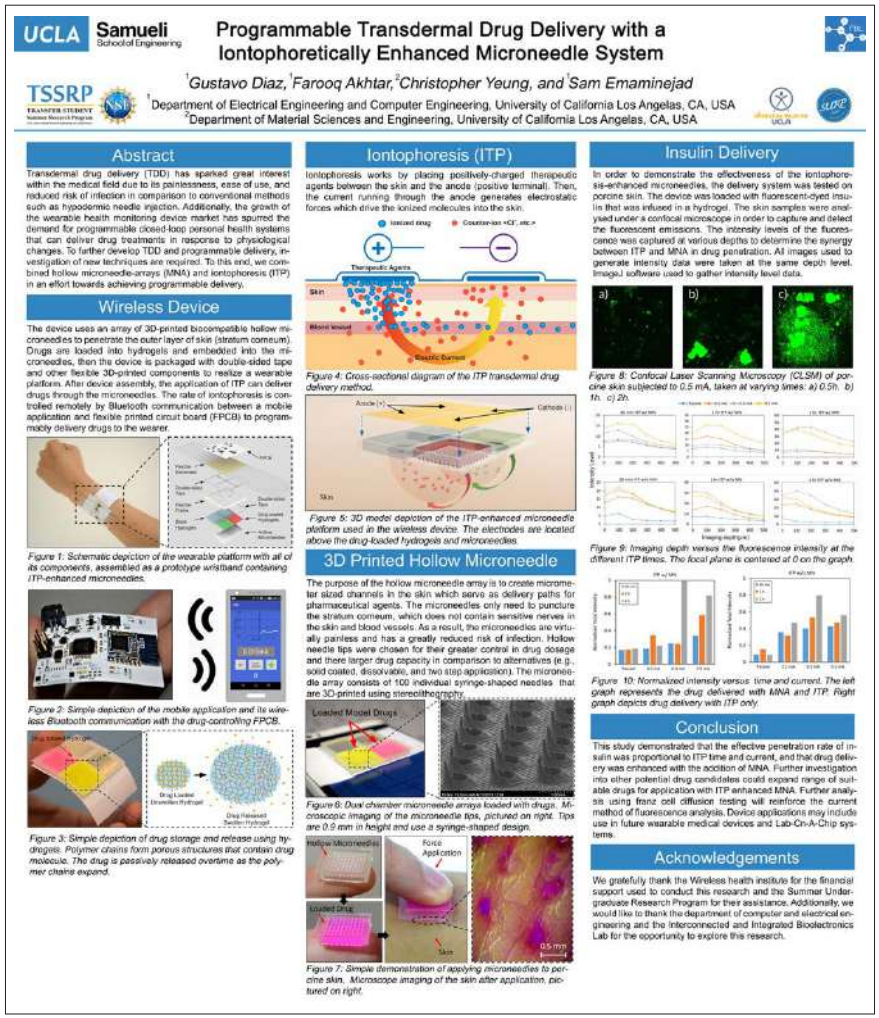

UCLA Samueli School of Engineering

Programmable Transdermal Drug Delivery with a Iontophoretically Enhanced Microneedle System

TSSRP Transfer Student Summer Research Program

[1]Gustavo Diaz, [1]Farooq Akhtar, [2]Christopher Yeung, and [1]Sam Emaminejad

[1]Department of Electrical Engineering and Computer Engineering, University of California Los Angeles, CA, USA

[2]Department of Material Sciences and Engineering, University of California Los Angeles, CA, USA

Abstract

Transdermal drug delivery (TDD) has sparked great interest within the medical field due to its painlessness, ease of use, and reduced risk of infection in comparison to conventional methods such as hypodermic needle injection. Additionally, the growth of the wearable health monitoring device market has spurred the demand for programmable closed-loop personal health systems that can deliver drug treatments in response to physiological changes. To further develop TDD and programmable delivery, investigation of new techniques are required. To this end, we combined hollow microneedle-arrays (MNA) and iontophoresis (ITP) in an effort towards achieving programmable delivery.

Wireless Device

The device uses an array of 3D-printed biocompatible hollow microneedles to penetrate the outer layer of skin (stratum corneum). Drugs are loaded into hydrogels and embedded into the microneedles, then the device is packaged with double-sided tape and other flexible 3D-printed components to realize a wearable platform. After device assembly, the application of ITP can deliver drugs through the microneedles. The rate of iontophoresis is controlled remotely by Bluetooth communication between a mobile application and flexible printed circuit board (FPCB) to programmably delivery drugs to the wearer.

Figure 1: Schematic depiction of the wearable platform with all of its components, assembled as a prototype wristband containing ITP-enhanced microneedles.

Figure 2: Simple depiction of the mobile application and its wireless Bluetooth communication with the drug-controlling FPCB.

Figure 3: Simple depiction of drug storage and release using hydrogels. Polymer chains form porous structures that contain drug molecule. The drug is passively released overtime as the polymer chains expand.

Iontophoresis (ITP)

Iontophoresis works by placing positively-charged therapeutic agents between the skin and the anode (positive terminal). Then, the current running through the anode generates electrostatic forces which drive the ionized molecules into the skin.

Figure 4: Cross-sectional diagram of the ITP transdermal drug delivery method.

Figure 5: 3D model depiction of the ITP-enhanced microneedle platform used in the wireless device. The electrodes are located above the drug-loaded hydrogels and microneedles.

3D Printed Hollow Microneedle

The purpose of the hollow microneedle array is to create micrometer sized channels in the skin which serve as delivery paths for pharmaceutical agents. The microneedles only need to puncture the stratum corneum, which does not contain sensitive nerves in the skin and blood vessels. As a result, the microneedles are virtually painless and has a greatly reduced risk of infection. Hollow needle tips were chosen for their greater control in drug dosage and there larger drug capacity in comparison to alternatives (e.g., solid coated, dissolvable, and two step application). The microneedle array consists of 100 individual syringe-shaped needles that are 3D-printed using stereolithography.

Figure 6: Dual chamber microneedle arrays loaded with drugs. Microscopic imaging of the microneedle tips, pictured on right. Tips are 0.9 mm in height and use a syringe-shaped design.

Figure 7: Simple demonstration of applying microneedles to porcine skin. Microscope imaging of the skin after application, pictured on right.

Insulin Delivery

In order to demonstrate the effectiveness of the iontophoresis-enhanced microneedles, the delivery system was tested on porcine skin. The device was loaded with fluorescent-dyed insulin that was infused in a hydrogel. The skin samples were analysed under a confocal microscope in order to capture and detect the fluorescent emissions. The intensity levels of the fluorescence was captured at various depths to determine the synergy between ITP and MNA in drug penetration. All images used to generate intensity data were taken at the same depth level. ImageJ software used to gather intensity level data.

Figure 8: Confocal Laser Scanning Microscopy (CLSM) of porcine skin subjected to 0.5 mA, taken at varying times: a) 0.5h. b) 1h. c) 2h.

Figure 9: Imaging depth verses the fluorescence intensity at the different ITP times. The focal plane is centered at 0 on the graph.

Figure 10: Normalized intensity versus time and current. The left graph represents the drug delivered with MNA and ITP. Right graph depicts drug delivery with ITP only.

Conclusion

This study demonstrated that the effective penetration rate of insulin was proportional to ITP time and current, and that drug delivery was enhanced with the addition of MNA. Further investigation into other potential drug candidates could expand range of suitable drugs for application with ITP enhanced MNA. Further analysis using franz cell diffusion testing will reinforce the current method of fluorescence analysis. Device applications may include use in future wearable medical devices and Lab-On-A-Chip systems.

Acknowledgements

We gratefully thank the Wireless health institute for the financial support used to conduct this research and the Summer Undergraduate Research Program for their assistance. Additionally, we would like to thank the department of computer and electrical engineering and the Interconnected and Integrated Bioelectronics Lab for the opportunity to explore this research.

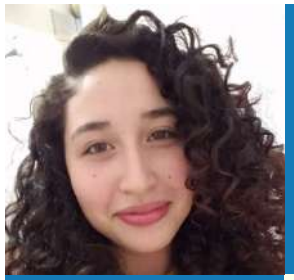

LAB NAME

Laboratory for the Chemistry of Construction Materials

FACULTY ADVISOR

Professor Gaurav Sant

GRADUATE STUDENT DAILY LAB SUPERVISOR

Steven Bustillos

DEPARTMENT

Civil and Environmental Engineering

Alyssa Eckley

Civil and Environmental Engineering

Third Year

El Camino College

Competitive Cation Exchange Behavior of Simulated Wastewater Streams Using Zeolites and Cation Exchange Resins for CO_2 Mineralization

Sodium based zeolites and resins, often used for gas adsorption and water softening processes, are proposed to be used to induce a pH shift required for CO_2 mineralization using a CO_2- rich stream. These materials initiate a Na^+ / H^+ exchange, which increases alkalinity, forming carbonate ions (CO_3^{2-}) for mineralization. Produced water, a waste stream rich in calcium and sodium ions, is proposed for mineralization (to produce calcium carbonate) and for the regeneration of materials. However, produced water streams also contain other polyvalent cations that could potentially compete with Na for exchange sites and inhibit regeneration. This research explores the competitive exchange of common ions found in produced water on various zeolites and exchange resins that may inhibit regeneration capacities. Ion exchange capacities and kinetics in single component systems using synthetic zeolites 13X and 4A, along with organic resins TP-207 and TP-260 were studied using calcium, magnesium and iron ions for exchange. Various concentrations of ions in solution over time were analyzed through inductively coupled plasma optical emission spectroscopy (ICP-OES). Dual component exchange capacities were further examined to determine competitive exchange behavior using fixed sodium concentration and varying calcium, magnesium and iron concentrations to simulate the concentrations within produced water streams.

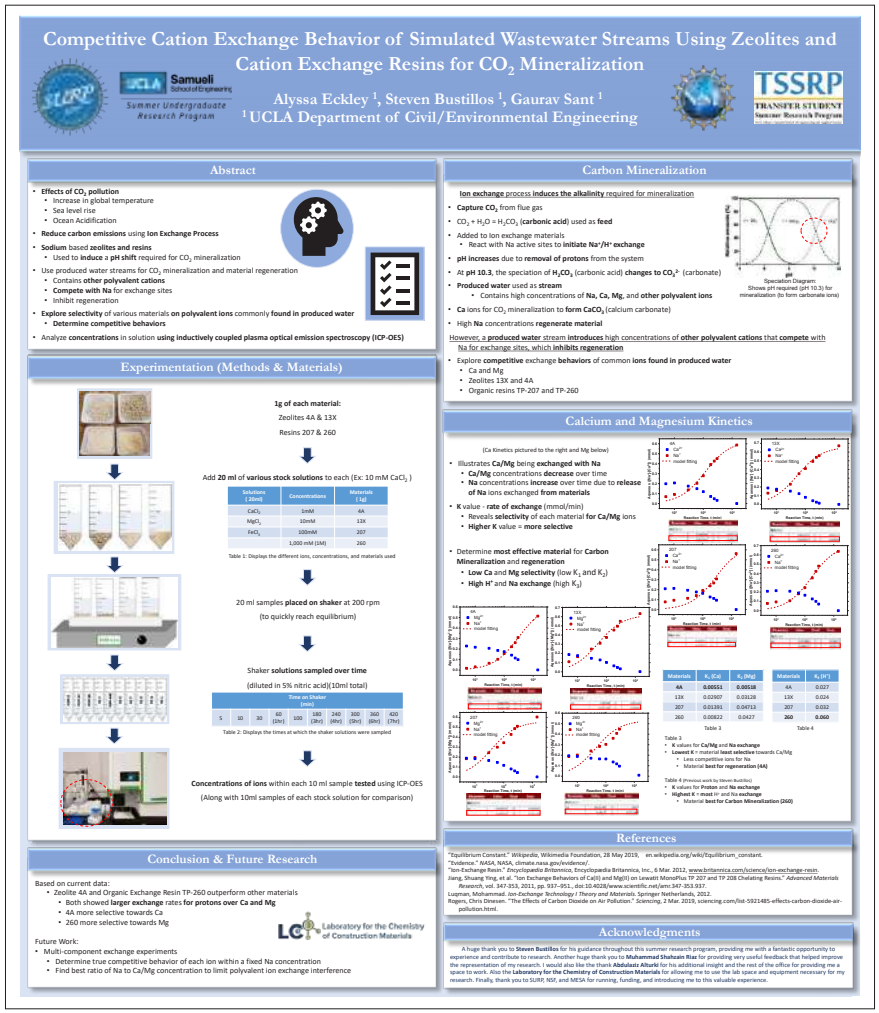

LAB NAME
Visual Machine Learning Group

FACULTY ADVISOR
Professor Achuta Kadambi

GRADUATE STUDENT DAILY LAB SUPERVISOR
Guanyang Zhou

DEPARTMENT
Electrical and Computer Engineering

Lucas He

Electrical Engineering

First Year

UCLA

Physics-Based Object Temporal Localization Via Video Segmentation

The field of object detection has seen much advancements over the past years, especially in videos with the implementation and improvements of architectures such as Optical Flow, Tubelets, and Temporal Action Localization. However, such methods are still limited in their speed, efficiency, and accuracy, with the current fastest method running at an average of two frames per second. Thus, we propose the usage of the Physics Guided Neural Network (PGNN) to aid this task. By specifically tailoring this to detection of cars we hope to produce a naive form of detection that can track and solve transformations (i.e. scale, sheer, and direction) of cars as they travel down a road. Using segmentation, we would then be able to establish instances of the cars as apply a physics model and determine each object's trajectory based on the previous frames of the object's path. The application of the physics model will serve to reduce the computational requirements of previous methods and allow for a more accurate prediction of an object's temporal location.

Implementing Kinematic Prediction via Physics-Guided Neural Networks

Brian Chap, Lucas He, Irfan Syed
Guangyuan Zhao, Achuta Kadambi
Department of Electrical and Computer Engineering, UCLA

Using Physics-Based Machine Learning to Track Objects

Physics-guided neural networks (PGNNs) are crucial for modeling resistive behaviors in real life scenarios ranging from vehicle tracking to aerial trajectories. In prior papers, bounding box construction for videos would entail construction for every individual frame, hindering progress in terms of speed without significant computational power. This paper aims to bridge the divide between image and video object detection, utilizing kinematic priors to predict the motion of subjects via the incorporation of affine transformations and perspective consideration (horizon, side-to-side, overhead, etc.). Approaches based on optical flow algorithms and tubelet architectures are considered and blended with physical modules to harness spatiotemporal coherence among individual frames. PyTorch 1.0 acts as the framework for code development and all code is expected to be open-source for future development.

Regional Convolutional Neural Networks

Figure 1 : Improvements such as clearer annotations and bounding box representations were made on a Faster R-CNN framework with 20 different classifications of objects. The physics model resulted from this framework of Faster R-CNN.

Dataset

Applications of physics-based calculations on the Faster R-CNN framework were tested on a self-made dataset of videos that captured optimal scenarios, including drops, tosses, and object sliding on surfaces to model the effects of gravity, resistance, and object motion. The added complexity of object occlusion was captured for the purpose of modeling realistic difficulties in object detection and motion prediction.

Physics-Based Model

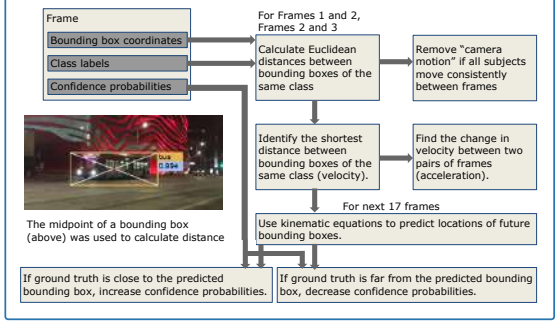

Future Plans

The proposed physics model performs with high confidence values in the ideal scenarios created within the dataset. Expectations for future improvements include higher efficiency rates, faster processing rates, greater accuracy between multiple objects, and more accurate predictions for accounted complexities such as occlusions, lighting, and camera motion.

Limitations of current model:

Inability to account for changing acceleration
Inability to predict object motion with occlusions
Prediction model accounts for only 2D object transformations.
Unidentified objects lack physics-based machine learning

Applications:

Self-Driving	Defense Industry
Autonomous Drones	Movement Prediction

Preliminary Results

Figure 4: Bottle detection without physics-based learning (left) and with physics-based learning (right)

Figure 5: Multiple object detection without physics-based learning (left) and with physics-based learning (right)

The physics-based model results indicate significant increases in the accuracy of the model when compared with simply the Faster R-CNN framework. Faster R-CNN with physics-based machine learning increases the confidence of object detection and removes classification errors for objects.

References

Saha, Sumit. A Comprehensive Guide to Convolutional Neural Networks — the ELI5 Way. *Towards Data Science*, (2018).

Lei, F.-F. et al. Detection and Segmentation. *Stanford University*, (2017).

Girshick, R. Fast R-CNN. CoRR 1504.08083 (2015).

Girshick, R., et al. Rich feature hierarchies for accurate object detection and semantic segmentation. CoRR 1311.2524 (2013).

Ren, S., et al. Faster R-CNN: Towards Real-Time Object Detection with Region Proposal Networks. CoRR 1506.01497 (2015).

Redmon, J., et al. You Only Look Once: Unified, Real-Time Object Detection. CoRR 1506.02640 (2015).

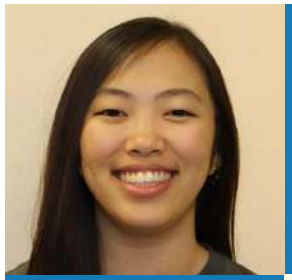

LAB NAME

Fang Lu Mesoscopic Optics and Quantum Electronics Laboratory

FACULTY ADVISOR

Professor Chee Wei Wong

GRADUATE STUDENT DAILY LAB SUPERVISOR

Dr. Wenting Wang

DEPARTMENT

Electrical and Computer Engineering

Tz-Wei Hung

Electrical Engineering

First Year

Pasadena City College

Ultrafast Real-Time Dynamics of Frequency Microcomb Transitions

Temporally stabilized optical solitons, also known as self-sustaining nonlinear pulses at a mid-infrared frequency, confined in a microcavity driven by a continuous-wave laser has attracted tremendous attention due to its fascinating spectral and temporal features and corresponding intriguing cavity dynamics. A real-time ultrafast oscilloscope characterization system demonstrates the dynamics in the microcavity with picosecond resolution and a 500 picosecond recording length over each frame. However, the recording length is limited by the sampling rate due to the restricted memory depth of the oscilloscope during data acquisition. To bypass this complication, time lens was used to stretch the timescale of the waveform without adding distortion or noise. After finding the optimum recording length and temporal resolution, a Kerr frequency comb is generated in the microresonator with a laser which is then sent through optical fibers to the oscilloscope to be studied. We were then able to record the mode-locking formation and the transitions between different soliton states during the formation process. The real-time observations of the ultrafast optical dynamics provides new physical insight for ultrafast phenomena that happens in the microcavity.

Ultrafast Real-Time Dynamics of Frequency Microcomb Transitions

Tz-Wei Hung, Wenting Wang, Xinghe Jiang, Chee Wei Wong

Department of Electrical and Computer Engineering

University of California - Los Angeles

Background

This research focuses on the mid-infrared part of the optical spectrum that encompasses visible light and infrared waves. Ultrafast optical dynamics such as a soliton, an undisturbed stable light waveform that sustains its pulse over time, happens at the nanosecond and picosecond scale. Studying its characteristics in a microresonator has immense significance to laser optics For the further development of optical technology and telecommunication.

Aim

Goal: Observe and record all the characteristics of different transitioning states a dissipative Kerr comb soliton in microcavities produce in real time.

Problem: Conventional oscilloscopes can miss extremely fast rare events as they have limitations of both the spatial and temporal domain. This makes the oscilloscope insufficient to characterize ultrafast waveforms.

Solution: Time lens are used to slow down and extend the signal without adding distortion or noise. It magnifies the image dispersing it in time and uses the quadratic phase shift which stretches the temporal domain. The longer recording length allowed the waveform to be analyzed and recorded.

Kerr Frequency Comb

- A frequency comb is generated on an optical spectrum analyzer from a signal on the time domain that uses the Fourier transform in the cavity to the frequency domain creating an equidistant spectrum of pulses.

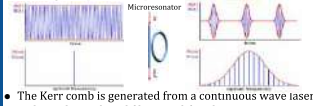

- The Kerr comb is generated from a continuous wave laser and an erbium-doped fiber amplifier that pumps a power of 35 dBm. That signal is then sent to the microcavity in the silicon chip that uses a Fourier transform to create the comb on a frequency and wavelength domain.

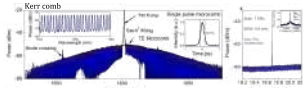

Time Lens Setup

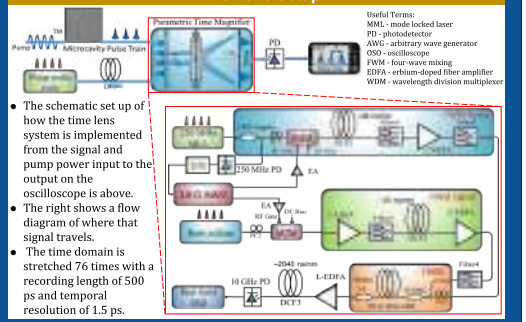

- The schematic set up of how the time lens system is implemented from the signal and pump power input to the output on the oscilloscope is above.
- The right shows a flow diagram of where that signal travels.
- The time domain is stretched 76 times with a recording length of 500 ps and temporal resolution of 1.5 ps.

Results

- The transmission used the voltage jumps to trigger the signal acquisition and transitions between different soliton states.
- The time lens increased the temporal resolution and abled the magnification of the pulse train to be studied.
- The oscilloscope received the signal and recorded the transition from high-noise to mode locking, 3 to 2 to 1 soliton, and 3 to 1 soliton transitions.

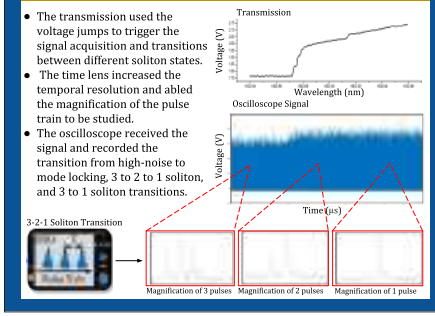

Conclusions and Future Works

- Observed new physical insight regarding ultrafast optical phenomena in the microcavity and observed the transitions between soliton states.
- Continue to study the dynamics and increase temporal resolution using different systems and methods to further the advancement in laser science, spectroscopy, precision measurements, and other optical physics fields.

Acknowledgements

Special thanks to Professor Chee Wei Wong for giving me this opportunity to work with his team and Dr. Wenting Wang for allowing me to be a part of such cutting edge advanced scientific research. Greatly appreciate the support of lab members, Xinghe Jiang, Jaime Flor, and Abhinav Vinod, who took the time to explain concepts. This would not be possible without the SURP program that lead to this incredible experience here at UCLA.

References

Godey, Cyril, et al. "Stability Analysis of the Spatiotemporal Lugiato-Lefever Model for Kerr Optical Frequency Combs in the Anomalous and Normal Dispersion Regimes." *Physical Review A*, vol. 89, no. 6, 2014, doi:10.1103/physreva.89.063814.

Huang, Shu-Wei, et al. "A Broadband Chip-Scale Optical Frequency Synthesizer at 2.7 × 10−16 Relative Uncertainty." *Science Advances*, vol. 2, no. 4, 22 Apr. 2016, doi:10.1126/sciadv.1501489.

Jalali, B., et al. "Silicon's Time Lens." *Nature Photonics*, vol. 3, no. 1, 2009, pp. 8–10., doi:10.1038/nphoton.2008.261.

Li, Bowen, et al. "Panoramic-Reconstruction Temporal Imaging for Seamless Measurements of Slowly-Evolved Femtosecond Pulse Dynamics." *Nature Communications*, vol. 8, no. 1, 2017, doi:10.1038/s41467-017-00093-7.

Stillman, Gregory E. "Optoelectronics." *Reference Data for Engineers*, 2002, doi:10.1016/b978-075067291-7/50023-6.

LAB NAME
Networkerd and Embedded Systems Laboratory

FACULTY ADVISOR
Professor Mani Srivastava

GRADUATE STUDENT DAILY LAB SUPERVISOR
Dr. Luis Garcia

DEPARTMENT
Electrical and Computer Engineering

Tyler Kaplan

Computer Science

Third Year

El Camino College

Environmental Detection Using Mobile Sensors

Machine learning has made significant strides in enhancing human situational awareness with respect to recollection. In order to improve this cognitive ability, it is necessary to have a baseline understanding of the environment, which can also provide context to particular applications. Although localization of a human combined with background knowledge of an area (e.g., having a map of a place) can provide some intrinsic understanding of an environment, there are limitations for both components. Typically, localization in outdoor settings relies on GPS, while indoor localization is dependent on existing infrastructure. In addition, it is neither scalable nor generalizable to rely on background information of an area for exploring new environments. In this work, we aim to provide a semantic understanding of human movement through different spaces using a mobile phone attached to the subject. In particular, we simplify the problem by detecting room-to-room movement instead of fine-grained localization. We further show that detecting room-to-room movement can be implemented using ubiquitous phone sensors that provide a less invasive means of interaction compared to that of a camera. Knowing when a user traverses from one room to another can provide a significant amount of information to make inferences about a specific location. These inferences can then be applied to a variety of applications, such as correlating environment with episodic brain activity.

UCLA Samueli School of Engineering — Summer Undergraduate Research Program

TSSRP

Environmental Detection Using Mobile Sensors

Tyler Kaplan, Sean Dao, Mani Srivastava, Luis Garcia, Joseph Noor

UCLA Wireless Health Institute

Networked and Embedded Systems Laboratory (NESL)

Motivation

- IoT and Ubiquitous computing has led to the advancement of medical technology and innovation
- Detecting room to room movement can correlate environment to brain activity and recollection
- Can be implemented on nearly any phone and is much more private than a camera

Background

- Localization has been done in outside environments through the use of GPS signals
- Indoor positioning systems rely on pedometers, speedometers, and predetermined maps
- Using sound and its properties may be the key to pinpointing someone's position regardless of location

Methods

- Recorded 800, three-second audio clips at 4 different locations
- Sample Set A – 400 samples with a High-Frequency Tone (HFT) of 22 kHZ played from an external source
- Sample Set B – 400 samples without HFT
- Extracted audio features from the data to train supervised machine learning classification model based on a Random Forest algorithm

Phone Lanyard

Fig 1) mobile device attached to plastic lanyard for capturing data

Results

Bruin Walk

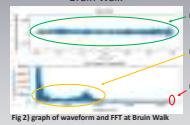

Fig 2) graph of waveform and FFT at Bruin Walk

- the overall loudness is greater in this outside area
- there is also a plethora of frequencies and noises occurring
- 22 kHZ can barely be heard, hardly any reverberations

Library

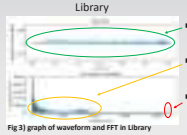

Fig 3) graph of waveform and FFT in Library

- the overall loudness is much quieter compared to outside
- however, there is still numerous sounds occurring
- 22 kHZ is louder; the area is quite large, but there is still some reverberations

Hallway

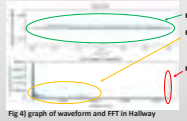

Fig 4) graph of waveform and FFT in Hallway

- the hallway is very quite
- there isn't that much ambient noise either
- however, the 22 kHZ is the loudest here; the most reverberations of any location

Without HFT Model – Results

	Bruin Walk	Student Store	Hallway	Library	NESL
Precision	100	90	100	96	100
Recall	100	100	90	96	100
Overall Accuracy			97 %		

Fig 5) specific results of Random Forest classifier model based on data without HFT

Conclusion and Future Works

- Utilize a variety of mobile sensors with time synchronization to dramatically increase accuracy of room detection
- Implement a neural network to learn distinguishing factors as much more data is collected
- Train better models based on better locations, more samples, and more representative audio features

References

- Lu, Hong, et al. "SoundSense: scalable sound sensing for people-centric applications on mobile phones." Proceedings of the 7th international conference on Mobile systems, applications, and services. ACM, 2009.
- Mao, Wenguang, Mei Wang, and Lili Qiu. "Mobile Imaging Using Acoustic Signals." GetMobile: Mobile Computing and Communications 22.4 (2019): 35-38.
- Shih, Oliver, and Anthony Rowe. "Can a phone hear the shape of a room?." Proceedings of the 18th International Conference on Information Processing in Sensor Networks. ACM, 2019.

printed by MegaPrint Inc. www.posteresession.com

LAB NAME

Laboratory for Embedded Machines and Ubiquitous Robots (LEMUR)

FACULTY ADVISOR

Professor Ankur Mehta

GRADUATE STUDENT DAILY LAB SUPERVISOR

Professor Ankur Mehta

DEPARTMENT

Electrical and Computer Engineering

Chelsea Lai

Electrical Engineering

Second Year

UCLA

Custom Printable Robotic Boats for Early STEM Education

Robotics engages students in multiple disciplines of engineering, which is increasingly important in our technology-based society. However, existing robotics kits are mostly geared toward middle- and high- school students and either cost hundreds or thousands of dollars or have limited hands-on design capabilities. This leaves customizable robotics unaffordable to many schools, as well as neglects to introduce robots to impressionable elementary-age children. Our project focused on concurrently addressing three concerns: cost, age group, and creative potential. We developed a modifiable template for an affordable robot that students design themselves, supporting a project-based learning approach, with the goal of inspiring interest in STEM in kindergartners.

Since most robotics kits are cars, we designed a robotic boat and a web-based app, which students use to create and steer the boat. One boat is made of a flat sheet of plastic folded into a 3D structure, with basic electronics propelling the vehicle, and costs under $40 total. In the app, powered by Robot Compiler technology, students change parameters on the boat to see the effect on the 2D printable template and 3D model of the finished boat. This focus on customization encourages iterative design and engages students firsthand in the engineering innovation process. Students have flexibility in designing their robots down to the component level, fostering a sense of ownership over their project and resulting in a more self-motivated learning experience.

Custom Printable Robotic Boats for Early STEM Education

Chelsea Lai, Shantinath Smyth, Dr. Ankur Mehta

Dept. of Electrical and Computer Engineering, University of California, Los Angeles

Introduction

Problems with Existing Robotics Kits

- Expensive
- Middle- and high-school age group
- Limited hands-on design

Our Solution

- Creating a design tool for low-cost foldable robotic boats

Educational Applications

- Students design, build, and redesign robotic boats
- Hands-on experience with cycle of scientific experimentation

Developing the Design Tool

Built prototypes of mechanically powered paddleboat design → Motorized boat and integrated electronics into design → Finalized boat template → Model 2D template and 3D structure on RoCo

Student Design Process

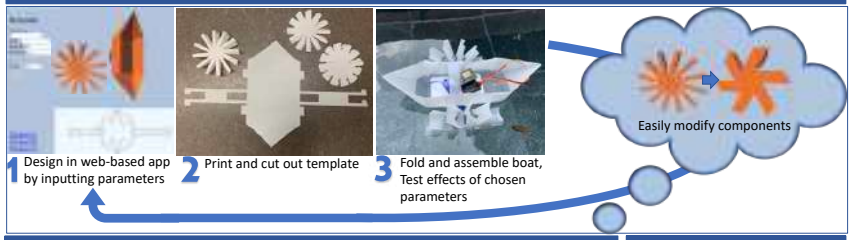

Results

- Iterative design process and customization allows for personalized products
- Encourages experimentation and hands-on learning approach
- Teaches gateway STEM skills and engineering/design process

Total cost: ~$30 (Retail), ~$15 (Bulk)

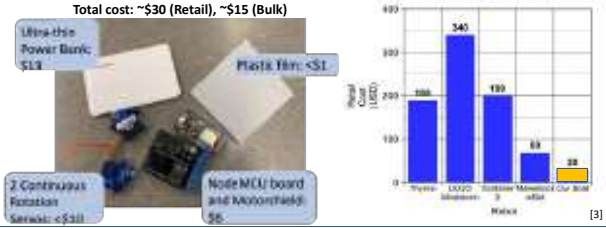

Acknowledgements

Summer Undergraduate Research Program

Fast Track to Success Program

LEMUR Lab, Dr. Ankur Mehta

Wireless Health Institute

References

[1] McLurkin, James, et al. "Using multi-robot systems for engineering education: Teaching and outreach with large numbers of an advanced, low-cost robot." IEEE transactions on education 56.1 (2012): 24-33.

[2] Blumenfeld, Phyllis C., et al. "Motivating project-based learning: Sustaining the doing, supporting the learning." Educational psychologist 26.3-4 (1991): 369-398.

[3] Rubenstein, Michael, et al. "AERobot: An affordable one-robot-per-student system for early robotics education." 2015 IEEE International Conference on Robotics and Automation (ICRA). IEEE, 2015.

[4] Mondada, Francesco, et al. "The e-puck, a robot designed for education in engineering." Proceedings of the 9th conference on autonomous robot systems and competitions. Vol. 1. No. CONF. IPCB: Instituto Politecnico de Castelo Branco, 2009.

[5] A.M. Mehta, J. DelPreto, B. Shaya, and D. Rus. "Cogeneration of Mechanical, Electrical, and Software Designs for Printable Robots from Structural Specifications". In: Intelligent Robots and Systems (IROS 2014), Chicago, IL, Sep 2014, pp. 2892-2897.

[6] Mehta, Ankur M., and Daniela Rus. "An end-to-end system for designing mechanical structures for print-and-fold robots." 2014 IEEE International Conference on Robotics and Automation (ICRA). IEEE, 2014.

LAB NAME

Neural Computation and Engineering Laboratory

FACULTY ADVISOR

Professor Jonathan Kao

GRADUATE STUDENT DAILY LAB SUPERVISOR

Professor Jonathan Kao

DEPARTMENT

Electrical and Computer Engineering

Michelle Lam

Computer Engineering

Third Year

UCLA

Studying changes of mind in decision-making

A decision is a commitment to an action after consideration of evidence and expected outcomes. The brain deliberates on available evidence to yield an action or decision. However, during cognition, we often change our minds; standard decision-making models do not fully explain why these changes of mind occur. The purpose of this study is to develop an experiment to study changes of mind, validating work by Resulaj and colleagues. It was hypothesized that noisy evidence, in the form of a random dot motion stimulus, is accumulated over time until it reaches a criterion level, or bound. An initial decision is made once this criterion is achieved. While the trials were conducted, subjects made decisions about a noisy visual stimulus, and then they indicated their choice of direction by moving a joystick according to the direction inferred. The brain then exploited further information that either reversed or reaffirmed the initial decision made. We conclude that this study supports Resulaj's findings and theory of post-initiation processing. This study is significant to understand decisions related to gambling, social selection, and probabilistic reasoning.

Studying changes of mind in decision-making

Michelle Lam[1], Alicia Mercado[2], Jonathan Kao[1]

[1]Department of Electrical and Computer Engineering, University of California – Los Angeles

[2]Department of Physical Sciences and Mathematics, Mount Saint Mary's University – Los Angeles

Ideas and Principles

Motivation

- A decision is a commitment to an action after consideration of evidence and expected outcomes.
- Standard decision-making models do not fully explain why changes of mind occur during the decision-making process.
- The purpose of this study is to develop an experiment to study changes of mind, validating work by Resulaj and colleagues.
- It was hypothesized that noisy evidence, in the form of a random dot motion stimulus, is accumulated over time until it reaches a criterion level, or bound.

Random Dot Motion Stimulus

- Random dot motions (RDM) are a classic stimulus used in psychophysical and physiological studies of motion processing.
- RDM occur in binary directions and can be modified to occur at different motion coherences.
  - Right v. Left
  - Up v. Down

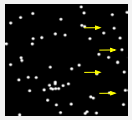

Figure 1. Random Dot Motion. Image of the random dot motion.

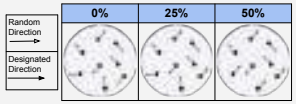

Figure 2. Motion Coherence. Motion coherence is equal to the number of dots in a designated direction divided by the number of dots total. We performed trials at motion coherences of 0%, 3.2%, 6.4%, 12.8%, 25.6%, 51.2%.

Materials and Methods

Experimental Setup

- Subjects perceive a specific direction upon viewing a random-dot stimulus. A mouse is used to move towards either a left or right target.
- The trial ends once the subject has reached one of the two targets.

Figure 3. Experimental Setup. Schematic of the monitor viewed by the subject during the experimental session.

Timeline of Trial

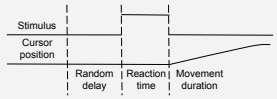

Figure 4. Timeline of Trial. The time course of events that make up a trial. Following a random delay, subjects viewed stimulus and indicated the direction of the dot motion by moving the cursor to leftward or rightward target. Motion stimulus vanished upon initiation of hand movement.

Coding

- Random dot stimulus is generated with Python, primarily tested with the PsychoPy IDE.
- The general structure of the experiment is based on the one presented in Resulaj's paper.
- Stimulus will be implemented on LiCoRICE machine to collect real-time data every millisecond of the cursor's position.

Figure 5. PsychoPy3 Logo. Primary IDE for development of the random dot stimulus used in experimental trials.

Data Collection

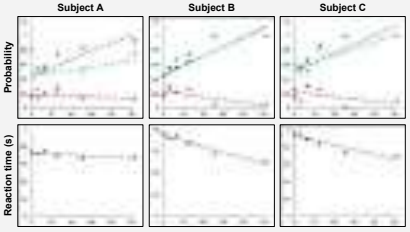

Figure 6. Accuracy improves through changes of mind. Data is from three subjects (A, B, and C). The top row shows the probability of a correct decision (blue), probability of change (red), and probability of a correct decision after change of mind (green) according to motion coherence strengths. Probability of a correct decision increases with motion strength, while probability of change decreases with motion strength. The bottom row shows that reaction times are higher for weaker motion strengths.

Conclusions

- We conclude that this study supports Resulaj's findings and theory of post-initiation processing.
- This study is significant to understand decisions related to gambling, social selection, and probabilistic reasoning.

Future Directions

- We plan to expand on the study by placing targets at 180° and comparing this to data using 45° targets.
- We anticipate, since a less natural movement to change direction is required, the frequency of changes of mind will decrease.

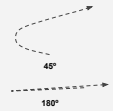

Figure 7. Contrast in movement. Arrows showing contrast in movement for targets placed at 45° versus 180°.

Figure 8. Experimental Setup. Schematic of the monitor viewed by the subject in a possible future study.

References

Pilly, P. K., & Seitz, A. R. (2009). What a difference a parameter makes: a psychophysical comparison of random dot motion algorithms. *Vision research*, *49*(13), 1599–1612. doi:10.1016/j.visres.2009.03.019

Resulaj, A., Kiani, R., Wolpert, D. M., & Shadlen, M. N. (2009). Changes of mind in decision-making. *Nature, 461*, 263-266.

Acknowledgements

This work was supported by the National Science Foundation through the UCLA Summer Undergraduate Research Program, specifically under the UCLA Electrical and Computer Engineering Department. We thank William Herrera and Muhammad Shahzain Raiz for their guidance throughout the program.

LAB NAME

Communications Sytems Laboratory

FACULTY ADVISOR

Professor Richard Wesel

GRADUATE STUDENT DAILY LAB SUPERVISOR

Ethan Liang

DEPARTMENT

Electrical and Computer Engineering

Vincent Lau

Electrical Engineering

Third Year

UCLA

Design of Cyclic Redundancy Check (CRC) for Tail-Biting Convolutional Codes

Reliable transmission of data requires channel codes that can correct errors introduced by the channel and/or detect that a received or decoded sequence is not valid. Convolutional encoders can correct errors in a distorted received sequence by using the Viterbi algorithm to find the closest convolutional codeword to the received sequence. Cyclic redundancy check (CRC) codes can detect whether the convolutional codeword identified by Viterbi decoding corresponds to a valid message. While both CRCs and convolutional codes have been developed in the past, they have been designed independently even though they are not independent when used together. For zero-terminated convolutional codes (ZTCCs) that are terminated by a final sequence of inputs that drives the encoder to the zero state, our research group has designed CRCs that are optimal for a given ZTCC. Tail-biting convolutional codes (TBCCs) avoid the overhead caused by ZTCCs and therefore can achieve higher rates with essentially the same performance. Rather than using additional input symbols to drive the final state to zero, TBCCs enforce the constraint that the starting state is the same as the final state. Our research is directed towards developing CRCs that are optimal for a given TBCC.

Design of Cyclic Redundancy Check (CRC) for Tail-Biting Convolutional Codes

Vincent Lau[1], Wenhui Sui[1], Ethan Liang[1], Richard Wesel[1]

[1]Communications Systems Laboratory, Department of Electrical and Computer Engineering
University of California, Los Angeles

Introduction

Reliable transmission of data requires channel codes that can correct errors introduced by the channel and/or detect that a received or decoded sequence is not valid. **Convolutional encoders** can correct errors in a distorted received sequence by using the Viterbi algorithm to find the closest convolutional codeword to the received sequence. We are particularly interested in the implementation of **tail-biting convolutional codes (TBCC)**, which reduce overhead and are capable of achieving higher rates at practically no expense to performance. **Cyclic redundancy check (CRC) codes** can detect whether the convolutional codeword identified by Viterbi decoding corresponds to a valid message. While both CRCs and convolutional codes have been developed in the past, they have been designed independently even though they are not independent when used together. Our research is directed towards developing CRCs that are optimal for a given TBCC. By first implementing an encoder and decoder for convolutional codes, we are building towards designing CRCs to ultimately accomplish this goal.

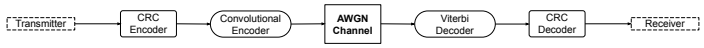

Figure 1. *Overall system structure of convolutional code and CRC for communications.*

Convolutional Codes

Convolutional codes are error-correcting codes that rely on memory storage in encoding, distinguishing them from traditional linear block codes. The encoder employs a shift-register structure that utilizes delay blocks to compute the output and track the state. We focus on rate-1/*n* encoders, which take 1-bit inputs and produce *n*-bit outputs.

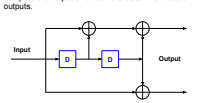

Figure 2. *A convolutional encoder can be represented as a block diagram. The values inside the delay blocks (blue) represent the state of the encoder.* [1]

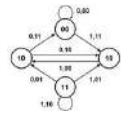

Figure 3. *A state machine is used to determine the output for a particular input and state. It also shows the evolution of states in a compact way.* [1]

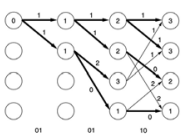

Figure 4. *The Trellis diagram aids in keeping track of path metrics and surviving paths, which are utilized in Viterbi decoding.* [1]

- The decoder we implement is based on the **Viterbi algorithm**, which can be realized with a Trellis diagram to keep track of the evolution of state paths over time, and helps us identify the most likely codeword given the received sequence.
- We are able to identify several performance metrics from the Trellis diagram, including free distance and number of nearest neighbors. The **free distance** represents the smallest Hamming distance between a pair of two valid codewords, while the number of nearest neighbors indicates the number of such pairs.
- While zero-terminated convolutional codes (ZTCCs) are terminated by a final sequence of inputs that drives the encoder to the zero state, **tail-biting convolutional codes (TBCCs)** require that the starting state be the same as the final state. These codes can achieve higher rates while maintaining nearly the same error-correcting performance.

Cyclic Redundancy Check (CRC)

Cyclic redundancy check (CRC) codes are error-detecting codes that help detect errors that may have been made by the decoder (e.g. the Viterbi decoder). At a high level, the CRC adds extra bits to the original codeword to serve as an extra layer of protection for decoding. This modification acts as an additional constraint to reduce the number of valid codewords, resulting in a smaller set of such valid codewords. This smaller set facilitates a larger minimum distance between codewords that provides a higher noise tolerance. In other words, the decoder will be less likely to select and validate an incorrect codeword.

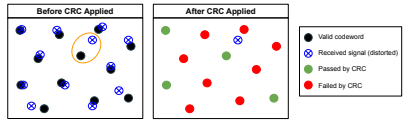

Figure 5. *Visual representation of CRC operation: The figure at the left shows the space of valid codewords (black). Transmission over a channel creates noise, resulting in distortion in the received signals (blue). Sometimes the noise distorts the codewords so much that the decoder may associate the received signal with a different codeword (yellow), leading to an error in decoding. To limit this effect, the CRC will only pass specific codewords (green) and fail all others (red) to make the valid codewords distinct.*

Materials and Methods

- This phase of the project primarily involved implementing a convolutional encoder and Viterbi decoder. This work was completed in MATLAB and was followed by extensive testing of both the codes and performance metrics for various examples of generator polynomials. We made sure to test different code rates and number of states.
- We started by simulating transmission across noiseless channels to make sure our encoder/decoder worked (i.e. zero errors occurred).
- For noisy channel transmission, we were interested in comparing bit-error rate (BER) vs. signal-to-noise ratio (Eb/No) for different rates and codes, as well as examining other properties like free distance, nearest neighbors, and analytic traceback depth.

Simulation Results

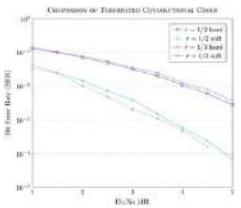

Figure 6. *A performance comparison of bit-error rate (BER) vs. signal-to-noise ratio (Eb/No) between different generator polynomials for ZTCC. We tested codes with rate-1/2 and 1/3, which were decoded with both hard decision and soft decision.*

- We compared two polynomials, (7,5) in purple and (13,12,16) in blue, which are of rate-1/2 rate-1/3, respectively.
- Two types of decoding were implemented and tested: hard-decision and soft-decision.
  - Hard-decision decoding uses a threshold value to decode a codeword.
  - Soft-decision decoding uses Euclidean distance to decode, which takes into account the impact of the noise on the transmission. Soft-decision decoding is the more refined and accurate technique of the two.
- As expected, the soft-decision decoding method outperformed the hard-decision decoding. Soft-decision required an Eb/No value about 2dB lower than hard-decision to produce the same BER.
- The rate-1/3 code performed better than the rate-1/2 code for soft-decision decoding, as expected. However, the two codes have similar performance for hard-decision decoding, which is an anomaly we are exploring (we expect the rate-1/3 to perform better).

Conclusions & Future Work

- Overall, our experience with the program was equal parts learning and re-implementing codes. We were able to develop a sound understanding of channel coding techniques and implement convolutional codes from scratch to supplement our learning process.
- For noiseless channels, we found that messages were decoded with zero error, as expected. Across noisy channels, noise was applied at different proportions, and we were also able to obtain good results (BER vs. Eb/No) for different parameters.
- We are looking towards the future to further develop our knowledge and bolster the significance of this project, with the ultimate goal of developing new CRCs for a range of CRC bit lengths. Specifically, we hope to eventually design new CRCs which are targeted for use with specific TBCCs, which we will implement.
- Our new CRCs will improve short-blocklength communications that are vital to sensor networks and the internet of things.

References

[1] R.D. Wesel, "Convolutional Codes", Wiley Encyclopedia of Telecommunications, John Wiley and Sons, 2003.
[2] H.H. Ma, J.K. Wolf, "On Tail Biting Convolutional Codes", IEEE Transaction on Communications, 1986.
[3] C.-Y. Lou, B. Daneshrad, R.D. Wesel, "Convolutional-Code-Specific CRC Code Design", IEEE Transactions on Communications, 2015.

Acknowledgments

We would like to thank the National Science Foundation and the Electrical and Computer Engineering Department for providing us the opportunity to conduct research. Additionally, we would like to acknowledge Ethan Liang and Hengjie Yang for providing guidance and mentorship throughout our research and learning process.

LAB NAME
Integrated Sensors Laboratory

FACULTY ADVISOR
Professor Aydin Babakhani

GRADUATE STUDENT DAILY LAB SUPERVISOR
Babak Jamali

DEPARTMENT
Electrical and Computer Engineering

Brandon Le

Electrical Engineering

Second Year

UCLA

Material Characterization Through THz-Wave Spectroscopy

Terahertz (THz) wave propagation allows for a large number of technological advances in modern systems, such as larger communication bandwidth and enhanced imaging resolution. THz wave signals also prove to be valuable in the practice of spectroscopy in order to characterize materials. The reason that THz waves present new advantages comes from two characteristics of millimeter waves. Because of their large bandwidth, these types of waves offer a larger absorption data set to uniquely identify materials. Secondly, their small wavelength nature allows these waves to have very high resolution in determining the thickness of a material.

This paper lays some groundwork of THz systems as a method of spectroscopy by testing its applications to solid materials. In our research, we set up a transmitter and a receiver to communicate with each other at varying sub-THz frequencies. An object of varying material is placed along the signal path to absorb some frequencies of communication dependent on the properties of that material. Intensity of the signals is measured at both the transmitter and the receiver and recorded in the frequency domain. Through a Support Vector Machine (SVM) machine learning algorithm, absorption plots obtained from various trials are used to identify the material obstructing the signal with 95% accuracy.

FAST TRACK TO SUCCESS
UCLA Electrical and Computer Engineering

Material Characterization Through THz-Wave Spectroscopy

Brandon Le, Rachel Schwall, Babak Jamali, Aydin Babakhani

UCLA Samueli School of Engineering

Background

- Absorption spectroscopy is used to identify specific materials based on its absorption of various wavelengths of electromagnetic waves
- This practice is often used to determine if a particular substance is present and if so, how much
- Different methods exist for measuring absorption spectra but a common one is to analyze the intensity of the radiation that passes through the object

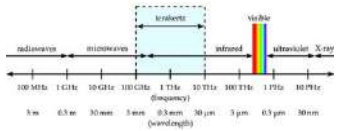

Introduction

- THz-waves pose a method of increasing the viable range of electromagnetic frequencies used for spectroscopy
- The goal of this experiment is to use a Support Vector Machine (SVM) algorithm to identify materials given its absorption of mm-waves
- SVMs classify data by determining an optimal hyperplane which acts as a separation boundary between different categories of data
- An SVM algorithm was used since it can effectively distinguish between complex sets of data, such as the various material absorptions, with much greater success than a human could

Materials and Methods

- Signal power received by the circuit was measured in the presence and absence of an object

- Absorption for each object was calculated by taking the difference in power with and without the object

- The SVM algorithm drew decision boundaries to differentiate the different materials' absorption data

Results

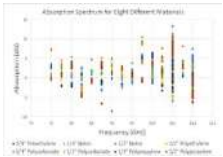

- An example of absorption data supplied to the SVM algorithm
- The SVM algorithm allows the machine to understand small differences in absorption that we could not observe ourselves for classification
- For these tests, absorption data at 105 and 110 GHz for all materials were unreliable, and thus were not necessarily used for training

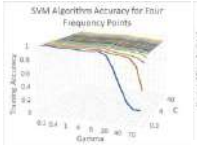

- The SVM algorithm was most accurate when using between two and six frequency points for training and using a low value for gamma
- For this range, the value of C didn't affect the accuracy very much

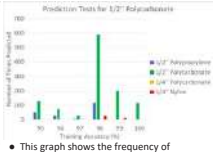

- This graph shows the frequency of predicting different materials from a new set of absorption data separate from the training
- For 95% training accuracy and above, an SVM algorithm proves effective in classifying the correct material over other possibilities

Conclusion/Future Works

Conclusion:

- From absorption spectra measurements, a Support Vector Machine algorithm can be trained to predict the material obstructing the signal with 95% accuracy
- Given new test data after training, higher training accuracy is required for consistently accurate classifications of objects

Future Works:

- Using other machine learning algorithms to separate absorption data and determine if other algorithms prove more accurate in predicting materials
- Create new absorption data to determine if other factors besides material type and thickness affect absorption
- Running these tests with a new set of materials to provide more data and materials for machine learning algorithms to classify

References

Jamali, Babak and Babakhani, Aydin. "A Fully Integrated 50–280-GHz Frequency Comb Detector for Coherent Broadband Sensing".

Pätzold, Martin. "Graphical Models and Simulation for THz-Imaging," *PhD Dissertation*, (2018).

Acknowledgements

We would like to thank the UCLA Summer Undergraduate Research Program for this research opportunity and the ECE Dean's Department for funding the experience. We would also like to thank Professor Babakhani for providing the opportunity to work in his lab as well as Babak Jamali for his support and guidance throughout the program.

LAB NAME

Interconnected and Integrated Bioelectronics Laboratory

FACULTY ADVISOR

Professor Sam Emaminejad

GRADUATE STUDENT DAILY LAB SUPERVISOR

Chris Yeung

DEPARTMENT

Electrical and Computer Engineering

Jifei Liu

Computer Engineering

First Year

Pasadena City College

Fabrication and Design of a Wearable Microfluidic Device Integrated with Electrochemical Sensors for the Detection of Glucose and Lactate Variation in Sweat

Traditionally, glucose and lactate levels are sampled via subcutaneously extracted blood tests. However, these previous methods often involve long and tedious processes such as laboratory testing, and they are susceptible to medical risks such as skin infections. In this study, we fabricated and designed a wearable microfluidic device that detects the glucose and lactate variation in sweat, which overcomes the shortcomings of previously reported methods. The microfluidic device is comprised of plastic, double-sided tape, microheaters, and thermoresponsive hydrogel valves to facilitate the active manipulation of sweat. Additionally, the device was integrated with a 3-electrode electrochemical sensor system capable of detecting changes in electrical current created by the chemical reactions between the sensors and biomarkers. Joined with a flexible printed circuit board, the final device can transmit the measured glucose and lactate levels to a mobile device. Interconnected with Internet of Things (IoT) devices, on-body microfluidics devices have the potential to switch the point of care from hospitals and labs to personalized health monitoring via wearable platforms.

Fabrication and Design of a Wearable Microfluidic Device Integrated with Electrochemical Sensors for the Detection of Glucose and Lactate Variation in Sweat

Jifei Liu[1], Jiawei Tan[1,2], Christopher Yeung[1,2], Sam Emaminejad[1]

[1]Department of Electrical and Computer Engineering, University of California, Los Angeles, CA, USA

[2]Department of Materials Science and Engineering, University of California, Los Angeles, CA, USA

Abstract

Traditionally, glucose and lactate levels are sampled via intravenously extracted blood tests. However, these previous methods often involve long and tedious processes such as laboratory testing, and they are susceptible to medical risks such as skin infections. In this study, we fabricated and designed a wearable microfluidic device that detects the glucose and lactate variation in sweat, which overcomes the shortcomings of previously reported methods. The microfluidic device is comprised of plastic, double-sided tape, microheaters, and thermoresponsive hydrogel valves to facilitate the active manipulation of sweat. Additionally, the device was integrated with a 3-electrode electrochemical sensor system capable of detecting changes in electrical current created by the chemical reactions between the sensors and biomarkers. Joined with a flexible printed circuit board, the final device can transmit the measured glucose and lactate levels to a mobile device. Interconnected with Internet of Things (IoT) devices, on-body microfluidics devices have the potential to switch the point of care from hospitals and labs to personalized health monitoring via wearable platforms.

Microfluidic Device

- "CAD to 3D Device" fabrication combined with laser cutting technology allows rapid and low-cost prototyping of microfluidic devices [1] .
- Double-sided tape and transparent polyethylene terephthalate (PET) are used to fabricate the device through vertical multi-layer integration.
- Laser-cut fabrication forms microchannels for fluid to pass.
- The adhesiveness and flexibility of the device allows the development of wearable devices for sweat sensing.
- Poly(N-isopropylacrylamide) (PNIAP)-based thermoresponsive polymer hydrogels combined with electrical microheaters create valves which enable sweat manipulation [2].
- Electrochemical sensor arrays sense the lactate and glucose variations in sweat.

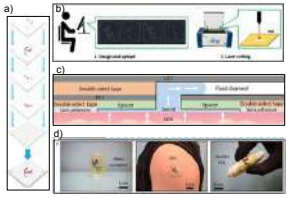

Figure 1: a) Double-sided tape and PET are stacked vertically to form the device. b) Devices designed on AutoCAD are fabricated using a laser cutter. c) Sample schematic of the microfluidic sweat collection device. Sweat passes through the skin adhesive and fluid channel layers. d) Sample microfluidic device attached to various interfaces: glass, human arm, and flexible printed circuit board (PCB) [1].

Electrochemical Sensors

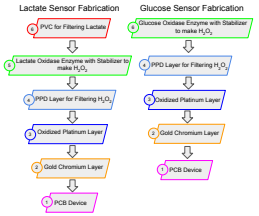

- The sensors are based on the three electrode system to monitor potential and current.
- ① PCB device controls the on/off of heaters and transmit signals of current to microcontroller.
- ② Gold-Chromium layer patterned using photolithography and evaporation of gold and chromium.
- ③ Platinum and H_2O_2 under oxidation generates electrical potential, allowing the electrodes to detect change in electrical current [3]. Silver chloride paste is used to cover the reference/counter electrode to set reference point 0 (as silver is not reactive).
- ④ M-Phenylenediamine (PPD), and organic polymer, is used to filter H_2O_2 from higher layer. Platinum and PPD are deposited onto the electrode surface via electrodeposition.
- ⑤ Lactate oxidase and glucose oxidase have enzymatic reaction with lactate and glucose, respectively, to make hydrogen peroxide (H_2O_2).
- ⑥ Polyvinyl Chloride (PVC), an industrial plastic polymer, is used to filter sodium lactate from sweat solution.

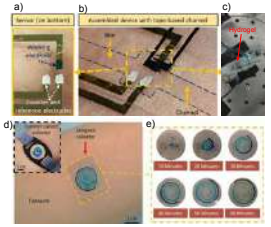

Figure 2: a) Sample 3-electrode sensor system. b) Fluid flows through a tape-based channel and comes in contact with sensors. c) Sample microfluidic device using a PNIAP hydrogel as a fluidic valve. d,e) Sample sweat collection demonstrating the volume of sweat captured over time [1].

Sensor Optimization

The initially-designed sensors are susceptible to significant noise/disruption. This noise can be caused by contaminated platinum or PPD solutions. Gold exposed during calibration can also contaminate the solutions. We addressed these issues by optimizing our fabrication process, which showed drastic improvements in noise reduction. Additionally, we discovered that the application of heat causes changes in sensor readings, which will be addressed in future studies.

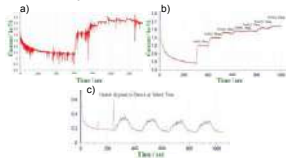

Figure 3: a) Noise/disruption in the current signal during initial sensor tests. b) Noise-reduced current variation of the lactate sensor responding to the addition of lactate. Tests here were performed in phosphate buffer saline solution to imitate lactate changes in the human body. c) Current levels with the heater applied on top of the device, showing that the applied heat causes changes in sensor readings.

Future Work

- To achieve reliable and stable lactate detection within the human body range (10-20 mM/L), additional testing is needed to determine the optimal PVC thickness (if the PCV is too thin, it will saturate sensor readings, and if it is too thick, the PVC will block lactate from the sensors).
- Current tests are done on synthetic sodium lactate and D(+) glucose in vitro. The device requires in vivo testing on a person exercising to capture and determine the variation of their lactate and glucose.
- PCB integration with microfluidic sensors and heaters require further testing and optimization.

References

[1] Lin, Haisong, et al. 2019. "A Rapid and Low-Cost Fabrication and Integration Scheme to Render 3D Microfluidic Architectures for Wearable Biofluid Sampling, Manipulation, and Sensing." Lab on a Chip, 2019

[2] Liu Junqiu, Yin Yanzhen. Temperature Responsive Hydrogels: Construction and Applications. Polym Sci, 2015

[3] Katsounaros, Ioannis, et al. 2012. "Hydrogen Peroxide Electrochemistry on Platinum: towards Understanding the Oxygen Reduction Reaction Mechanism." Physical Chemistry Chemical Physics 14 (20), 2012

Acknowledgement

This program was funded by Dr. Gregory Pottie's NSF grant for Wireless Health Institute and the Transfer Student Summer Research Program (TSSRP). The research was performed at the Interconnected and Integrated Bioelectronics Lab and UCLA Nanolab.

LAB NAME
Seidlits Laboratory

FACULTY ADVISOR
Professor Stephanie Seidlits

GRADUATE STUDENT DAILY LAB SUPERVISOR
Joshua Karam

DEPARTMENT
Bioengineering

Kajal Maran

Bioengineering

Fourth Year

UCLA

Effect of Hyaluronic Acid Molecular Weight on CD44 Clustering

The regeneration of tissue after spinal cord injury (SCI) has proven difficult as a result of the complex pathophysiology at the injury site. One biomolecule that plays an important role in the wound healing response is hyaluronic acid (HA), a long-chain polysaccharide in the extracellular matrix. It is known that HA signals cells to directly influence the inflammatory response in a molecular weight-dependent manner. One possible explanation for this effect is that different molecular weights of HA bind differentially to the CD44 receptor to induce varying levels of clustering. A model cell line, human embryonic kidney (HEK293T), was transduced with CD44 overexpression lentiviral vectors and treated with HA of varying molecular weights. CD44 clustering was characterized using both fluorescent resonant energy transfer (FRET) and Western blotting assays. Measurements of receptor clustering levels were made using HEK293T cells infected with two different viruses, CD44-YPet and CD44-CyPet, which promote expression of the CD44 receptor coupled to the YPet and CyPet fluorophores, respectively, which are well established FRET pairs. To quantify expression of clustered and unclustered CD44 via Western blotting, the crosslinker bis(sulfosuccinimidyl)suberate (BS^3) was used to preserve the CD44 receptors clustered in the cell membrane prior to cell lysis. Both FRET and Western blot analysis demonstrated that CD44 receptors in the presence of HA undergo greater clustering. Furthermore, data suggests that increasing molecular weight of HA may correspond with higher levels of CD44 clustering, although additional experimental repeats are required for verification.

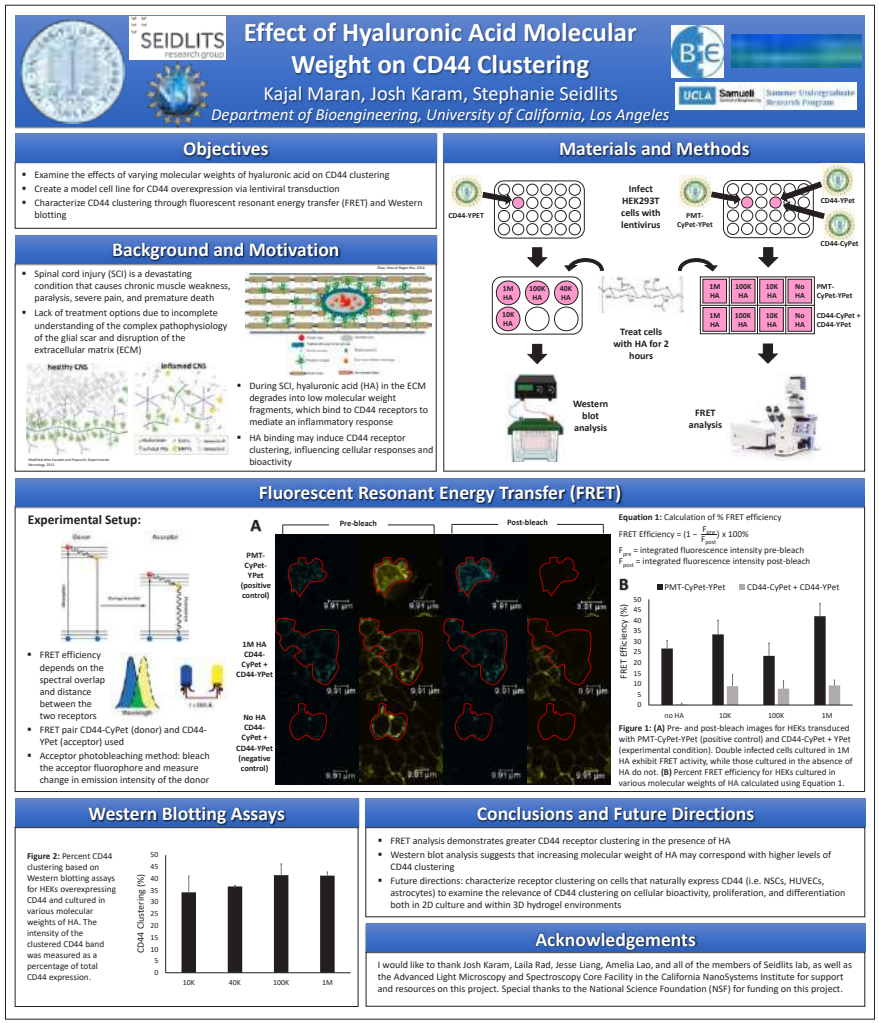

LAB NAME

Neural Computation and Engineering Laboratory

FACULTY ADVISOR

Professor Jonathan Kao

GRADUATE STUDENT DAILY LAB SUPERVISOR

Professor Jonathan Kao

DEPARTMENT

Electrical and Computer Engineering

Alicia Mercado

Biochemistry and Mathematics

Second Year

Mount Saint Mary's University

Studying changes of mind in decision-making

A decision is a commitment to an action after consideration of evidence and expected outcomes. The brain deliberates on available evidence to yield an action or decision. However, during cognition, we often change our minds; standard decision-making models do not fully explain why these changes of mind occur. The purpose of this study is to develop an experiment to study changes of mind, validating work by Resulaj and colleagues. It was hypothesized that noisy evidence, in the form of a random dot motion stimulus, is accumulated over time until it reaches a criterion level, or bound. An initial decision is made once this criterion is achieved. While the trials were conducted, subjects made decisions about a noisy visual stimulus, and then they indicated their choice of direction by moving a joystick according to the direction inferred. The brain then exploited further information that either reversed or reaffirmed the initial decision made. We conclude that this study supports Resulaj's findings and theory of post-initiation processing. This study is significant to understand decisions related to gambling, social selection, and probabilistic reasoning.

Studying changes of mind in decision-making

Michelle Lam[1], Alicia Mercado[2], Jonathan Kao[1]

[1]Department of Electrical and Computer Engineering, University of California – Los Angeles

[2]Department of Physical Sciences and Mathematics, Mount Saint Mary's University – Los Angeles

Ideas and Principles

Motivation

- A decision is a commitment to an action after consideration of evidence and expected outcomes.
- Standard decision-making models do not fully explain why changes of mind occur during the decision-making process.
- The purpose of this study is to develop an experiment to study changes of mind, validating work by Resulaj and colleagues.
- It was hypothesized that noisy evidence, in the form of a random dot motion stimulus, is accumulated over time until it reaches a criterion level, or bound.

Random Dot Motion Stimulus

- Random dot motions (RDM) are a classic stimulus used in psychophysical and physiological studies of motion processing.
- RDM occur in binary directions and can be modified to occur at different motion coherences.
  - Right v. Left
  - Up v. Down

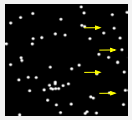

Figure 1. Random Dot Motion. Image of the random dot motion.

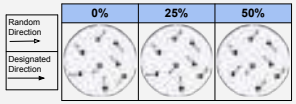

Figure 2. Motion Coherence. Motion coherence is equal to the number of dots in a designated direction divided by the number of dots total. We performed trials at motion coherences of 0%, 3.2%, 6.4%, 12.8%, 25.6%, 51.2%.

Materials and Methods

Experimental Setup

- Subjects perceive a specific direction upon viewing a random-dot stimulus. A mouse is used to move towards either a left or right target.
- The trial ends once the subject has reached one of the two targets.

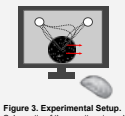

Figure 3. Experimental Setup. Schematic of the monitor viewed by the subject during the experimental session.

Timeline of Trial

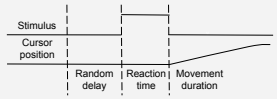

Figure 4. Timeline of Trial. The time course of events that make up a trial. Following a random delay, subjects viewed stimulus and indicated the direction of the dot motion by moving the cursor to leftward or rightward target. Motion stimulus vanished upon initiation of hand movement.

Coding

- Random dot stimulus is generated with Python, primarily tested with the PsychoPy IDE.
- The general structure of the experiment is based on the one presented in Resulaj's paper.
- Stimulus will be implemented on LiCoRICE machine to collect real-time data every millisecond of the cursor's position.

Figure 5. PsychoPy3 Logo. Primary IDE for development of the random dot stimulus used in experimental trials.

Data Collection

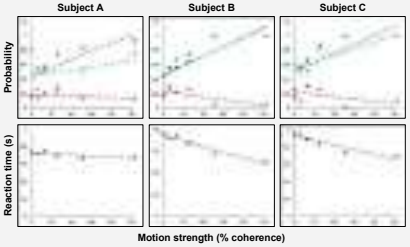

Figure 6. Accuracy improves through changes of mind. Data is from three subjects (A, B, and C). The top row shows the probability of a correct decision (blue), probability of change (red), and probability of a correct decision after change of mind (green) according to motion coherence strengths. Probability of a correct decision increases with motion strength, while probability of change decreases with motion strength. The bottom row shows that reaction times are higher for weaker motion strengths.

Conclusions

- We conclude that this study supports Resulaj's findings and theory of post-initiation processing.
- This study is significant to understand decisions related to gambling, social selection, and probabilistic reasoning.

Future Directions

- We plan to expand on the study by placing targets at 180° and comparing this to data using 45° targets.
- We anticipate, since a less natural movement to change direction is required, the frequency of changes of mind will decrease.

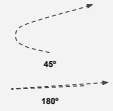

Figure 7. Contrast in movement. Arrows showing contrast in movement for targets placed at 45° versus 180°.

Figure 8. Experimental Setup. Schematic of the monitor viewed by the subject in a possible future study.

References

Pilly, P. K., & Seitz, A. R. (2009). What a difference a parameter makes: a psychophysical comparison of random dot motion algorithms. *Vision research*, *49*(13), 1599–1612. doi:10.1016/j.visres.2009.03.019

Resulaj, A., Kiani, R., Wolpert, D. M., & Shadlen, M. N. (2009). Changes of mind in decision-making. *Nature, 461*, 263-266.

Acknowledgements

This work was supported by the National Science Foundation through the UCLA Summer Undergraduate Research Program, specifically under the UCLA Electrical and Computer Engineering Department. We thank William Herrera and Muhammad Shahzain Raiz for their guidance throughout the program.

LAB NAME

Center for Heterogenous Integration and Performance Scaling (CHIPS)

FACULTY ADVISOR

Professor Subramanian Iyer

GRADUATE STUDENT DAILY LAB SUPERVISOR

Arsalan Alam

DEPARTMENT

Electrical and Computer Engineering

Michael Molter

Electrical Engineering

Third Year

UCLA

Design of Flexible, Wireless Surface Electromyography System

According to the CDC 1 in every 7,250 males are afflicted by Duchenne and Becker muscular dystrophy, a disease that affects muscle strength and leads to muscle degeneration. Surface Electromyography (EMG) is a non-invasive method used to measure muscle activity that can help in the diagnosis and treatment of musculoskeletal diseases such as muscular dystrophy. Typical Surface Electromyography machines are often bulky, rigid, and heavy which makes them difficult to use in a clinical setting, and it means they cannot be used as wearable devices. In addition, these systems are often single-channel systems which limit the spatial and temporal information that the system can gather, making readings incomplete. To help solve these issues, a full multi-channel electromyography system that is lightweight, flexible, and wireless will be integrated on FlexTrate™ , a flexible electronic platform based on Fan-Out Wafer Level Packaging (FOWLP). The surface EMG will take advantage of FlexTrate™ to integrate a variety of different integrated circuit (IC) dies such as amplifiers, passive components, and a Bluetooth Low Energy (BLE) chip as well as electrodes to detect the EMG signal. For wireless communication, the Nordic nRF52840 BLE module is used for low system power. Using FlexTrate™, the overall system will be lightweight, thickness less than 1 mm, and flexible enough to conform to skin allowing for a wearable device that can be used easily in a clinical setting.

Design of Flexible, Wireless Surface Electromyography System

M. Molter, A. Alam, and S. S. Iyer (UCLA CHIPS)

Motivation

- According to the CDC Muscular dystrophy effects 1 in 7250 males
- Surface Electromyography (EMG) measures the electrical activity of muscles for diagnoses of muscular disorders
- Existing Surface Electromyography systems are bulky, non-flexible, and heavy making them difficult to use
- FlexTrate™ is a flexible electronic platform based on Fan Out Wafer Level Packaging allowing integration of high performance dies
- FlexTrate™ is an ideal platform for a complete flexible and lightweight EMG system due to flexibility and ability to integrate many high performance dies

Traditional Surface Electromyography

System Design

Surface EMG on FlexTrate™ Layout

In the figure below, we see the simple layout and size EMG system. Total system thickness will be less than 1 mm and weigh approximately 10 g.

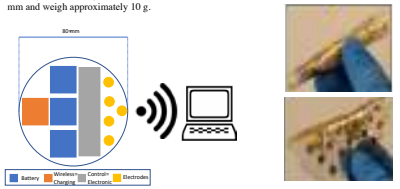

FlexTrate™ Surface EMG Electrodes Bent and Rolled

Control Electronics

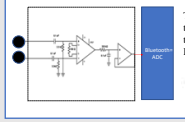

The control electronics amplify the EMG signal from microvolts to a voltage readable by the Bluetooth ADC.

The Nordic 52840 BLE chip sends data wirelessly to central computer

Verification of Wireless Communication

Cross Correlation of a sinusoid from a signal generator was recorded simultaneously from an oscilloscope and our Bluetooth controller at 10 Hz and 500 Hz. High correlation coefficients of 0.9923 and 0.9545 were calculated from cross correlation of both signals sources.

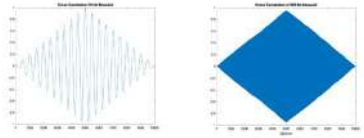

Verification of Wireless Communication Cont.

A comparison of EMG signals gathered simultaneously from an oscilloscope and Bluetooth controller. We can see that the EMG signals are visually the same from both.

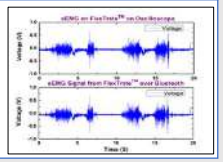

Signal Post Processing

Filtering Process

Surface EMG signals have only been recorded in the range of 5 – 500 Hz allowing filtering outside those ranges. Filtering allows removals of DC and low frequency noises associated with wire movement below 5 Hz and high frequency noises above 300 Hz.

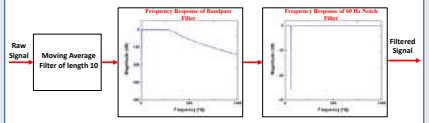

The pre and post processed signals Filtered EMG signal can be seen in the figure to the right.

In the close up view, we can see the pre-processed signal is subject to a large power line noise. Removing noise allows us to clearly see muscle activation signals that are not visible before.

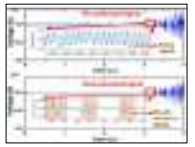

Conclusions/Future and Ongoing Work

Demonstrated the beginning steps towards a fully flexible, wireless, and lightweight surface EMG system including:

- Flexible electrodes
- Robust Wireless system capable of recording EMG
- Design of control electronics

Full System integration onto FlexTrate™ including the Bluetooth controller and control electronics.

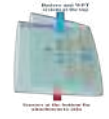

References/Acknowledgements

[1] M.B.I Raez et al. Techniques of EMG signal analysis: detection, processing, classification and applications, Biol Proced, 2006

[2] G. Ezhilarasu et al., IEDM, 2019.

[3] Romitti PA, Zhu Y, Puzhankara S, et al. Prevalence of Duchenne and Becker Muscular Dystrophies in the United States, Pediatrics. 2015

I would like to acknowledge CHIPS at UCLA for allowing me to research this summer as well as the UCLA engineering and SURP for providing their support for undergraduate research.

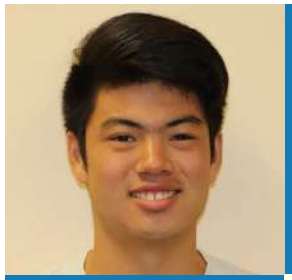

LAB NAME
UCLA Plasma Accelerator Group

FACULTY ADVISOR
Professor Chandrashekhar Joshi

GRADUATE STUDENT DAILY LAB SUPERVISOR
Zan Nie

DEPARTMENT
Electrical and Computer Engineering

Noa Nambu

Electrical Engineering

Third Year

UCLA

Spin-polarized Electrons by Photoionization with Intense Ultrashort Lasers

High-energy spin-polarized electrons are important for the investigation of pathways in high- energy collisions. However, generation of such electrons is difficult using conventional methods. Photoionization is a very common phenomenon that shows potential to provide a simpler way to produce spin-polarized electrons. Developments in laser technology have made it possible to create extremely high intensity light, which leads to various ionization processes. Multiphoton ionization involves the transfer of energy from multiple photons to an electron in order to surpass the ionization potential. Tunneling ionization occurs when higher field strength and lower frequencies allow the laser to be treated as an electric field which changes the shape of the potential barrier and allows the electron to escape through tunneling. The rates of ionization in these regimes have been described by several theories developed by Landau, Keldysh, ADK, PPT, and Barth and Smirnova. Different models of ionization rates were compared in order to find the areas in which they can be used to accurately describe ionization. The incorporation of magnetic and angular momentum quantum numbers into ionization rates allows for selective ionization of spin-polarized electrons, leading to predictions of up to 30% spin polarization. This may open a new avenue for the generation of high-energy, spin-polarized electrons in combination with the laser wakefield acceleration technique.

Spin-polarized Electrons by Photoionization with Intense Ultrashort Lasers

Noa Nambu, Zan Nie, Ken Marsh, Chan Joshi
Department of Electrical and Computer Engineering
University of California, Los Angeles

Introduction

- High-energy spin-polarized electrons are of interest to high-energy and particle physics, which are very difficult to generate by conventional methods.
- Laser technology has made it possible to create extremely high intensity light, suitable for tunneling and multiphoton ionization. Theories by Landau, Keldysh, ADK, PPT, and Barth and Smirnova describe rates of photoionization.
- Photoionization shows potential to provide a simpler way to produce spin-polarized electrons

Multiphoton and Tunneling Ionization

- Keldysh parameter differentiates multiphoton or tunneling
- $\gamma = \frac{\omega\sqrt{2m_e I_p}}{eE}$
- Multiphoton ionization ($\gamma > 1$) occurs when the energy of a single photon is lower than the ionization potential, but the intensity is high enough that multiple photons can interact with the electron at once
- Tunneling ($\gamma < 1$) occurs at higher intensities and lower frequency, where the electric field changes the shape of the potential barrier and allows the electron to escape by tunneling

Barrier Suppression Ionization

- High enough electric fields will deform the potential barrier to the point that an electron can freely escape without tunneling
- Critical field: $E_c = \frac{I_p^2 m_e}{2e^3}$

Figure 1: Multiphoton , tunneling, and barrier suppression ionization

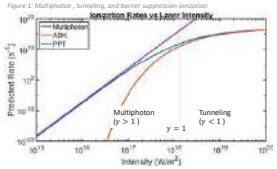

Figure 2: Ionization rates of Ar in 800 nm light predicted by different models: ADK (tunneling), multiphoton, and PPT.

Temporal Evolution of Ionization by Laser Pulse

- Electric field can be expressed as either a carrier or envelope, but using corrected rates yields similar results for ionization
- $E = E_0 \exp\left(\frac{t^2}{2\sigma^2}\right)\cos(\omega t)$ $\quad I = \frac{|E_0|^2}{2\eta_0}$

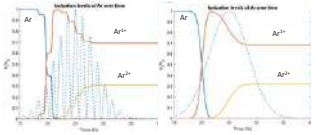

Figure 3: Ionization of Ar over time by laser pulse. Pulse is 12 fs with 800 nm light, 10^{14}W/cm² peak intensity. Instantaneous (left) vs time-averaged (right)

References

M. V. Ammosov, N. B. Delone, and V. P. Krainov, Sov. Phys. JETP **64**, 1191 (1986).
Augst, S., Meyerhofer, D.D., Strickland, D. & Chin, S.L. (1991). Laser ionization of noble gases by Coulomb-barrier suppression. *J. Opt. Soc. Am. B* 8, 858–867.
L. V. Keldysh, "Ionization in field of a strong electromagnetic wave," Sov. Phys. JETP **20**, 1307–1314 (1965).
A. M. Perelomov, V. S. Popov, and M. V. Terentev, "Ionization of atoms in an alternating electric field," Sov. Phys. JETP **50**, 1393–1409 (1966).
Jens Schwarz, Patrick Rambo, Mark Kimmel, and Briggs Atherton, "Measurement of nonlinear refractive index and ionization rates in air using a wavefront sensor," Opt. Express **20**, 8791-8803 (2012).
I. Barth and O. Smirnova, Phys. Rev. A **84**, 063415 (2011)

Electron orbitals

- Bound electrons have quantized energy levels, angular momentum, and projection of angular momentum, given by n, l, and m quantum numbers
- m quantum number describes the projection of the angular momentum onto an axis

m-dependent Ionization Rates

- For p-electrons exposed to circularly polarized light, projection of angular momentum onto the direction of the light can be seen as a sense of rotation of the electron
- Counter-rotating electrons have a higher ionization rate, than co-rotating electrons
- For linearly polarized light, m = 0 has the highest ionization rate

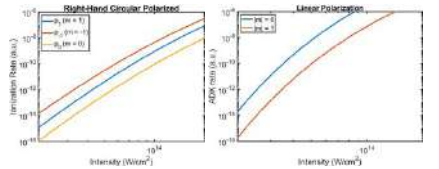

Figure 3: Different ionization rates for p-electrons of Ar depending on their magnetic quantum number in both linearly (right) and circularly (left) polarized light, using Barth and Smirnova's extension to PPT and the ADK model.

Summary of Models

	Range of γ	Atomic shell	Polarization	AC or DC
BSI	High intensity field above critical field	Doesn't depend on shell	Doesn't depend on polarization	Instantaneous
Landau	DC Tunneling (γ < 1)	Hydrogen (n=1, l=m=0)	N/A	DC
Keldysh	Multiphoton and tunneling	Hydrogen (n=1, l=m=0)	Linear	Time-averaged
ADK	Tunneling (γ < 1)	Any n, l, m	Linear, circular for s-orbitals	Instantaneous, time-averaged for linearly polarized
PPT	Multiphoton and tunneling	Any n, l, m	Linear, circular for s-orbitals	Time-averaged?
Barth and Smirnova	Multiphoton and tunneling	Any n, l, m	p-orbitals with circularly polarized light	Time-averaged?

Spin Selectivity

- Spin is coupled to m numbers, so selecting for m allows spin-selectivity
- Ionization into the $^2P_{3/2}$ state has a lower ionization potential, and occurs at a higher rate

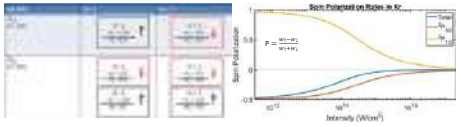

Figure 4: Spin polarization based on ionization rates in Kr

Conclusions and Future Work

- Different theories of ionization are investigated and summarized to gain an understanding of photoionization under many conditions
- Theories of multiphoton and tunneling ionization predict that spin-polarized electrons can be generated by photoionization This can be combined with the laser wakefield acceleration technique to create high-energy spin-polarized electrons

LAB NAME
Professor Greg J. Pottie's Laboratory

FACULTY ADVISOR
Professor Greg J. Pottie

GRADUATE STUDENT DAILY LAB SUPERVISOR
Kartik Ahuja

DEPARTMENT
Electrical and Computer Engineering

Marcel Nwaukwa

Computer Science

Fourth Year

University of Arkansas at Pine Bluff

Precision in Computing and Communication with Feedback

The 1940s marked the beginning of modern computing and communications. The two potential competing approaches that were about to drive these technologies were digital and analog. At that time digital computing was unreliable and analog computing was imprecise. Digital paradigm witnessed advancement in the theory and the development of hardware that scaled speed, cost, and energy. While the analog paradigm did not have any significant advances and as a result digital emerged as the winner. Modern-day integrated circuits use CMOS transistors and a lot of success of the integrated circuit technology is attributed to the decrease in the size of the CMOS over the last few decades. However, due to the impending end of CMOS scaling, we need to find alternative ways to continue to scale speed and power. If we are able to return to analog and improve the precision with today's modern integrated circuit technology, we might be able to get results competing with digital in some applications. In this work, we focus on characterizing the types of impairments in computation that can be tolerated for two important classes of problems: those that can be solved with linear methods using LMS adaptation, and those that can be solved using neural nets with backpropagation. Studying the impact of these impairments helps us understand the range of imprecision that analog circuits can operate while still being able to result in a desirable behavior.

Precision in Computing and Communication with Feedback

Marcel Nwaukwa[1], Naveene Naya[1], Professor Greg Pottie[1,2], Kartik Ahuja[1,2]

[1]Professor Greg Pottie's Laboratory

[2]Department of Electrical and Computer Engineering

Background

The 1940s marked the beginning of modern computing and communications. The two potential competing approaches that were about to drive these technologies were digital and analog. At that time digital computing was unreliable and analog computing was imprecise. Digital paradigm witnessed advancement in the theory and the development of hardware that scaled speed, cost, and energy. While the analog paradigm did not have any significant advances and as a result digital emerged as the winner.

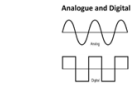

Figure 1. A comparison of digital and analog signals. Digital is the conversion of analog signals into digits.

Motivation

Modern-day integrated circuits use CMOS transistors and a lot of success of the integrated circuit technology is attributed to the decrease in the size of the CMOS over the last few decades. However, due to the impending end of CMOS scaling, we need to find alternative ways to continue to scale speed and power. If we are able to return to analog and improve the precision with today's modern integrated circuit technology, we might be able to get results competing with digital in some applications.

Figure 2. A CMOS image sensor

Figure 3. A simple layout of CMOS

Methods

Our goal in the simulations is to compare the digital paradigm with the analog computation paradigm for the problem of filtering. We used Matlab and Octave to carry out the simulations. Digital setup: computations are exact. Analog setup: computations are impaired. We used linear models (LMS adaptation) and neural network models (backpropagation) to compute the solution to the filtering problem in both digital and analog setups. We particularly focused on problems for which there is an analytical solution (or a computable brute force numerical solution) so that we could evaluate how well the calculations were working.

MATLAB GNU Octave

Figure 4. A simplified flowchart showing the steps taken towards achieving the results shown below.

Results

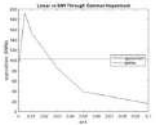

Figure 5. The graph of the linear method against SNi impairment, that has run 85000 times.

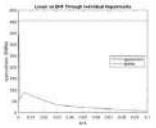

Figure 6. The graph of the linear method against SNi impairment, that has run 85000 times. This iteration has individual impairments throughout.

Comparing both figures 5 and 6 there is a clear trendline between both of them. The eventual decline towards the higher impairment value shows that both methods, one with a common impairment for each iteration and one with individual impairment values for each iteration, only have the potential to compete with exact digital solution in low impairment regime. The common impairment value signifies a more idealistic scenario where the same noise value is used. However the individual impairment values is more realistic due to how each multiplier would be different in different cases.
Unfortunately the neural network method did not come to fruition although it would have shown similar trends but with slower adaptation.

Other Problems

The different problems we looked at are all signal processing problems. There were two antenna problems that can be also tackled similarly to the filtering problem: antenna and multipath. The difference between the multipath and antenna problems is that in multipath the signals are coming from the same source. Though the antenna problems are different from the filter problem, the results should be the same.

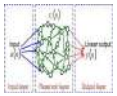

Figure 7. A visual representation of how the multipath problem adapts.

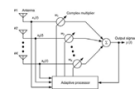

Figure 8. A visual representation of how the antenna problem adapts.

Future Applications

We can further our work and its application in various ways. One way would be to create an analog GPU that could solve all the problems neutral networks could solve. This will be substantially valuable for wireless health and self-driving cars, where there are incredibly complicated inference problems. Applications of an analog GPU will be to perform fast computations that are low in power in a compact unit. Also, analog computing would be more effective that digital computing in pattern recognition, like speech: speech, image recognition because of its inherent non-deterministic nature. One future work could be to improve the algorithm used for the neural network to enable them to converge in the presence of impairments as well as the linear method. A hypothesis for improving the algorithm for the neural network may be adding more layers or nodes. In a recapitulation, the future applications mentioned above are just a few of many circumstances analog computing is feasible, and further works could open a whole realm of possibilities. Hence, bringing analog computation out of the shadows of our digital world.

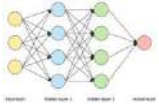

Figure 9. A visual representation of a neural network with two hidden layers

Acknowledgements

We would like to thank everyone who has supported us throughout this project. We want to use this medium to appreciate Professor Greg Pottie, Kartik Ahuja, Muhammed Shahzain Riaz, Arturo Hernandez, and William Herrera for their contributions to our academic and career growth this summer. We would also like to acknowledge organizations like NSF, TSSRP, WHI and the MESA Program.

LAB NAME

Speech Processing and Auditory Perception Laboratory

FACULTY ADVISOR

Professor Abeer Alwan

GRADUATE STUDENT DAILY LAB SUPERVISOR

Gary Yeung

DEPARTMENT

Electrical and Computer Engineering

Robert Ozturk

Electrical Engineering

First Year

UCLA

Automated Speech Database Organization

The development of an autonomous social robot, able to deliver clinical and educational assessments to young children, has great potential to aid in the efforts of educators and help students reach age-appropriate levels of proficiency in reading and oral language skills. A study researching the feasibility of the JIBO robot for such purposes, as well as gathering data needed to improve child automated speech recognition (ASR), resulted in a large dataset of verbal interactions between the robot and children via the administration of the Goldman-Fristoe Test of Articulation (GFTA) and other language tasks. Prior to database publication, time consuming and error-prone tasks such as matching audio data with corresponding prompt-answer pairs and the notation of private information for removal must be performed. We present a design and Python implementation for software automating and simplifying such processes. As robot prompts are known and consistent, timestamps are detected in audio files using a cross- correlation approach. We propose several methods of avoiding computationally expensive operations during such a search. For files with transcripts, processing is done using both a brute force search and the SpaCy natural language processing package, the latter to identify possible private information. Results are compared and combined with those from audio processing. Finally, we propose a database organizational structure and documentation in preparation for future publication.

Automated Speech Database Organization

Robert C. Ozturk[1], Dan Song[1], Gary Yeung[1] and Abeer Alwan[1]

[1]Department of Electrical and Computer Engineering, University of California, Los Angeles

Introduction

Figure 1. *The JIBO personal assistant robot was released in November of 2017.*

- What if a robot could help in the classroom?
- Recent research by Yeung et al. (2019) explored the feasibility of having the social robot JIBO (Figure 1) deliver educational assessments to young children [1].
- Additionally, data it produced was intended to be used towards developing better child automatic speech recognition (ASR), the current state of which has held back child human-robot interaction research [2].
- JIBO's administration of a letter and digit naming task and the 3rd Goldman Fristoe Tests of Articulation (GFTA-3) resulted in a large database containing 60 hours of child-robot interaction.
- This work presents an attempt to automate the necessary pre-processing of this database, as well as propose a database organizational structure.

Database

Subjects and Recordings:
- 156 children were recorded interacting with JIBO over 236 sessions.
- Sessions lasted between 5 and 40 minutes.
  - Session length varied based on child engagement and experience.
- Children were recorded in a classroom study space with limited noise.

Tasks:
- 3rd Goldman Fristoe Tests of Articulation (GFTA-3)
- Letter and digit naming task

Transcriptions:
- Full transcripts of the audio were produced by trained transcribers.
- Phonetic transcriptions were produced by trained phoneticians.

Objectives

- Create an easy to use interface for extracting/creating file information
- Automate the removal of private and sensitive data in audio
- Prepare database for publication and distribution for research

Methods

SciPy

/^[Reg]ular[Ex]pression$/

NumPy

SPYDER

Design: Text Processing

- Processing of audio transcripts was utilized in multiple ways:
  - To extract task completion data for documentation
  - To identify private information
  - As a guiding tool when labeling and cutting audio
- Regular expression (regex) use on the predictable transcript layout allowed for such analysis.
  - Ex. "\((\d+:\d\d)\)" searches for timestamps of the form (min:sec)
- spaCy:
  - This open-source package for Natural Language Processing aided in identifying private information within files, decreasing manual work.
  - Part-of-Speech tagging and Named Entity Recognition (NER) were the two main features of the package utilized.

Design: Audio Processing

- Template-based recognition was used to perform time-delay estimation to find robot speech in an audio file (Figure 2). Results shown in Figure 3.

Figure 2. *Flow-chart of template-based recognition*

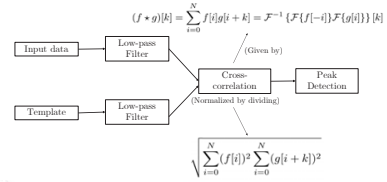

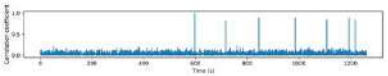

Figure 3. *Results of one normalized cross-correlation. The large peaks are matches to some JIBO voice line. A vertical axis value of 1 indicates an exact match. Due to noise and microphone placement inconsistencies, an exact match was very rare and thresholding was used to determine whether a match took place.*

Deliverables

- A new database layout was designed and accompanied with documentation using combined data from the designed processing methods.
- User interface was created for labeling and cutting audio. It decreases manual work by giving the user certain features:
  - Jump to audio containing private info or the beginning of certain tasks
  - Switch between textual and audio analysis (Figure 4) of child interviews

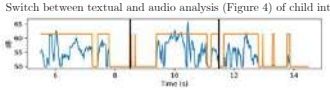

Figure 4. *A small section of a sound file. The user selected section is between the two black vertical lines. The orange sound blocks can be snapped to while scrubbing or can be ignored if fine scrubbing is desired.*

Conclusion and Future Work

- This database will assist in research for a number of diverse applications:
  - Child automatic speech recognition
  - Child speech science and linguistics
  - Human-robot interaction
- Going forward, we hope to generalize the methods for preliminary processing to all speech databases.

References

[1] Yeung, G., Afshan, A., Quintero, M., Martin, A., Spaulding, S., Park, H. W., ... and Alwan, A. (2019). Towards the development of personalized learning companion robots for early speech and language assessment. *2019 Annual Meeting of the American Educational Research Association (AERA)*.

[2] Yeung, G., & Alwan, A. (2018). On the Difficulties of Automatic Speech Recognition for Kindergarten-Aged Children. *Interspeech*, 1661–1665.

We would like to thank Professor Alwan, Gary Yeung, Amber Afshan, and Morgan Tinkler for the opportunity, guidance, and warm welcome given to us.
Additional thanks to the UCLA Wireless Health Institute, UCLA ECE Fast Track Program, and the NSF for their continuing support, financially and otherwise, for undergraduate research.

LAB NAME
Professor Greg J. Pottie's Laboratory

FACULTY ADVISOR
Professor Greg J. Pottie

GRADUATE STUDENT DAILY LAB SUPERVISOR
Kartik Ahuja

DEPARTMENT
Electrical and Computer Engineering

Naveene Raya

Computer Science

Third Year

El Camino College

Precision in Computing and Communication with Feedback

The 1940s marked the beginning of modern computing and communications. The two potential competing approaches that were about to drive these technologies were digital and analog. At that time digital computing was unreliable and analog computing was imprecise. Digital paradigm witnessed advancement in the theory and the development of hardware that scaled speed, cost, and energy. While the analog paradigm did not have any significant advances and as a result digital emerged as the winner. Modern-day integrated circuits use CMOS transistors and a lot of success of the integrated circuit technology is attributed to the decrease in the size of the CMOS over the last few decades. However, due to the impending end of CMOS scaling, we need to find alternative ways to continue to scale speed and power. If we are able to return to analog and improve the precision with today's modern integrated circuit technology, we might be able to get results competing with digital in some applications. In this work, we focus on characterizing the types of impairments in computation that can be tolerated for two important classes of problems: those that can be solved with linear methods using LMS adaptation, and those that can be solved using neural nets with backpropagation. Studying the impact of these impairments helps us understand the range of imprecision that analog circuits can operate while still being able to result in a desirable behavior.

Precision in Computing and Communication with Feedback

Naveene Naya[1], Marcel Nwaukwa[1], Professor Greg Pottie[1,2], Kartik Ahuja[1,2]

[1]Professor Greg Pottie's Laboratory

[2]Department of Electrical and Computer Engineering

TSSRP TRANSFER STUDENT Summer Research Program

Background

The 1940s marked the beginning of modern computing and communications. The two potential competing approaches that were about to drive these technologies were digital and analog. At that time digital computing was unreliable and analog computing was imprecise. Digital paradigm witnessed advancement in the theory and the development of hardware that scaled speed, cost, and energy. While the analog paradigm did not have any significant advances and as a result digital emerged as the winner.

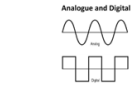

Figure 1. A comparison of digital and analog signals. Digital is the conversion of analog signals into digits.

Motivation

Modern-day integrated circuits use CMOS transistors and a lot of success of the integrated circuit technology is attributed to the decrease in the size of the CMOS over the last few decades. However, due to the impending end of CMOS scaling, we need to find alternative ways to continue to scale speed and power. If we are able to return to analog and improve the precision with today's modern integrated circuit technology, we might be able to get results competing with digital in some applications.

Figure 2. A CMOS image sensor

Figure 3. A simple layout of CMOS

Methods

Our goal in the simulations is to compare the digital paradigm with the analog computation paradigm for the problem of filtering. We used Matlab and Octave to carry out the simulations. Digital setup: computations are exact. Analog setup: computations are impaired. We used linear models (LMS adaptation) and neural network models (backpropagation) to compute the solution to the filtering problem in both digital and analog setups. We particularly focused on problems for which there is an analytical solution (or a computable brute force numerical solution) so that we could evaluate how well the calculations were working.

MATLAB GNU Octave

Figure 4. A simplified flowchart showing the steps taken towards achieving the results shown below.

Results

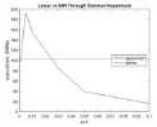

Figure 5. The graph of the linear method against SNi impairment, that has run 85000 times.

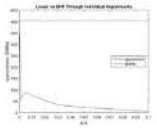

Figure 6. The graph of the linear method against SNi impairment, that has run 85000 times. This iteration has individual impairments throughout.

Comparing both figures 5 and 6 there is a clear trendline between both of them. The eventual decline towards the higher impairment value shows that both methods, one with a common impairment for each iteration and one with individual impairment values for each iteration, only have the potential to compete with exact digital solution in low impairment regime. The common impairment value signifies a more idealistic scenario where the same noise value is used. However the individual impairment values is more realistic due to how each multiplier would be different in different cases.
Unfortunately the neural network method did not come to fruition although it would have shown similar trends but with slower adaptation.

Other Problems

The different problems we looked at are all signal processing problems. There were two antenna problems that can be also tackled similarly to the filtering problem: antenna and multipath. The difference between the multipath and antenna problems is that in multipath the signals are coming from the same source. Though the antenna problems are different from the filter problem, the results should be the same.

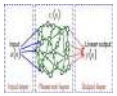

Figure 7. A visual representation of how the multipath problem adapts.

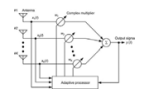

Figure 8. A visual representation of how the antenna problem adapts.

Future Applications

We can further our work and its application in various ways. One way would be to create an analog GPU that could solve all the problems neutral networks could solve. This will be substantially valuable for wireless health and self-driving cars, where there are incredibly complicated inference problems. Applications of an analog GPU will be to perform fast computations that are low in power in a compact unit. Also, analog computing would be more effective that digital computing in pattern recognition, like speech: speech, image recognition because of its inherent non-deterministic nature. One future work could be to improve the algorithm used for the neural network to enable them to converge in the presence of impairments as well as the linear method. A hypothesis for improving the algorithm for the neural network may be adding more layers or nodes. In a recapitulation, the future applications mentioned above are just a few of many circumstances analog computing is feasible, and further works could open a whole realm of possibilities. Hence, bringing analog computation out of the shadows of our digital world.

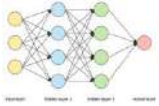

Figure 9. A visual representation of a neural network with two hidden layers

Acknowledgements

We would like to thank everyone who has supported us throughout this project. We want to use this medium to appreciate Professor Greg Pottie, Kartik Ahuja, Muhammed Shahzain Riaz, Arturo Hernandez, and William Herrera for their contributions to our academic and career growth this summer. We would also like to acknowledge organizations like NSF, TSSRP, WHI and the MESA Program.

LAB NAME

Algorithmic Research in Network Information Flow Laboratory

FACULTY ADVISOR

Professor Christina Fragouli

GRADUATE STUDENT DAILY LAB SUPERVISOR

Yahya Ezzeldin

DEPARTMENT

Electrical and Computer Engineering

Tara Sadjadpour

Electrical Engineering

Third Year

UCLA

Distributed Quantization for Classification Tasks

When using quantization schemes for distributed classification, the goal is not to reconstruct quantized data perfectly; rather, it is to create a quantization approach such that the classifier maintains the accuracy it had before the large, high-precision data was quantized. If a communication quality constraint exists between different devices in the system, then the number of bits that can be used in our quantization approach is further limited. In applications, such as brain-machine interface and Google Cloud Internet of Things, there is a pretrained classifier that resides in a central node in a communication network, where it receives unclassified data that is distributedly generated. In the case of brain-machine interface, sensors are distributed on a subject's body, and thus, high-precision features are generated from these body parts. This data is then classified for an actuator to carry out some action. Previously published solutions present a greedy algorithm that uses a recursive binning technique to quantize the data. We propose a more efficient, adaptable quantization approach implemented with neural networks. This approach achieves approximately the same accuracy as the greedy algorithm on an sEMG dataset with lower time complexity.

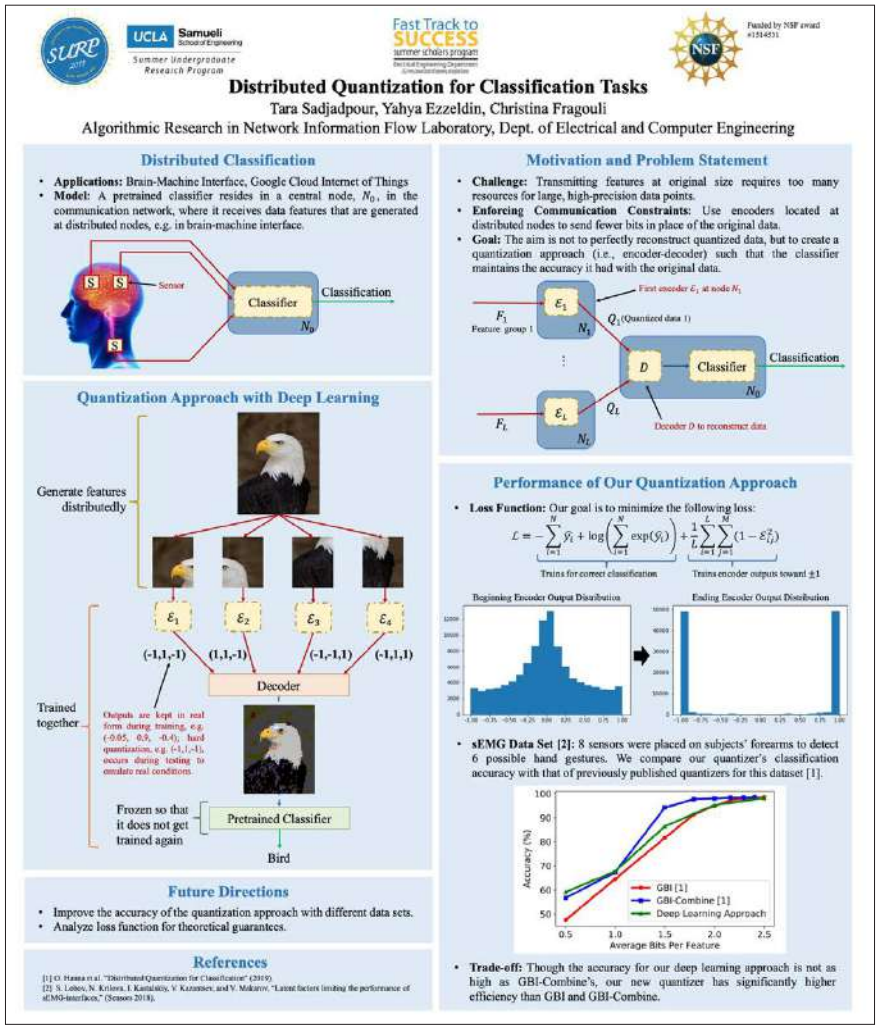

LAB NAME
Integrated Sensors Laboratory

FACULTY ADVISOR
Professor Aydin Babakhani

GRADUATE STUDENT DAILY LAB SUPERVISOR
Babak Jamali

DEPARTMENT
Electrical and Computer Engineering

Rachel Schwall

Electrical Engineering

Second Year

UCLA

Absorption Spectroscopy Using Millimeter-Wave and Sub-Terahertz Frequencies

Sensing and retrieving data from millimeter-wave and sub-terahertz frequencies are useful for many different applications including faster data transmission in wireless communication and enhanced resolution in imaging systems. In this frequency regime, broadband systems are also useful for spectroscopy and detecting different absorption frequencies of gas molecules. A comb- based method can be used to enhance bandwidth to include these frequencies and coherent detection techniques can be used to implement a receiver that can detect them. Integrated circuits designed using this method exhibit improved bandwidth, and detection resolution as well as reduced power consumption compared to current CMOS wideband coherent receivers. One specific use for these transmitter and receiver circuits is absorption spectroscopy where the power of the signal generated by the transmitter is measured after it passes through a specific material and is recorded by the receiver. A support vector machine (SVM) algorithm can then be trained with the absorption data of multiple materials to identify a new material given its absorption data collected from the receiver. SVMs are machine learning models that can classify data by determining an optimal hyperplane which acts as a separation boundary between different categories of data. An algorithm that utilizes SVM is quite effective when it comes to distinguishing between complex sets of data since it is able to determine boundaries in the data that may not be the most obvious to the human eye.

FAST TRACK TO SUCCESS
UCLA Electrical and Computer Engineering

Material Characterization Through THz-Wave Spectroscopy

Rachel Schwall, Brandon Le, Babak Jamali, Aydin Babakhani

UCLA Samueli School of Engineering

Background

- Absorption spectroscopy is used to identify specific materials based on its absorption of various wavelengths of electromagnetic waves
- This practice is often used to determine if a particular substance is present and if so, how much
- Different methods exist for measuring absorption spectra but a common one is to analyze the intensity of the radiation that passes through the object

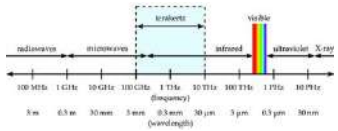

Introduction

- THz-waves pose a method of increasing the viable range of electromagnetic frequencies used for spectroscopy
- The goal of this experiment is to use a Support Vector Machine (SVM) algorithm to identify materials given its absorption of mm-waves
- SVMs classify data by determining an optimal hyperplane which acts as a separation boundary between different categories of data
- An SVM algorithm was used since it can effectively distinguish between complex sets of data, such as the various material absorptions, with much greater success than a human could

Materials and Methods

- Signal power received by the circuit was measured in the presence and absence of an object

- Absorption for each object was calculated by taking the difference in power with and without the object

- The SVM algorithm drew decision boundaries to differentiate the different materials' absorption data

Results

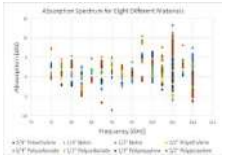

- An example of absorption data supplied to the SVM algorithm
- The SVM algorithm allows the machine to understand small differences in absorption that we could not observe ourselves for classification
- For these tests, absorption data at 105 and 110 GHz for all materials were unreliable, and thus were not necessarily used for training

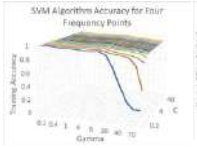

- The SVM algorithm was most accurate when using between two and six frequency points for training and using a low value for gamma
- For this range, the value of C didn't affect the accuracy very much

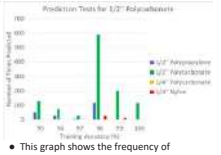

- This graph shows the frequency of predicting different materials from a new set of absorption data separate from the training
- For 95% training accuracy and above, an SVM algorithm proves effective in classifying the correct material over other possibilities

Conclusion/Future Works

Conclusion:

- From absorption spectra measurements, a Support Vector Machine algorithm can be trained to predict the material obstructing the signal with 95% accuracy
- Given new test data after training, higher training accuracy is required for consistently accurate classifications of objects

Future Works:

- Using other machine learning algorithms to separate absorption data and determine if other algorithms prove more accurate in predicting materials
- Create new absorption data to determine if other factors besides material type and thickness affect absorption
- Running these tests with a new set of materials to provide more data and materials for machine learning algorithms to classify

References

Jamali, Babak and Babakhani, Aydin. "A Fully Integrated 50–280-GHz Frequency Comb Detector for Coherent Broadband Sensing".

Pätzold, Martin. "Graphical Models and Simulation for THz-Imaging," *PhD Dissertation*, (2018).

Acknowledgements

We would like to thank the UCLA Summer Undergraduate Research Program for this research opportunity and the ECE Dean's Department for funding the experience. We would also like to thank Professor Babakhani for providing the opportunity to work in his lab as well as Babak Jamali for his support and guidance throughout the program.

LAB NAME
Sensors and Technology Laboratory

FACULTY ADVISOR
Professor Rob Candler

GRADUATE STUDENT DAILY LAB SUPERVISOR
Jimmy Wu

DEPARTMENT
Electrical and Computer Engineering

Justin Shao

Electrical Engineering

Second Year

UCLA

Millimeter-Scale Electroplated Multilayer Magnetic Shielding

Many devices that rely on atomic spectroscopy, like gyroscopic sensors and atomic clocks, require magnetic shielding to function as intended because of interference by external magnetic fields. Although no known material is able to stop a magnetic field, high permeability materials are able to effectively redirect magnetic field lines, creating protected regions of low magnetic field strength. Current methods of magnetic shielding involve inserting a sheet of high permeability material on a circuit board underneath a device or wrapping a region in a sheet of the high permeability material. In this project, we fabricate high performance chip-scale magnetic shields by electroplating alternating layers of nickel-iron alloy, which has a high relative permeability, and copper, which has a low relative permeability, onto a cylindrical shell. By alternating layers of high and low permeabilities, we minimize the influence of the demagnetization field, achieving a higher ability to redirect magnetic field lines. To test the shields, we use an electromagnet to generate a magnetic field and a magnetometer to measure the magnetic field inside the shield. We record the shielding factor of the shield, which is defined as the ratio of the external magnetic field strength to the internal magnetic field strength. Successful millimeter-scale shielding would allow for effective chip-scale implementation of devices that would function in external magnetic fields while conserving space.

Millimeter-Scale Electroplated Multilayer Magnetic Shielding

Justin Shao, Sydney Walsh, Hou Seng Wong, Jimmy C. Wu, and Rob N. Candler*

Sensors and Technology Laboratory, Electrical and Computer Engineering Department, University of California, Los Angeles*

UCLA Samueli School of Engineering — Summer Undergraduate Research Program

Introduction

Motivation

- Devices like atomic clocks and sensors require magnetic shielding because of sensitivity to external magnetic fields
- Using high magnetic permeability materials, magnetic shields can create protected regions of low magnetic field
- Current machining methods are limited to larger scales
- We use electroplating to fabricate more compact and efficient magnetic shields
- Successful implementation of chip-scale magnetic shields can lead to new innovations like GPS-free location tracking

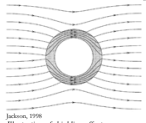

Jackson, 1998
Illustration of shielding effect

Design and Fabrication

Magnetic Shielding Mechanism

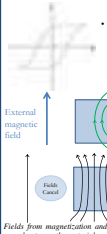

- Magnetization in a material follows a nonlinear curve and maximizes at saturation

Fields from magnetization and external magnetic field cancel out near the material

Multilayer Shielding Design

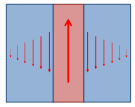

Magnetic field of red region opposes magnetization of blue regions

- Magnetization of a region opposes magnetization of neighboring regions
- By removing a layer of magnetic material, the neighboring regions reach higher magnetization
- A multilayer shield can better oppose external magnetic fields

Fabrication

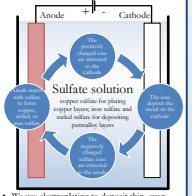

- We use electroplating to deposit thin, even layers onto a cylindrical wax mold
- After electroplating, the wax mold is dissolved in xylene, leaving just the metal shell

Results

Measurement Procedure

Shielding factor measurement setup

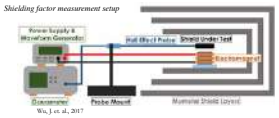

Wu, J. et. al., 2017

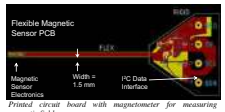

Printed circuit board with magnetometer for measuring magnetic field

- We apply a known magnetic field to a magnetometer using an electromagnet
- Measure the magnetic field using a magnetometer inside the magnetic shield
- Calculated shielding factor defined as $S \equiv \frac{H_{external}}{H_{internal}}$

Experimental Results

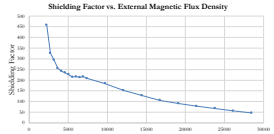

Internal magnetic flux density and shielding factor plotted against external magnetic flux density

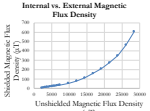

Internal magnetic field plotted against external magnetic field

From our experiments, the shield is most effective at in weaker magnetic fields. The performance of the shield decreases as the magnetic field gets stronger because the magnetic material in the shield approaches saturation, and its ability to cancel magnetic fields reaches a maximum.

COMSOL Physics Simulation

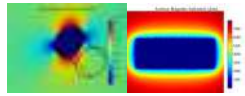

Cross sectional views of a simulated cylindrical shield inside a uniform external magnetic field

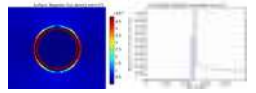

Simulation of magnetic flux density in a multilayer cylindrical shield

We demonstrate the magnetic shielding effect in COMSOL Multiphysics simulations, showing that the magnetic field is concentrated within the shield's material and redirected around the region enclosed by the cylinder.

Discussion and Future Work

Results Analysis

In comparison with current methods of magnetic shielding, our cylindrical shield is more effective at protecting regions from magnetic fields. For weaker magnetic fields, we recorded shielding factors higher than 400, while a flat sheet of similarly high permeability metal, as those found in current methods of magnetic shielding, could not achieve a shielding factor higher than 1.2.

Future Work

- Shielding factor greatly dependent on geometry of the shield
- From Maxwell's equations, the magnetic field around the surfaces of the magnetic material satisfies the boundary conditions at every surface:

$$(\mathbf{B}_2 - \mathbf{B}_1) \cdot \hat{\mathbf{n}} = 0$$
$$(\mathbf{H}_2 - \mathbf{H}_1) \times \hat{\mathbf{n}} = 0$$

- Using electroplating to generate the shields, it is possible to create shields of more complex geometries not achievable with traditional machining methods

x, y, and z components of internal magnetic fields within the protected regions of the plate and cylinder shaped shields

- Electroplate magnetic shield directly onto devices
- Conserves space and improves shielding factor

NIST, 2018
Chip-scale atomic clock

Acknowledgements

We would like to acknowledge the UCLA Summer Undergraduate Research Program, the UCLA Electrical and Computer Engineering Department, National Science Foundation, Functional Nanomaterials, the Sensors and Technology Laboratory. We would also like to acknowledge Erik Hodges, the previous undergraduate who worked on this project.

References

Jackson, John David (10 August 1998). *Classical Electrodynamics* (third ed.).

"NIST Unveils Chip-Scale Atomic Clock." NIST, 21 Mar 2018, www.nist.gov/news-events/news/2004/08/nist-unveils-chip-scale-atomic-clock.

Wu, J., Li, L., Harrison, J., and Candler, R. Micro- to Millimeter Scale Magnetic Shielding. 2017.

LAB NAME

Actuated Sensing & Coordinated Embedded Networked Technologies Laboratory

FACULTY ADVISOR

Professor William Kaiser

GRADUATE STUDENT DAILY LAB SUPERVISOR

Susie Tan

DEPARTMENT

Electrical and Computer Engineering

Robert Shi

Computer Science and Engineering

Second Year

Pasadena City College

Gait Recognition Using SensorTile – A State Machine Approach

Personal devices, such as smart phones and wristbands, can be turned into mobile health devices with the help of embedded systems with wearable motion sensors and Internet of Things (IoT). Such devices are capable of providing real time monitoring and feedback about training performance for outpatients with hemiparesis during their rehabilitation process. A reliable algorithm for gait recognition is required for the system to give accurate feedback. The goal of this research is to design and improve the performance of a custom-built state machine algorithm on a STMicroelectronics SensorTile utilizing only the onboard accelerometer module (LSM6DSM). The motion path of a foot in a gait cycle is divided into four states and mapped to a horizontal surface. The recognition of a complete gait cycle is then accomplished by moving SensorTile along the path. Results have shown high reliability, with an identification accuracy of 90% when the cutoff frequency is set to 5 Hz for the low-pass filter applied to the acceleration signal, and 0.7 Hz for the high-pass filter applied to the velocity and displacement signals. The high accuracy demonstrates that accelerometer data can be used to identify two-dimensional gait cycles.

Gait Recognition Using SensorTile – A State Machine Approach

Robert Y. Shi[1], Susie Tan[1], William Kaiser[1]

1. Department of Electrical and Computer Engineering, University of California Los Angeles

Introduction

Motivation: Lack of specialized equipment for stroke home rehabilitation

Background: Personal devices with wearable motion sensors and Internet of Things (IoT) can provide real time monitoring and feedback about training performance

Objective: Design and improve the performance of a state machine algorithm on a STMicroelectronics SensorTile utilizing only the onboard accelerometer module (LSM6DSM)

Fig. 1 Leg sensors to detect motion and muscle activity

Fig. 2 SensorTile core system board with LSM6DSM in the red box (left) and SensorTile soldered to cradle board packaged in plastic case (right)

Materials and Methods

- Motion path of a foot in a gait cycle is divided into four states and mapped to a horizontal surface
- Recognition of a complete gait cycle is accomplished while SensorTile is moved along the path (Fig. 9)
- Integrate filtered acceleration signals to obtain velocity signals
- Integrate filtered velocity signals to obtain displacement signals
- Integrations in both steps are done by performing trapezoidal integral with the formulae bellow on the discrete acceleration data samples
- Analyze displacement signals to identify foot motions

$$v_1 = v_0 + \left(a_0 + \frac{a_1 - a_0}{2}\right) \times \Delta t = v_0 + \frac{a_1 + a_0}{2} \times \Delta t$$

$$d_1 = d_0 + \left(v_0 + \frac{v_1 - v_0}{2}\right) \times \Delta t = d_0 + \frac{v_1 + v_0}{2} \times \Delta t$$

d_0, v_0, a_0 are the **previous** displacement, velocity, and acceleration samples respectively
d_1, v_1, a_1 are the **current** displacement, velocity, and acceleration samples respectively
Δt is the **sampling period** and is equal to 0.01 millisecond in this programming project

Fig. 3 Programming SensorTile on Cradle Expansion Board (left) connected to STM32 Nucleo-64 (right)

Fig. 4 Packaged SensorTile on Cradle board

Signal Processing

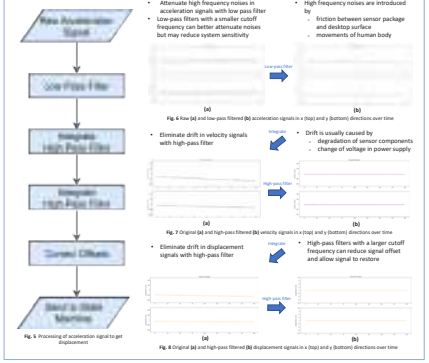

- Attenuate high frequency noises in acceleration signals with low-pass filter
- Low-pass filters with a smaller cutoff frequency can better attenuate noises but may reduce system sensitivity
- High frequency noises are introduced by
  - friction between sensor package and desktop surface
  - movements of human body

Fig. 5 Processing of acceleration signal to get displacement

Fig. 6 Raw (a) and low-pass filtered (b) acceleration signals in x (top) and y (bottom) directions over time

- Eliminate drift in velocity signals with high-pass filter
- Drift is usually caused by
  - degradation of sensor components
  - change of voltage in power supply

Fig. 7 Original (a) and high-pass filtered (b) velocity signals in x (top) and y (bottom) directions over time

- Eliminate drift in displacement signals with high-pass filter
- High-pass filters with a larger cutoff frequency can reduce signal offset and allow signal to restore

Fig. 8 Original (a) and high-pass filtered (b) displacement signals in x (top) and y (bottom) directions over time

State Machine Design

Fig. 9 Motion states of right foot in a gait cycle including stationary (blue), heel lifted (green), moved forward (red), and heel dropped (purple).

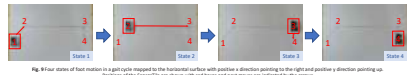

Fig. 9 Four states of foot motion in a gait cycle mapped to the horizontal surface with positive x direction pointing to the right and positive y direction pointing up. Positions of the SensorTile are shown with red boxes and next moves are indicated by the arrows.

- **State 0: Calibration**
  Transition 0 → 1: Signal offset of the sensor is calibrated using samples collected in 10 seconds
- **State 1: Stationary**
  Transition 1 → 2: Heel lifts, positive displacements in both x and y directions
- **State 2: Heel lifted**
  Transition 2 → 3: Foot moves forward, positive displacement in x direction, little to no displacement in y direction
- **State 3: Moved forward**
  Transition 3 → 4: Heel drops, little to no displacement in x direction, negative displacement in y direction
- **State 4: Heel dropped**
  Transition 4 → 1: Increase step count and go back to initial state

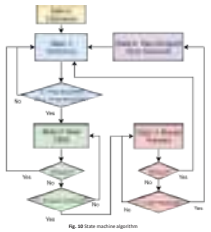

Fig. 10 State machine algorithm

Results

The system demonstrates high reliability, with an identification accuracy of 90% when the cutoff frequency is set to 5 Hz for the low-pass filter, and 0.7 Hz for the high-pass filter.

Fig. 11 Filtered and corrected displacement signals in x (top) and y (bottom) directions of a complete gait cycle

Conclusions

- Accelerometer data could possibly be used to identify two-dimensional gait cycles and/or other human motions
- Estimation of small displacements using the method above using accelerometer gives relatively large errors but does not affect identification of motion patterns
- Future works may include utilization of gyroscope to detect 3-dimensional motions and reduce errors introduced by the tilting of SensorTile

Acknowledgements

- National Science Foundation (grant no. IIS-1560483)
- UCLA Henry Samueli School of Engineering and Applied Science Summer Undergraduate Research Program
- UCLA Wireless Health Institute
- UCLA Transfer Student Summer Research Program

LAB NAME

Laboratory for Embedded Machines and Ubiquitous Robots (LEMUR)

FACULTY ADVISOR

Professor Ankur Mehta

GRADUATE STUDENT DAILY LAB SUPERVISOR

Professor Ankur Mehta

DEPARTMENT

Electrical and Computer Engineering

Shantinath Smyth

Electrical Engineering

Second Year

UCLA

Custom Printable Robotic Boats for Early STEM Education

Robotics engages students in multiple disciplines of engineering, which is increasingly important in our technology-based society. However, existing robotics kits are mostly geared toward middle- and high- school students and either cost hundreds or thousands of dollars or have limited hands-on design capabilities. This leaves customizable robotics unaffordable to many schools, as well as neglects to introduce robots to impressionable elementary-age children. Our project focused on concurrently addressing three concerns: cost, age group, and creative potential. We developed a modifiable template for an affordable robot that students design themselves, supporting a project-based learning approach, with the goal of inspiring interest in STEM in kindergartners.

Since most robotics kits are cars, we designed a robotic boat and a web-based app, which students use to create and steer the boat. One boat is made of a flat sheet of plastic folded into a 3D structure, with basic electronics propelling the vehicle, and costs under $40 total. In the app, powered by Robot Compiler technology, students change parameters on the boat to see the effect on the 2D printable template and 3D model of the finished boat. This focus on customization encourages iterative design and engages students firsthand in the engineering innovation process. Students have flexibility in designing their robots down to the component level, fostering a sense of ownership over their project and resulting in a more self-motivated learning experience.

Custom Printable Robotic Boats for Early STEM Education

Chelsea Lai, Shantinath Smyth, Dr. Ankur Mehta

Dept. of Electrical and Computer Engineering, University of California, Los Angeles

Introduction

Problems with Existing Robotics Kits

- Expensive
- Middle- and high-school age group
- Limited hands-on design

Our Solution

- Creating a design tool for low-cost foldable robotic boats

Educational Applications

- Students design, build, and redesign robotic boats
- Hands-on experience with cycle of scientific experimentation

Developing the Design Tool

Built prototypes of mechanically powered paddleboat design → Motorized boat and integrated electronics into design → Finalized boat template → Model 2D template and 3D structure on RoCo

Student Design Process

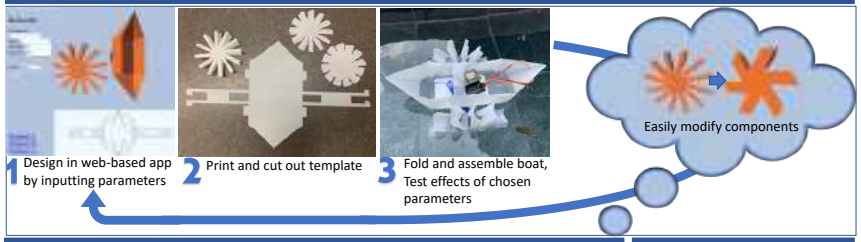

1 Design in web-based app by inputting parameters

2 Print and cut out template

3 Fold and assemble boat, Test effects of chosen parameters

Results

- Iterative design process and customization allows for personalized products
- Encourages experimentation and hands-on learning approach
- Teaches gateway STEM skills and engineering/design process

Total cost: ~$30 (Retail), ~$15 (Bulk)

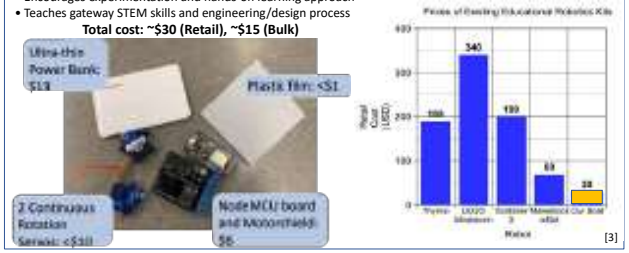

Acknowledgements

Summer Undergraduate Research Program

Fast Track to Success Program

LEMUR Lab, Dr. Ankur Mehta

Wireless Health Institute

References

[1] McLurkin, James, et al. "Using multi-robot systems for engineering education: Teaching and outreach with large numbers of an advanced, low-cost robot." IEEE transactions on education 56.1 (2012): 24-33.

[2] Blumenfeld, Phyllis C., et al. "Motivating project-based learning: Sustaining the doing, supporting the learning." Educational psychologist 26.3-4 (1991): 369-398.

[3] Rubenstein, Michael, et al. "AERobot: An affordable one-robot-per-student system for early robotics education." 2015 IEEE International Conference on Robotics and Automation (ICRA). IEEE, 2015.

[4] Mondada, Francesco, et al. "The e-puck, a robot designed for education in engineering." Proceedings of the 9th conference on autonomous robot systems and competitions. Vol. 1. No. CONF. IPCB: Instituto Politecnico de Castelo Branco, 2009.

[5] A.M. Mehta, J. DelPreto, B. Shaya, and D. Rus. "Cogeneration of Mechanical, Electrical, and Software Designs for Printable Robots from Structural Specifications". In: Intelligent Robots and Systems (IROS 2014), Chicago, IL, Sep 2014, pp. 2892-2897.

[6] Mehta, Ankur M., and Daniela Rus. "An end-to-end system for designing mechanical structures for print-and-fold robots." 2014 IEEE International Conference on Robotics and Automation (ICRA). IEEE, 2014.

LAB NAME

Speech Processing and Auditory Perception Laboratory

FACULTY ADVISOR

Professor Abeer Alwan

GRADUATE STUDENT DAILY LAB SUPERVISOR

Gary Yeung

DEPARTMENT

Electrical and Computer Engineering

Dan Song

Electrical Engineering

First Year

UCLA

Automated Speech Database Organization

The development of an autonomous social robot, able to deliver clinical and educational assessments to young children, has great potential to aid in the efforts of educators and help students reach age-appropriate levels of proficiency in reading and oral language skills. A study researching the feasibility of the JIBO robot for such purposes, as well as gathering data needed to improve child automated speech recognition (ASR), resulted in a large dataset of verbal interactions between the robot and children via the administration of the Goldman-Fristoe Test of Articulation (GFTA) and other language tasks. Prior to database publication, time consuming and error-prone tasks such as matching audio data with corresponding prompt-answer pairs and the notation of private information for removal must be performed. We present a design and Python implementation for software automating and simplifying such processes. As robot prompts are known and consistent, timestamps are detected in audio files using a cross- correlation approach. We propose several methods of avoiding computationally expensive operations during such a search. For files with transcripts, processing is done using both a brute force search and the SpaCy natural language processing package, the latter to identify possible private information. Results are compared and combined with those from audio processing. Finally, we propose a database organizational structure and documentation in preparation for future publication.

Automated Speech Database Organization

Robert C. Ozturk[1], Dan Song[1], Gary Yeung[1] and Abeer Alwan[1]

[1]Department of Electrical and Computer Engineering, University of California, Los Angeles

Introduction

Figure 1. *The JIBO personal assistant robot was released in November of 2017.*

- What if a robot could help in the classroom?
- Recent research by Yeung et al. (2019) explored the feasibility of having the social robot JIBO (Figure 1) deliver educational assessments to young children [1].
- Additionally, data it produced was intended to be used towards developing better child automatic speech recognition (ASR), the current state of which has held back child human-robot interaction research [2].
- JIBO's administration of a letter and digit naming task and the 3rd Goldman Fristoe Tests of Articulation (GFTA-3) resulted in a large database containing 60 hours of child-robot interaction.
- This work presents an attempt to automate the necessary pre-processing of this database, as well as propose a database organizational structure.

Database

Subjects and Recordings:
- 156 children were recorded interacting with JIBO over 236 sessions.
- Sessions lasted between 5 and 40 minutes.
  - Session length varied based on child engagement and experience.
- Children were recorded in a classroom study space with limited noise.

Tasks:
- 3rd Goldman Fristoe Tests of Articulation (GFTA-3)
- Letter and digit naming task

Transcriptions:
- Full transcripts of the audio were produced by trained transcribers.
- Phonetic transcriptions were produced by trained phoneticians.

Objectives

- Create an easy to use interface for extracting/creating file information
- Automate the removal of private and sensitive data in audio
- Prepare database for publication and distribution for research

Methods

SciPy

/^[Reg]ular[Ex]pression$/

NumPy

SPYDER

Design: Text Processing

- Processing of audio transcripts was utilized in multiple ways:
  - To extract task completion data for documentation
  - To identify private information
  - As a guiding tool when labeling and cutting audio
- Regular expression (regex) use on the predictable transcript layout allowed for such analysis.
  - Ex. "\((\d+:\d\d)\)" searches for timestamps of the form (min:sec)
- spaCy:
  - This open-source package for Natural Language Processing aided in identifying private information within files, decreasing manual work.
  - Part-of-Speech tagging and Named Entity Recognition (NER) were the two main features of the package utilized.

Design: Audio Processing

- Template-based recognition was used to perform time-delay estimation to find robot speech in an audio file (Figure 2). Results shown in Figure 3.

Figure 2. *Flow-chart of template-based recognition*

$$(f \star g)[k] = \sum_{i=0}^{N} f[i]g[i+k] = \mathcal{F}^{-1}\{\mathcal{F}\{f[-i]\}\mathcal{F}\{g[i]\}\}[k]$$

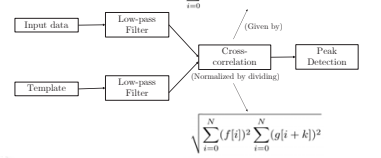

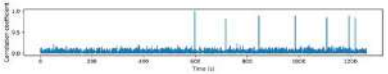

Figure 3. *Results of one normalized cross-correlation. The large peaks are matches to some JIBO voice line. A vertical axis value of 1 indicates an exact match. Due to noise and microphone placement inconsistencies, an exact match was very rare and thresholding was used to determine whether a match took place.*

Deliverables

- A new database layout was designed and accompanied with documentation using combined data from the designed processing methods.
- User interface was created for labeling and cutting audio. It decreases manual work by giving the user certain features:
  - Jump to audio containing private info or the beginning of certain tasks
  - Switch between textual and audio analysis (Figure 4) of child interviews

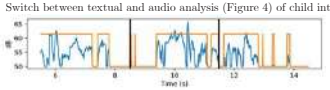

Figure 4. *A small section of a sound file. The user selected section is between the two black vertical lines. The orange sound blocks can be snapped to while scrubbing or can be ignored if fine scrubbing is desired.*

Conclusion and Future Work

- This database will assist in research for a number of diverse applications:
  - Child automatic speech recognition
  - Child speech science and linguistics
  - Human-robot interaction
- Going forward, we hope to generalize the methods for preliminary processing to all speech databases.

References

[1] Yeung, G., Afshan, A., Quintero, M., Martin, A., Spaulding, S., Park, H. W., ... and Alwan, A. (2019). Towards the development of personalized learning companion robots for early speech and language assessment. *2019 Annual Meeting of the American Educational Research Association (AERA)*.

[2] Yeung, G., & Alwan, A. (2018). On the Difficulties of Automatic Speech Recognition for Kindergarten-Aged Children. *Interspeech*, 1661–1665.

We would like to thank Professor Alwan, Gary Yeung, Amber Afshan, and Morgan Tinkler for the opportunity, guidance, and warm welcome given to us.
Additional thanks to the UCLA Wireless Health Institute, UCLA ECE Fast Track Program, and the NSF for their continuing support, financially and otherwise, for undergraduate research.

LAB NAME

Communications Systems Laboratory

FACULTY ADVISOR

Professor Richard Wesel

GRADUATE STUDENT DAILY LAB SUPERVISOR

Ethan Liang

DEPARTMENT

Electrical and Computer Engineering

Wenhui Sui

Electrical Engineering

First Year

UCLA

Design of Cyclic Redundancy Check (CRC) for Tail-Biting Convolutional Codes

Reliable transmission of data requires channel codes that can correct errors introduced by the channel and/or detect that a received or decoded sequence is not valid. Convolutional encoders can correct errors in a distorted received sequence by using the Viterbi algorithm to find the closest convolutional codeword to the received sequence. Cyclic redundancy check (CRC) codes can detect whether the convolutional codeword identified by Viterbi decoding corresponds to a valid message. While both CRCs and convolutional codes have been developed in the past, they have been designed independently even though they are not independent when used together. For zero-terminated convolutional codes (ZTCCs) that are terminated by a final sequence of inputs that drives the encoder to the zero state, our research group has designed CRCs that are optimal for a given ZTCC. Tail-biting convolutional codes (TBCCs) avoid the overhead caused by ZTCCs and therefore can achieve higher rates with essentially the same performance. Rather than using additional input symbols to drive the final state to zero, TBCCs enforce the constraint that the starting state is the same as the final state. Our research is directed towards developing CRCs that are optimal for a given TBCC.

Design of Cyclic Redundancy Check (CRC) for Tail-Biting Convolutional Codes

Vincent Lau[1], Wenhui Sui[1], Ethan Liang[1], Richard Wesel[1]

[1]Communications Systems Laboratory, Department of Electrical and Computer Engineering
University of California, Los Angeles

Introduction

Reliable transmission of data requires channel codes that can correct errors introduced by the channel and/or detect that a received or decoded sequence is not valid. **Convolutional encoders** can correct errors in a distorted received sequence by using the Viterbi algorithm to find the closest convolutional codeword to the received sequence. We are particularly interested in the implementation of **tail-biting convolutional codes (TBCC)**, which reduce overhead and are capable of achieving higher rates at practically no expense to performance. **Cyclic redundancy check (CRC) codes** can detect whether the convolutional codeword identified by Viterbi decoding corresponds to a valid message. While both CRCs and convolutional codes have been developed in the past, they have been designed independently even though they are not independent when used together. Our research is directed towards developing CRCs that are optimal for a given TBCC. By first implementing an encoder and decoder for convolutional codes, we are building towards designing CRCs to ultimately accomplish this goal.

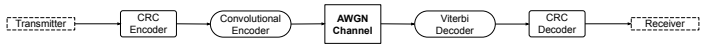

Figure 1. *Overall system structure of convolutional code and CRC for communications.*

Convolutional Codes

Convolutional codes are error-correcting codes that rely on memory storage in encoding, distinguishing them from traditional linear block codes. The encoder employs a shift-register structure that utilizes delay blocks to compute the output and track the state. We focus on rate-1/*n* encoders, which take 1-bit inputs and produce *n*-bit outputs.

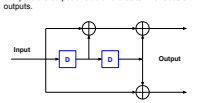

Figure 2. *A convolutional encoder can be represented as a block diagram. The values inside the delay blocks (blue) represent the state of the encoder.* [1]

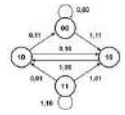

Figure 3. *A state machine is used to determine the output for a particular input and state. It also shows the evolution of states in a compact way.* [1]

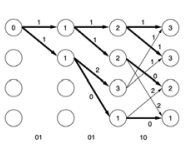

Figure 4. *The Trellis diagram aids in keeping track of path metrics and surviving paths, which are utilized in Viterbi decoding.* [1]

- The decoder we implement is based on the **Viterbi algorithm**, which can be realized with a Trellis diagram to keep track of the evolution of state paths over time, and helps us identify the most likely codeword given the received sequence.
- We are able to identify several performance metrics from the Trellis diagram, including free distance and number of nearest neighbors. The **free distance** represents the smallest Hamming distance between a pair of two valid codewords, while the number of nearest neighbors indicates the number of such pairs.
- While zero-terminated convolutional codes (ZTCCs) are terminated by a final sequence of inputs that drives the encoder to the zero state, **tail-biting convolutional codes (TBCCs)** require that the starting state be the same as the final state. These codes can achieve higher rates while maintaining nearly the same error-correcting performance.

Cyclic Redundancy Check (CRC)

Cyclic redundancy check (CRC) codes are error-detecting codes that help detect errors that may have been made by the decoder (e.g. the Viterbi decoder). At a high level, the CRC adds extra bits to the original codeword to serve as an extra layer of protection for decoding. This modification acts as an additional constraint to reduce the number of valid codewords, resulting in a smaller set of such valid codewords. This smaller set facilitates a larger minimum distance between codewords that provides a higher noise tolerance. In other words, the decoder will be less likely to select and validate an incorrect codeword.

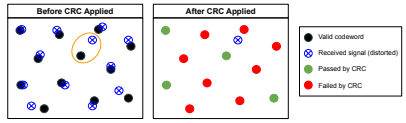

Figure 5. *Visual representation of CRC operation: The figure at the left shows the space of valid codewords (black). Transmission over a channel creates noise, resulting in distortion in the received signals (blue). Sometimes the noise distorts the codewords so much that the decoder may associate the received signal with a different codeword (yellow), leading to an error in decoding. To limit this effect, the CRC will only pass specific codewords (green) and fail all others (red) to make the valid codewords distinct.*

Materials and Methods

- This phase of the project primarily involved implementing a convolutional encoder and Viterbi decoder. This work was completed in MATLAB and was followed by extensive testing of both the codes and performance metrics for various examples of generator polynomials. We made sure to test different code rates and number of states.
- We started by simulating transmission across noiseless channels to make sure our encoder/decoder worked (i.e. zero errors occurred).
- For noisy channel transmission, we were interested in comparing bit-error rate (BER) vs. signal-to-noise ratio (Eb/No) for different rates and codes, as well as examining other properties like free distance, nearest neighbors, and analytic traceback depth.

Simulation Results

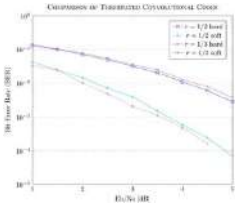

Figure 6. *A performance comparison of bit-error rate (BER) vs. signal-to-noise ratio (Eb/No) between different generator polynomials for ZTCC. We tested codes with rate-1/2 and 1/3, which were decoded with both hard decision and soft decision.*

- We compared two polynomials, (7,5) in purple and (13,12,16) in blue, which are of rate-1/2 rate-1/3, respectively.
- Two types of decoding were implemented and tested: hard-decision and soft-decision.
  - Hard-decision decoding uses a threshold value to decode a codeword.
  - Soft-decision decoding uses Euclidean distance to decode, which takes into account the impact of the noise on the transmission. Soft-decision decoding is the more refined and accurate technique of the two.
- As expected, the soft-decision decoding method outperformed the hard-decision decoding. Soft-decision required an Eb/No value about 2dB lower than hard-decision to produce the same BER.
- The rate-1/3 code performed better than the rate-1/2 code for soft-decision decoding, as expected. However, the two codes have similar performance for hard-decision decoding, which is an anomaly we are exploring (we expect the rate-1/3 to perform better).

Conclusions & Future Work

- Overall, our experience with the program was equal parts learning and re-implementing codes. We were able to develop a sound understanding of channel coding techniques and implement convolutional codes from scratch to supplement our learning process.
- For noiseless channels, we found that messages were decoded with zero error, as expected. Across noisy channels, noise was applied at different proportions, and we were also able to obtain good results (BER vs. Eb/No) for different parameters.
- We are looking towards the future to further develop our knowledge and bolster the significance of this project, with the ultimate goal of developing new CRCs for a range of CRC bit lengths. Specifically, we hope to eventually design new CRCs which are targeted for use with specific TBCCs, which we will implement.
- Our new CRCs will improve short-blocklength communications that are vital to sensor networks and the internet of things.

References

[1] R.D. Wesel, "Convolutional Codes", Wiley Encyclopedia of Telecommunications, John Wiley and Sons, 2003.
[2] H.H. Ma, J.K. Wolf, "On Tail Biting Convolutional Codes", IEEE Transaction on Communications, 1986.
[3] C.-Y. Lou, B. Daneshrad, R.D. Wesel, "Convolutional-Code-Specific CRC Code Design", IEEE Transactions on Communications, 2015.

Acknowledgments

We would like to thank the National Science Foundation and the Electrical and Computer Engineering Department for providing us the opportunity to conduct research. Additionally, we would like to acknowledge Ethan Liang and Hengjie Yang for providing guidance and mentorship throughout our research and learning process.

LAB NAME
Visual Machines Laboratory

FACULTY ADVISOR
Professor Achuta Kadambi

GRADUATE STUDENT DAILY LAB SUPERVISOR
Guangyuan Zhao

DEPARTMENT
Electrical and Computer Engineering

Irfan Syed

Electrical Engineering

First Year

El Camino College

Tracking Objects Using Physics-Guided Neural Networks

Incorporating physics into neural networks, known as physics guided neural networks (PGNN), has been explored for object detection and tracking. The proposed method aims to enhance accuracy by merging regional convolutional neural networks (R-CNN) and physics-guided models. Using video segmentation methods, it uses a physics guided neural network to classify, detect, and track objects. A self-made dataset created with ideal scenarios involving linear motion such as object drops and tosses is the testing framework for the physics-guided model. The dataset contains scenarios involving the complexity of object occlusion for future development of the prediction model to increase accuracy in realistic, occluded situations. Classification and motion tracking of objects through predicted patterns rely on physics-based learning. By predicting trajectories in later frames based on kinematic calculation in earlier frames within the video, the model is able to detect and track the target object and increase accuracy. Pytorch 1.0 is the framework used for developing this platform and the code will be open source for future development.

Implementing Kinematic Prediction via Physics-Guided Neural Networks

Brian Chap, Lucas He, Irfan Syed
Guangyuan Zhao, Achuta Kadambi
Department of Electrical and Computer Engineering, UCLA

Using Physics-Based Machine Learning to Track Objects

Physics-guided neural networks (PGNNs) are crucial for modeling resistive behaviors in real life scenarios ranging from vehicle tracking to aerial trajectories. In prior papers, bounding box construction for videos would entail construction for every individual frame, hindering progress in terms of speed without significant computational power. This paper aims to bridge the divide between image and video object detection, utilizing kinematic priors to predict the motion of subjects via the incorporation of affine transformations and perspective consideration (horizon, side-to-side, overhead, etc.). Approaches based on optical flow algorithms and tubelet architectures are considered and blended with physical modules to harness spatiotemporal coherence among individual frames. PyTorch 1.0 acts as the framework for code development and all code is expected to be open-source for future development.

Regional Convolutional Neural Networks

Figure 1 : Improvements such as clearer annotations and bounding box representations were made on a Faster R-CNN framework with 20 different classifications of objects. The physics model resulted from this framework of Faster R-CNN.

Dataset

Applications of physics-based calculations on the Faster R-CNN framework were tested on a self-made dataset of videos that captured optimal scenarios, including drops, tosses, and object sliding on surfaces to model the effects of gravity, resistance, and object motion. The added complexity of object occlusion was captured for the purpose of modeling realistic difficulties in object detection and motion prediction.

Physics-Based Model

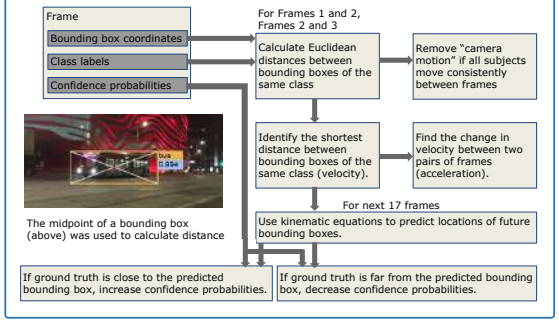

The midpoint of a bounding box (above) was used to calculate distance

Future Plans

The proposed physics model performs with high confidence values in the ideal scenarios created within the dataset. Expectations for future improvements include higher efficiency rates, faster processing rates, greater accuracy between multiple objects, and more accurate predictions for accounted complexities such as occlusions, lighting, and camera motion.

Limitations of current model:

Inability to account for changing acceleration
Inability to predict object motion with occlusions
Prediction model accounts for only 2D object transformations.
Unidentified objects lack physics-based machine learning

Applications:

Self-Driving	Defense Industry
Autonomous Drones	Movement Prediction

Preliminary Results

Figure 4: Bottle detection without physics-based learning (left) and with physics-based learning (right)

Figure 5: Multiple object detection without physics-based learning (left) and with physics-based learning (right)

The physics-based model results indicate significant increases in the accuracy of the model when compared with simply the Faster R-CNN framework. Faster R-CNN with physics-based machine learning increases the confidence of object detection and removes classification errors for objects.

References

Saha, Sumit. A Comprehensive Guide to Convolutional Neural Networks — the ELI5 Way. *Towards Data Science*, (2018).

Lei, F.-F. et al. Detection and Segmentation. *Stanford University*, (2017).

Girshick, R. Fast R-CNN. CoRR 1504.08083 (2015).

Girshick, R., et al. Rich feature hierarchies for accurate object detection and semantic segmentation. CoRR 1311.2524 (2013).

Ren, S., et al. Faster R-CNN: Towards Real-Time Object Detection with Region Proposal Networks. CoRR 1506.01497 (2015).

Redmon, J., et al. You Only Look Once: Unified, Real-Time Object Detection. CoRR 1506.02640 (2015).

LAB NAME
Terahertz Electronics Laboratory

FACULTY ADVISOR
Professor Mona Jarrahi

GRADUATE STUDENT DAILY LAB SUPERVISOR
Dr. Nezih Yardimci and Deniz Turan

DEPARTMENT
Electrical and Computer Engineering

Madeline Taylor

Electrical Engineering

Second Year

UCLA

Optimization of Delay Stage of Terahertz Time-Domain Spectroscopy System

Terahertz time-domain spectroscopy (THz-TDS) allows us to analyze materials using pulses of terahertz radiation created by a femtosecond laser. Materials are analyzed based on their absorption patterns of the THz radiation. In the laboratory system, the detector receives pulses of THz radiation along with optical light pulses. The optical light path length is shifted by a delay stage which enables analysis of materials over a time domain and frequency domain.

Our goal is to miniaturize and improve the delay stage to convert the large laboratory system into a mobile, commercial device. The previous delay stage utilizes linear motion; a platform with mirrors accelerates back and forth to alter the path length of the radiation. Our main focus is designing a smaller prototype that relies on rotational acceleration to decrease the loss of speed from linear acceleration and deceleration.

Once a full prototype has been designed, it is tested in the laboratory setup and compared with previous data for accuracy. The frequency domain results of THz-TDS can be analyzed and used to determine chemical composition. When testing for accuracy, the Fourier graphs and THz pulses of our delay stage are directly compared with those of the laboratory stage. Our first test displayed broadening and shifting in the Fourier transformed waves which both indicate a worsened accuracy. However, the new delay stage works at almost double the frequency of the old one (2.2 Hz compared to 1.2 Hz) and only weighs 861 grams.

Optimization of Delay Stage of Terahertz Time-Domain Spectroscopy System

Madeline Taylor, Arhison Bharathan, Deniz Turan, Nezih Tolga Yardimci, Mona Jarrahi
Terahertz Electronics Laboratory, Department of Electrical and Computer Engineering

Background and Motivation

Terahertz Time-Domain Spectroscopy
- Allows analysis of chemical composition of materials using time-delayed pulses of terahertz radiation
- More efficient than prior methods because it is sensitive to amplitude and phase of radiation
- Materials and environments are analyzed based on their absorption patterns of the radiation
- Laboratory system utilizes a femtosecond laser source that produces electromagnetic radiation which follows two paths as depicted below

- One optical path passes through a terahertz emitter. The other is delayed by a mechanical stage to allow results to be made over a time domain
- Objects can be placed in the path of terahertz pulses for time-based spectroscopic analysis as shown below

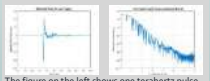

The figure on the left shows one terahertz pulse detection over a time domain. Each dip and spike gives information that can be processed using Fourier analysis to create the figure on the right. The graph on the right gives detailed information about the material being analyzed over a frequency domain. In this case, the graph's dips show the water vapor content in the air since no specific object is being analyzed

Motivation
- Create a smaller, cost-efficient system for analyzing various materials specifically for agricultural, environmental purposes

Delay Stage

The current delay stage is based on linear motion.

The current delay stage performs too slowly for desired results so the proposed solution is to convert from linear acceleration to rotational motion.

Materials and Methods

Delay Stage
- DC motor powered by Arduino and H-bridge IC, L293D
- Initial prototypes of delay stage created by 3D printer with goals to outsource for final design

Prototype Designs

First Design:
- Uses slider-crank mechanism to drive platform
- Powered by stepper motor

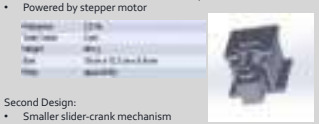

Second Design:
- Smaller slider-crank mechanism
- Powered by DC motor
- Much faster, but inconsistent speeds
- 101 grams (decrease in weight)

Third Design:
- Crank-inspired eccentric design
- Powered by DC motor and feedback system to stabilize speed (in progress)
- Greater inertia with the use of gears to drive the platform

This table compares the second and third design in the two left columns. The third column design is currently in progress.

Testing and Results

We test our delay stage in the laboratory set up by aligning the mirrors to accurately reflect the laser beam on its path. We compare the pulses and Fourier transformed data using MATLAB to compare accuracy and efficiency.

First design in laboratory setup

Results of First Design:

The Fourier transformed graphs of the first design's results (left) display a broadening in the dips compared to the standard results shown on the right. This depicts a decrease in accuracy.

The figure above shows our new data overlapping the data from the original laboratory delay stage. The shallow absorption lines and shifts in the absorption lines are indicated above. It shows promising results that also demonstrate a need for greater accuracy.

Current Work/Conclusion

We are currently improving each design by ordering new parts to improve stability and reciprocation. We are also implementing a PID feedback system using a proximity sensor to increase reliability and control. A crank mechanism presents promising results for use in the actuation of a THz-TDS delay stage so we hope to continue improving on accuracy and speed with this next design shown to the right.

Acknowledgements

This work was supported by the National Science Foundation through the UCLA Summer Undergraduate Research Program organized by William Herrera.

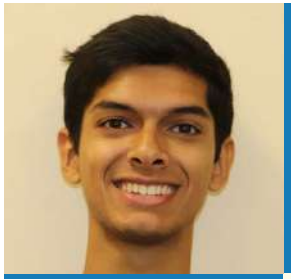

LAB NAME
Neptune Laser Laboratory

FACULTY ADVISOR
Professor Chan Joshi

GRADUATE STUDENT DAILY LAB SUPERVISOR
Daniel Matteo

DEPARTMENT
Electrical and Computer Engineering

Ravi Varma

Electrical Engineering

First Year

UCLA

Sub-micrometer Precision Optical Delay Stage for Synchronization of Ultrafast Laser Pulse

As laser systems produce shorter and shorter pulses to push the limits of ultrafast and high field science, the requirements for precision timing and optical synchronization in the lab have increased accordingly. The coordination and control of the relative time delay between ultrafast pump and probe laser pulses is required to resolve short lived physical events. Time and space are intimately connected for light, and on picosecond and femtosecond time scales, errors and uncertainties in the optical path length on the order of micrometers and nanometers can drastically degrade the time resolution of measurements in the laboratory. We have implemented an optical delay stage powered by a DC servo motor and controlled by a LabVIEW program. To evaluate the accuracy of positioning two laser pulses, we study the stage's accuracy and repeatability in creating an optical path length delay with a HeNe laser Michelson interferometer. The pointing stability and reproducibility of the spatial beam profile after the stage is also determined. Understanding of the stage's precision will enable us to perform picosecond pump-probe experiments, or synchronize ultrafast laser pulses using cross-correlation.

Sub-micrometer Precision Optical Delay Stage for Synchronization of Ultrafast Laser Pulse

Ravi Varma, Daniel Matteo, Sergei Tochitsky, Chan Joshi
Neptune Laboratory
Department of Electrical and Computer Engineering
University of California, Los Angeles

Introduction and Motivation

- In order to resolve ultrafast events, synchronization of short laser pulses is crucial
  - As pulses become shorter, optical systems must become more accurate and stable to ensure correct measurements
- Synchronization of such pulses will result in more accurate pump-probe experiments
- Pump-Probe: One intense pulse interacts with the experimental sample while the weak probe pulse is affected by the interaction
  - Used to study laser-matter interactions in many fields including plasma physics, femtochemistry, and condensed matter physics

Methods

- We assembled a delay stage, translated by a DC motor, which can control the optical path length of the probe pulse relative to the pump pulse
- A LabVIEW program controls the motor and collects data from an oscilloscope in either single shot or continuous shot modes
- We move the delay stage back and forth repeatedly to measure the pointing stability of a CW Helium-Neon (HeNe) laser beam (λ = 632.8 nm)
  - We measure stability by tracking the beam's centroid on a CCD camera
- We then set up Michelson interferometer using a HeNe laser to distinguish the stage's positional precision
  - We track movement of the fringes across the CCD

Interferometry

- Using the wave nature of light to extract phase information from overlapped beams
  - Once combined, constructively interfering parts of the beam will produce bright fringes and destructively interfering parts will produce dark fringes
  - We use a beam splitter to split the HeNe laser into two paths
  - Light traveling along those paths are reflected back by mirrors, one static and one dynamic, its position controlled by the delay stage (Michelson Interferometer)
  - Movement of our delay stage changes the relative phase of the two interfering beams

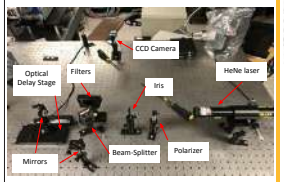

Pointing Stability Experimental Setup

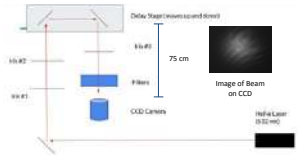

Distribution of the Beam positions after translating the delay stage in either µm or mm steps

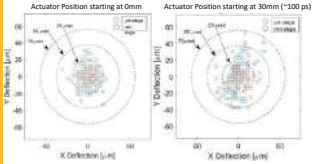

- µm steps allow for higher precision compared to mm steps

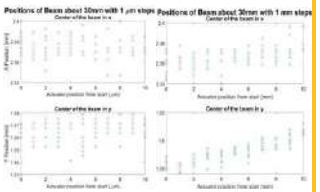

- Plotting Trends of X and Y displacements of beam starting from 30mm vs actuator position
- For 1 µm steps, the system jitters, but is reproducible within 40 µrad
- For 1mm steps, the system is reproducible, but systematic mechanical errors begin to arise, and the beam starts to drift significantly in the vertical direction

References

- A. J. Alcock and P. B. Corkum, Can. J. Phys., **57**, 1280
- *Introduction to Optics*, "Chapter 11." by Frank L. Pedrotti and Leno S. Pedrotti, Prentice Hall, 1993.

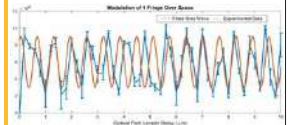

- Integrate full image to get fringe intensity, which should vary with a period of 632.8 nm path length delay (orange curve)
- Over 8 µm of stage movement, we accumulate approximately 700 nm of error from our expected path length delay

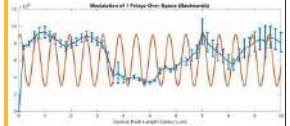

- We repeated the experiment, translating the actuator in the backwards direction
- Sub-µm accuracy was not reproducible (min. possible step = 2.5 µm)

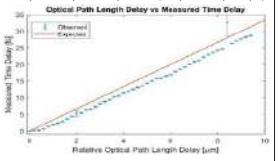

- By measuring the position of fringes, we determined the total accumulated phase at each stage position, and thus the true position of the stage
- We relate this to the time delay via the speed of light, and find that for every 8µm we accumulate an error of 3 fs

Conclusion

- We find that our delay stage gives us a pointing stability of 25 µrad within µm steps, but increases to 50 µrad at mm steps
  - Stability is worse the farther away the stage is from its origin
- Using interferometric techniques, we determined that:
  - For every 8 µm, we accumulate 700 nm of translational error or about 3 fs of time delay error
  - Movement in the forward direction is reliable, whereas movement backwards is inconsistent
- We demonstrated the optical delay stage's ability to synchronize ultrafast laser pulses on sub-picosecond time scales

LAB NAME
Sensors and Technology Laboratory

FACULTY ADVISOR
Professor Robert Candler

GRADUATE STUDENT DAILY LAB SUPERVISOR
Jimmy Wu

DEPARTMENT
Electrical and Computer Engineering

Sydney Walsh

Electrical Engineering

Second Year

UCLA

Millimeter-Scale Magnetic Shielding

Devices that rely on atomic spectroscopy, such as nuclear magnetic resonance gyroscopes and atomic clocks, are strongly affected by external magnetic fields. Thus, in order to miniaturize these devices while maintaining precision, small-scale magnetic shields must be developed to properly redirect magnetic field lines away from the enclosed devices. The purpose of our research is to fabricate and test potential shield designs. Based on previous research, we determined that the optimal design would consist of concentric cylinders of alternating high permeability and low permeability material. By alternating layers, we partially prevented adjacent ferromagnetic material from reducing the magnetization of that layer. Moreover, multilayer shielding allowed us to mitigate the effects of magnetic saturation, as a single layer of magnetic material would reach saturation more quickly, limiting the shield's ability to generate an opposing field. We conducted our research by simulating potential shield designs in COMSOL Multiphysics, developing an appropriate test setup to assess the effectiveness of our shields, and fabricating shields to test. For our test setup, we generated a magnetic field using an electromagnet and measured the magnetic flux density using a printed circuit board with a magnetometer mounted at its tip; shielding factor was determined by taking the ratio of external to internal magnetic field. Shields were fabricated by electroplating alternating layers of permalloy and copper.

Millimeter-Scale Magnetic Shielding

Sydney Walsh, Hou Seng Wong, Justin Shao, Jimmy Wu, Robert Candler

Department of Electrical and Computer Engineering, University of California, Los Angeles

Purpose

Figure 1: Chip-scale atomic clock[2].

- Devices that rely on atomic spectroscopy (atomic clocks, NMR gyroscopes, etc.) are sensitive to external magnetic fields
- In order to miniaturize these devices while maintaining precision, we must enclose them in small-scale magnetic shields
- Our research serves primarily to test and fabricate potential shield designs

Magnetic Shielding Overview

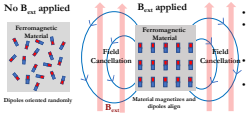

Figure 2: Depiction of DC magnetic shielding process.

- Shields created from high permeability ferromagnetic material
- When an external magnetic field (B_{ext}) is applied, the previously randomly ordered dipoles align in the direction of the applied field, generating an opposing magnetic field
- These fields cancel, redirecting B_{ext} away from the device enclosed in the shield
- Magnetic material reaches saturation when a strong enough external magnetic field is applied that the material cannot magnetize further, decreasing effectiveness of shielding

Shield Design

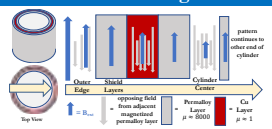

Figure 3: Visualization of multilayered cylindrical shield design.

- Concentric cylinders of alternating high permeability and low permeability material
- Magnitude of external magnetic field decreases each successive layer with max shielding in the center
- Alternating material prevents adjacent layers of ferromagnetic material from demagnetizing each other
- Having multiple layers mitigates effects of saturation

Methods

Test Setup

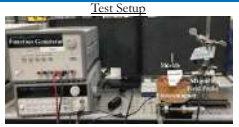

Figure 4: Picture of test setup.

- External magnetic field generated by electromagnet with current outputted by function generator
- Magnetic flux density inside (B_{in}) and outside (B_{out}) the shield measured by printed circuit board with magnetometer mounted at its tip
- We perform 2 trials: one increasing the magnetic field without the shield (B_{out}) and another with the shield (B_{in})
- Shielding Factor: $S = B_{out}/B_{in}$

Fabrication

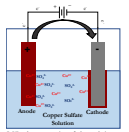

Figure 5: Visual representation of electroplating process

- Electroplate alternating layers of permalloy and copper onto cylindrical wax mold and then dissolve wax in xylene solution
- To electroplate permalloy, use nickel and iron as anode instead of copper

Results & Discussion

COMSOL Simulations for Multilayer Cylinder

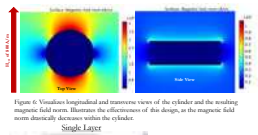

Figure 6: Visualizes longitudinal and transverse views of the cylinder and the resulting magnetic field norm. Illustrates the effectiveness of this design, as the magnetic field norm drastically decreases within the cylinder.

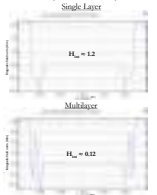

Figure 7: Comparison between multilayer and single layer cylindrical shields of same material, dimensions, and thickness in order to access the effectiveness of multilayered shielding. Charts depict magnetic field norm in a line through the center of the cylinder in the direction of the applied magnetic field. The results prove that multilayer designs are more effective than single layer designs before saturation, as shielding factor for the multilayer shield is considerably larger for cylinders of the same dimensions, material, and external magnetic field.

Plate vs. Cylinder Design

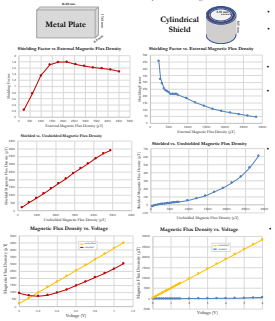

- Cylindrical shield: alternating permalloy and copper layers
- Metal plate shield: single permeandar layer

- Cylindrical design observed to have higher shielding factors overall
- Shielding factors appear to decrease as materials approach saturation

- Metal plate B_{in} seems to have linear relationship with B_{out} while cylinder continues to shield with decreasing effectiveness as it approaches saturation

- B_{in} of permeduar plate seems to increase at a similar rate to B_{out} while for the cylinder, the rate B_{in} increases is much less than that of B_{out}

Figure 8: Results collected from our test setup for cylindrical and metal plate shield designs.

Plate vs. Cylinder_Mapping

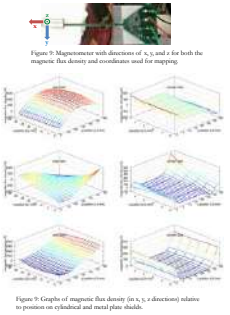

Figure 9: Magnetometer with directions of x, y, and z for both the magnetic flux density and coordinates used for mapping.

Figure 9: Graphs of magnetic flux density (in x, y, z directions) relative to position on cylindrical and metal plate shields.

Conclusion and Future Work

- Our simulation and test setup results imply that our multilayer, cylindrical design provides more optimal shielding than the commonly used plate design
  - COMSOL simulations confirmed that alternating layers of high and low permeability material produced a higher shielding factor than a single layer of the same thickness, inner radius, and material
  - By applying different magnetic fields and measuring B_{out} and B_{inside}, we found that our cylindrical design had higher shielding factors overall and that B_{out} increased at a much slower rate when increasing B_{out} compared to the plate design
  - In the future, we plan on testing and fabricating more shields of different geometries and examining the possibility of electroplating metal directly onto devices

References

[1] Donley E., Hodby, E., Hollberg, L., and Kitching, J, Demonstration of high-performance compact magnetic shields for chip-scale atomic devices. 2007.

[2] Dubay, L., NIST scientists win 2014 Rank Prizes for chip-scale atomic clock. 2013.

[3] Hodges, E., Millimeter-Scale Electroplated Conformal Magnetic Shields. 2018.

[4] Wu, J., Li, L., Harrison, J., and Candler, R. Micro- to Millimeter Scale Magnetic Shielding. 2017.

Acknowledgements

I would like to thank the Sensors and Technology Laboratory for having me in their lab, the National Science Foundation and Functional Nanomaterials Summer Scholars Program for funding my research, and the UCLA SURP program for giving me this unique opportunity.

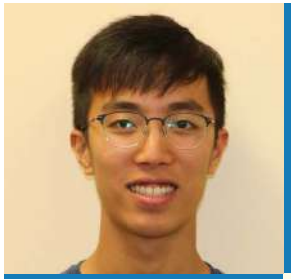

LAB NAME
Sensors and Technology Laboratory

FACULTY ADVISOR
Professor Robert Candler

GRADUATE STUDENT DAILY LAB SUPERVISOR
Jimmy Wu

DEPARTMENT
Electrical and Computer Engineering

Hou Seng Wong

Computer Science

First Year

Pasadena City College

Miniaturized magnetic shielding for chip-scale atomic devices

Atomic devices such as atomic clocks and nuclear magnetic resonance (NMR) gyroscopes are excellent for taking measurements because of their well-defined quantum properties. The miniaturization of atomic devices would allow for them to be combined with phones and wearables, which allow for extremely precise, low power positioning systems. However, such devices must be extremely well-isolated against external interference, such as a magnetic field, to preserve their accuracy. For example, atomic clocks need to be shielded to prevent magnetic fields from interfering with the energy spectrum of atoms and to maintain the clock's frequency. Recent efforts have been made to miniaturize chip-scale atomic devices. But to further scale down the size of atomic devices, smaller magnetic shields must be fabricated to accommodate the compact environment inside electronic devices. In this research, the magnetic behavior of a flat piece of Permendur and a cylinder of Permalloy was measured to study the shape-dependency of magnetic shields as well as their effectiveness to attenuate an external magnetic field. The results of this research would provide insights for the optimal design of a miniaturized magnetic shield.

UCLA Samueli School of Engineering

TSSRP TRANSFER STUDENT Summer Research Program

Miniaturized magnetic shielding for chip-scale atomic devices

Hou Seng Wong, Justin Shao, Sydney Walsh, Jimmy Wu, Robert Candler
Pasadena City College
Sensors and Technology Laboratory, UCLA

Introduction

- Atomic devices are excellent measurement tools given their well-defined quantum states.

- However, their fragility toward external interferences such as magnetic fields is a significant limitation.
- Materials with high permeability provide an alternate path for magnetic field lines to travel through.

Wu, J. et. al., 2017[1]

Fig. 1: Illustration of a magnetic shield. When the shield has the same permeability as the air ($\mu_r = 1$), it does not affect the magnetic field. When $\mu_r \approx 8000$, field lines travel along the shield instead of cutting through the shield.

Methods

- Two iron alloy shields are tested: a 2mm diameter electroplated cylinder and a piece of 1mm thick Permendur.
- Shielding factor $\equiv \frac{H_{ext}}{H_{int}} \approx \frac{\mu_r t}{D}$

Fig. 2: Photo of setup.

- The magnetic field is generated by running direct current through a coil.

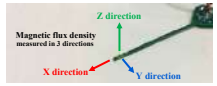

Fig. 3: Close-up photo of the magnetometer.

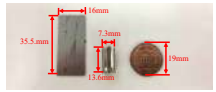

Fig. 4: Dimensions of shields. The plate is made up of Permendur (49Fe-49Co-2V) and the cylinder is made up of wax electroplated with Permalloy (80Ni-20Fe). Both iron alloys have high permeability[2] ($\mu_r \geq 800$).

Results

Cylinder Plate

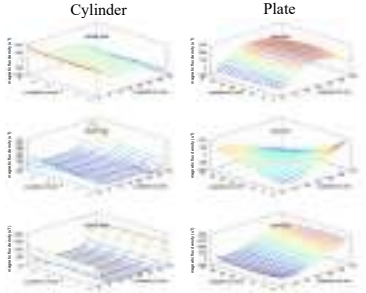

Fig. 5: The XYZ magnetic flux density mappings of two shields. Magnetometer is scanned across a horizontal plane on the shield.

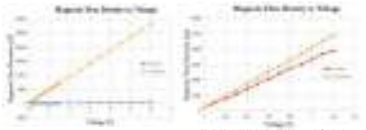

Fig. 6: (Cylinder) Shielded and unshielded magnetic flux density against voltage. It is apparent that the unshielded flux density relates linearly to voltage, whereas the shielded does not.

Fig. 7: (Plate) Shielded and unshielded magnetic flux density against voltage respectively. Both of the shielded and unshielded magnetic flux densities appear to be linear as voltage increases.

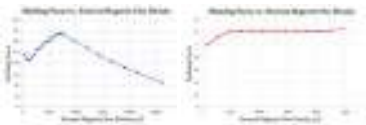

Fig. 8: (Cylinder) Shielding factor against external magnetic flux density. The effect of saturation is noticeable after 7500μT external flux density where the shielding factor peaks.

Fig. 9: (Plate) Shielding factor against external magnetic flux density. No apparent effects of saturation are observed. However, the overall shielding factor is considerably lower than that of the cylindrical shield.

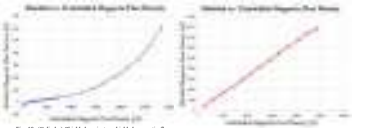

Fig. 10: (Cylinder) Shielded against unshielded magnetic flux density using cylindrical shield. Saturation is apparent after 10000μT unshielded flux density where the plot losses linearity.

Fig. 11: (Plate) Shielded against unshielded magnetic flux density using Permendur plate. Linearity is observed between the shielded and unshielded flux densities.

Discussion

	Permalloy cylinder	Permendur plate
Max. shielding factor measured	134.2	1.25
saturation	at 6927μT EXT	Not observed

- Saturation effects are apparent for the Permalloy cylinder after 10000μT EXT in figure 10 where the plot loses linearity. This is confirmed by a previous work[3]. The decrease of shielding factor after 7500μT EXT in figure 8 also suggests for saturation. This is consistent with another previous work[1]. The saturation point in the table above is the point at which the shielding factor is the highest.
- Based on the xyz mappings, the Permalloy cylinder is able to attenuate the magnetic flux density to nearly zero inside its shielded region in both x, y and z directions. This is consistent with the results of our COMSOL simulations.

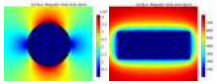

Fig. 12: COMSOL simulations of the shielding effects of the Permalloy cylinder. Permeability (μ_r) is set to 8000. The deep-blue color of the cylinder's interior shows that the magnetic field is attenuated to an extremely low level.

- However, the Permendur plate manifested poor shielding abilities relative to the Permalloy cylinder. This is partly due to the fact that Permendur has a lower permeability than Permalloy. Their geometries could have contributed to their shielding capabilities as well. The plate seems to attenuate the magnetic field symmetrically in one direction yet nonuniformly across different directions.

Conclusion

- The Permalloy cylinder has a higher maximum shielding factor than the Permendur plate.
- Saturation is observed for the cylinder but not for the plate.
- Cylindrical shape is a more effective design.

Acknowledgements

STL MESA

References

[1]Wu, J., Li, L., Harrison, J., and Candler, "R. Micro- to Millimeter Scale Magnetic Shielding". 2017.

[2]Jiles, D. C.,1998, *Introduction to Magnetism and Magnetic Materials*, 2nd Edition, CRC Press, p. 354.

[3]Donley, E. A., et al. "Demonstration of high-performance compact magnetic shields for chip-scale atomic devices." Review of Scientific Instruments 78.8 (2007): 083102

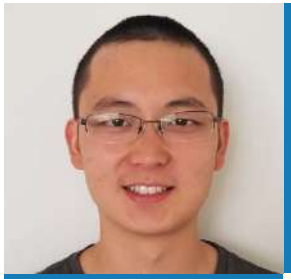

LAB NAME
Communications Systems Laboratory

FACULTY ADVISOR
Professor Richard Wesel

GRADUATE STUDENT DAILY LAB SUPERVISOR
Ethan Liang

DEPARTMENT
Electrical and Computer Engineering

Derek Xiao

Electrical Engineering

Third Year

UCLA

Computing Channel Capacity using the Blahut-Arimoto Algorithm

The maximum rate at which information can be reliably transmitted over a communication channel is the channel capacity, usually represented in units of bits per channel use. The ability to compute the capacity of any discrete memoryless channel based on its statistical description is a powerful and fundamental result of information theory. Broadly speaking, the noisier a channel, the lower its capacity.

Mathematically, the channel capacity is the maximum mutual information between the input and output of the channel, where the maximum is taken over possible input distributions. My research is focused on developing tools to identify the mutual-information-maximizing input distribution for a channel and consequently its capacity. As an initial project, I have implemented the Blahut-Arimoto algorithm, which finds the capacity-achieving distribution for any discrete memoryless channel with a finite input alphabet.

For many practical channels, the input alphabet is not finite. For example, even a simple amplitude shift keying system has an uncountably infinite number of possible amplitudes. Furthermore, there are practical communication systems where the optimal input distribution turns out to be asymmetric, such as on-off keying over an additive white Gaussian noise channel. My future research is directed towards identifying the optimal input distributions in these cases and developing practical encoders that can approximate those optimal input distributions.

Computing Channel Capacity Using the Blahut-Arimoto Algorithm

Derek Xiao, Ethan Liang, Prof. Richard D. Wesel
Department of Electrical and Computer Engineering
University of California, Los Angeles

Motivation

In our communication technology, whether it's TV or satellite communications, the fundamental goal is to **send bits** with **low power** and **low error**.

This initial project is focused on finding the highest rate at which information can be transmitted with **zero error**, the channel capacity. Since analytic derivation of the capacity is sometimes unfeasible, I implement an iterative algorithm that can find the optimal input distribution, and consequently the capacity.

What is Channel Capacity?

Definition

- Channel Capacity: The maximum information rate (in bits per transmission) at which information can be transmitted reliably (with no error) through a noisy channel.

Example

- noisy typewriter channel
  - Capacity: $\log_2(26/2)$, achieved by using only half of the inputs

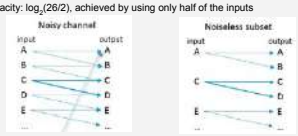

Some Intuition

- *noisier* typewriter channel (n equiprobable outputs given an input)
  - Capacity: $\log_2(26/n)$, achieved by using only 1/n of the inputs.
  - *noisier channels have a lower capacity*

What is Mutual information?

- mutual information: measurement of how much information X and Y share. how much knowing one of the variables reduces uncertainty about the other.

Examples

- X = dice roll, Y = indicator of whether the roll is even or odd
  - I(X;Y) = 1 (bit)
- X = dice roll, Y = a different, independant dice roll
  - I(X;Y) = 0 (bits)

Computation of Channel Capacity

$$C = \max_{p(x)} I(X;Y)$$

C	= channel capacity
p(x)	= input probability distribution
I(X;Y)	= mutual information between X and Y
X,Y	= random variables

- It turns out that mutual information, I(X;Y), is convex over the possible input distributions, p(x), allowing for application of convex optimization techniques.
- I implement the **Balhut-Arimoto algorithm** to solve for capacity of a few example channels.

Acknowledgements

We would like to thank the UCLA ECE Fast Track to Success Program, NSF Summer Undergraduate Research Program for their financial support, and for this opportunity to explore research.

What is the Blahut-Arimoto Algorithm?

Projection on Convex Sets (POCS)

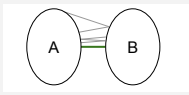

- we can find the minimum distance between two convex sets by randomly picking a $x \in A$ and finding the closest $y \in B$, then repeating until convergence.

- it turns out that I(X;Y) is a distance which satisfies the right properties, and we can write the capacity maximization expression in the form of a POCS problem, so we apply the iterative procedure described above.

Results

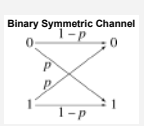

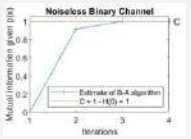

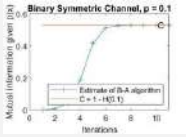

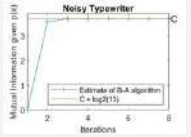

Conclusions and Future Work

All results converge to the correct theoretical values, validating my implementation of the Blahut-Arimoto algorithm.

My implementation works for discrete memoryless channels with a finite input alphabet. However, for many practical channels, the input alphabet is not finite. For example, even a simple amplitude shift keying system has an uncountably infinite number of possible amplitudes.

My future research is directed towards identifying the optimal input distributions in these cases and developing practical encoders that can approximate those optimal input distributions.

My immediate next project is to find the optimal input distribution given any average power constraint on an on-off keying channel with additive Gaussian noise.

If you would like to find out more about the Summer Undergraduate Research Program, please contact Director William Herrera:

William Herrera
Director
Undergraduate Research Program
310.825.9478
williamh@seas.ucla.edu
Engineering Student Resource Center, 6288 Boelter Hall

Or visit our website at https://tinyurl.com/uclasurp.

UCLA Samueli School of Engineering